Fall 2019

Changes in fresh properties of flowable concrete induced by pumping and composition of the lubrication layer

Alexis Salinas

Department:

CHANGES IN FRESH PROPERTIES OF FLOWABLE CONCRETE INDUCED BY PUMPING AND COMPOSITION OF THE LUBRICATION LAYER

by

ALEXIS SALINAS

A THESIS

Presented to the Faculty of the Graduate School of the

MISSOURI UNIVERSITY OF SCIENCE AND TECHNOLOGY

In Partial Fulfillment of the Requirements for the Degree

MASTER OF SCIENCE IN CIVIL ENGINEERING

2019

Approved by:

Dr.Dimitri Feys, Advisor
J Dr. Kamal H. Khayat
Dr. Cesar Mendoza

ABSTRACT

Pumping is an easy method to move concrete while keeping stability. It is worldwide accepted as one of the principal methods for concrete placement, as it accelerates construction. Typically, concrete acceptance in terms of fresh quantitative empirical properties (i.e. slump/slump flow and air content) are performed prior to the pumping process. However, empirical measurements have the drawback that they only measure 1 point. Rheology is better tool to evaluate the behavior of concrete. Pumping is a process that induces considerable shearing in the concrete that can impact its rheological properties. Therefore, the magnitude of these changes in fresh properties depends on a combination of mix design, flow rate, boom length and configuration, and concrete drop height. This research work evaluates the interaction between fresh concrete properties and pumping parameters on several mixtures with different workability levels and air contents. Large scale concrete batches were produced with different types and contents of admixtures and subjected to different pumping conditions. The tests used to address the workability changes were slump/slump flow, T50, air content (pressure method), unit weight, segregation resistance and rheology. The results showed that the fresh concrete properties are affected in diverse ways by pumping, with the results being dependent on the concrete fresh properties, and pumping parameters. Additionally, an attempt was performed to reverse engineer the composition of the so called “lubrication layer” through the science of rheology. Main results indicated a composition of purely paste.

ACKNOWLEDGMENTS

I would like to thank my advisor and friend Dr. Dimitri Feys for the given opportunity to be involved in this project. I will be always thankful for his patience, guidance and for this good experience that resulted from my graduate studies. Next, I would like to thank my committee members Dr. Kamal Khayat and Dr. Cesar Mendoza for their time and help given through my education. Also, I would like to thank Dr. Riding for his support on this project. I would like to thank John Bullock, Jason Cox, Greg Leckrone, Michael Lusher, for their assistance in this project.

I would like to thank to my teammates Daniel Galvez Moreno, Margarita Ley Hernandez, Alexandra Wehar, Piyush Lunkad, for their work put into this project, for everything they thought me and for treating me as a family member.

I would also like to thank my family buy especially to my parents Florentino Salinas and Maria Reyes for their support and encouragement. To my sister Neiba Salinas for her support. To my cousin Monico Solis and his wife Lydia Aguilar for their help in relocating to San Antonio. And my fiancé Arisbel Chapa for tolerating me, I Love you!

Finally, to CIES who provided with multiple equipment. And ACI-RE-CAST for their funding.

TABLE OF CONTENTS

Page

LIST OF ILLUSTRATIONS

Page

LIST OF TABLES

Page

NOMENCLATURE

Symbol	Description
ASTM	American society for testing materials
τ	Shear stress (Pa)
G	Shear modulus (Pa)
γ	Angle of deformation (Pa)
σ	Axial stress (Pa)
E	Young's modulus (Pa)
ε	Strain (-)
η	Coefficient of viscosity (Pa.s)
$\dot{\gamma}$	Shear rate (1/s)
τ_0	Yield stress (Pa)
ηs	Viscosity of the suspending medium (Pa.s)
φ	Volume fraction (-)
η_R	Relative viscosity (-)
φ_{max}	Maximum volume fraction (-)
$\tau_{surface}$	Surface friction (Pa)
τ_{oi}	Yield stress of the interface (Pa)

K	Consistency factor (-)
n	Consistency power index (-)
μ	Coefficient of viscosity (Pa.s)
c	Second order parameter ($Pa.s^2$)
$\propto$	Time-dependent parameter (s)
η_∞	Apparent viscosity at very high shear rate (Pa s)

1. INTRODUCTION

1.1. GENERAL

After water; concrete is the most widely used material in the world. Since human lives depend on this material (i.e. bridges, buildings), characterization to achieve adequate quality control is required. In the construction field, qualitative terms are used to describe the behavior of fresh concrete such as: workability, flowability, compactability, stability, finishability, pumpability, consistency, etc. However, these terms depend on the subjectivity of the technician/engineer [1]. Over time, quantitative empirical tests were developed to characterize the behavior of fresh concrete. For example, the slump test, using a plate and the Abrams cone classifies the behavior of concrete in a set of circumstances. However, an empirical test has the drawback that it is a "single point measurement". As a result, two different materials can give the same reading while having completely different behavior. Also, the measurement depends on the ability of the operator and can be easily influenced depending on the goal of the test.

In order to have a better understanding of the behavior of fresh cement-based materials, fundamental quantitative measurements were developed. The underlying science to study fundamentally the flow behavior of cement-based materials is rheology: the science of deformation of matter [2]. The device designed to measure the flow properties is called a rheometer [3]. Typically for cement-based materials, a rheometer measures the required torque to maintain a certain speed, after which the data are transformed into fundamental units. The use of rheological parameters in the world of concrete has been a powerful strategy to control and optimize the quality, cost and

performance of concrete mixtures. Additionally, interface rheology has helped with concrete pumping [4]. When a concrete mixture is pumped a layer rich in paste with lower rheological properties, also known as the "lubrication layer" is shown to exist [4]. The composition and properties of that lubrication layer can be better described by the science of interface of properties (also named tribology in the past). This layer requires extra attention since it is influential to the required pumping pressure [5], avoidance of blockages [6, 7] and concrete behavior inside a pipe [8].

1.2. SIGNIFICANCE

Pumping concrete is a technique that accelerates the construction process. It has been used in the United States since the early 1930s, allowing to move fresh concrete from point A to point B in a matter of seconds. Pumpability can be described as: "the ability of a mixture to be transported through a pipeline under pressure". Kaplan et al. show that pumpability is not an intrinsic quality of concrete but is a concept that involves all pumping parameters the concrete composition [8]. Increasing the pumpability of concrete is a strategy to find the equilibrium between flowability and stability [13]. Kaplan showed that a lubrication layer is formed inside the pipe with the use of a so-called tribometer [8]. This layer formed on the walls facilitates the flow of concrete as it contains less coarse particles and is richer in cement paste. As a result, the rheological properties are lower compared to the bulk concrete. If the lubrication layer cannot be adequately formed or maintained, a concrete blockage can occur which can potentially damage the equipment. Multiple studies have aimed to understand the flow inside a pipe using full scale equipment [5,10,11]. But describing what is happening inside of a pipe is

not an easy task since there are multiple factors playing a role (flow rate, pipe diameter, pumping position, material properties of concrete etc.). Not only is it necessary to understand the rheological properties of the concrete mixture, but if a lubrication layer is presumed to occur, the rheological properties of the lubrication layer need to be known. To be able to predict pumping behavior and to estimate rheological properties of the lubrication layer, the composition needs to be known. This is a topic of debate in literature. This work will attempt to reverse engineer the composition of the lubrication layer through the science of rheology.

Conventional vibrated concrete (CVC) has been pumped since early 1930s. However, self-consolidating concrete (SCC) has more sensitivity to changes induced by pumping. SCC is a highly flowable concrete where slump/slump flow measurements are higher compared to CVC. With the use of SCC, the construction process can be accelerated since less construction workers are necessary to consolidate the mixture. In addition, the risk of blockages is reduced.

In literature, several reports review mainly stability or mobility under pressure. Multiple studies have focused on understanding the difference between pumping regular CVC and SCC and the formation of the lubrication layer. However, relatively speaking, just a few projects focus on the entire set of parameters that deal with the entire picture: including the changes in fresh properties induced by pumping. However, this is important as the fresh properties which are of importance for the quality of the structure are those.

1.3. SCOPE OF WORK

Pumpability is a qualitative measurement that is hard to define. The overall objective of this research is to investigate the composition and formation of the lubrication layer that is presumed to occur inside the pipe and to determine the influence that pumping has concrete fresh properties. To do so, rheological properties of bulk concrete and lubrication layer are required. To achieve this, the composition of the lubrication layer was investigated by measuring the rheology of cement paste, mortar with four different maximum aggregate sizes, and concrete, and comparing the values to the output of the interface device mounted on the ICAR rheometer. To obtain the variation in rheological properties as a function of sand volume fractions for the mortars, Krieger-Dougherty types of equations were developed. A main obstacle encountered is that different rheometers give different results [9] and a direct comparison between them is not straightforward.

In this experimental research, a rheometer comparison was conducted between the ICAR, contec 5 (mortar and concrete configuration), contec 6 and Anton Paar MCR 302 rheometers, using a reference material at 3 different temperatures. Transformation equations between rheometers where obtained in a “2 step transformation”.

The influence of pumping was determined with full scale pumping experiments at a ready-mix plant. 16 mixtures were pumped and evaluated to investigate the influence of a different pumping parameters. The experiments used to evaluate the pumping influence were slump/slump flow, T50, fresh air content, sieve stability, segregation resistance and rheological and interface properties using the ICAR rheometer.

2. JUSTIFICATION, HYPOTHESIS AND OBJECTIVES

2.1. JUSTIFICATION

SCC is a type of concrete mixture that was developed in Japan during the 1980s due to the lack of skilled workers. However, in the United States, it has not taken over a large portion of the concrete market as it requires a stricter quality control. However, SCC is being used in complex projects.

Pumping is widely accepted as the easiest way to place concrete inside a formwork. Multiple studies aimed to avoid problems that can damage equipment and cause injuries, such as blockages, other studies were performed to identify the flow pattern of concrete in pipes, explaining the difference between pumping SCC and CVC. But not only material properties are playing a role, the influence of pumping parameters can make considerable changes in the concrete fresh properties. Typically, in the industry pumping parameters are changed without taking those changes into consideration (i.e. different boom configurations, use of reducers, pumping height, etc.) and every variable creates a different change in the behavior of fresh concrete that is not easy to estimate. Pumping is a procedure that induces high shear rates to the mixture, which is believed to disperse more cement particles. How this is going to affect the fresh properties of concrete? A better understanding of the influence of each parameter not only from the scientific point of view but from the technical aspect is required to estimate the changes. Adequate knowledge on this topic can avoid rejecting potential non-acceptable material after pumping.

2.2. HYPOTHESIS

The evaluation of pumping parameters including the formation and composition of the lubrication layer can be a powerful tool, if is well understood, to prevent negative changes in workability, durability and mechanical strength of flowable concrete. Another benefit is that minor adjustments in concrete composition can lead to lower pumping pressure required to mobilize concrete, which is translated as a financial benefit. It is believed that lowering pumping pressure and reducing the shear rate can minimize changes induced by pumping.

2.3. OBJECTIVES

Overall Objective. The overall objective is to analyze the effects of pumping parameters and to evaluate the changes induced to highly flowable concrete through empirical and fundamentals measurements. Therefore, an evaluation of the composition and thickness of the lubrication layer investigated on laboratory scale can be used as a tool to better understand the complexity of the pumping process. To achieve the goal of this research, the following detailed objectives are proposed:

Detailed Objectives. A first objective is to evaluate the effect of different pumping parameters, including flow rate, boom configuration, and the use of a reducer on the following concrete properties: slump or slump flow, T50 if applicable, fresh concrete air content, static stability (if applicable), rheological properties of bulk concrete, rheological properties of interface zone, and any potential interactions.

A second objective is to determine the composition of the lubrication layer by reverse engineering the thicknesses of different layers of paste, mortar with four different maximum aggregate sizes and concrete.

However, to perform this task, a comparison between the rheometers available at Missouri S&T had to be performed with a Bingham-like reference material. To estimate the rheological properties of mortars with different volume fractions of sand with different sizes, Krieger-Dougherty type relationships needed to be established as well.

3. LITERATURE REVIEW

3.1. SELF-CONSOLIDATING CONCRETE

Self-Consolidating Concrete, also known as Self-Compacting Concrete (SCC), was first developed in Japan in the 1980s. SCC is a concrete mixture that does not require external vibration. This concrete flows by its own weight and is at the same time sufficiently cohesive to fill the formwork entirely without segregation or bleeding [12]. In 1988, Dr. Okamura at Tokyo University [13] proposed the first concept of SCC to counter the lack of skilled workers. The SCC consistency was achieved by fixing the coarse and fine aggregates first, and then obtain self-compactability by adjusting the water-to-cementitious materials ratio (w/cm) and superplasticizer dosage. To ensure SCC consistency and stability, a low yield stress and relatively high viscosity are required. The superplasticizers are a powerful tool to reduce the yield stress without adding more water and the viscosity needs to be sufficiently high to avoid segregation. This is the reason why SCC typically has a low a w/cm ratio. An example of typical volumetric proportions are shown in Figure 3-1.

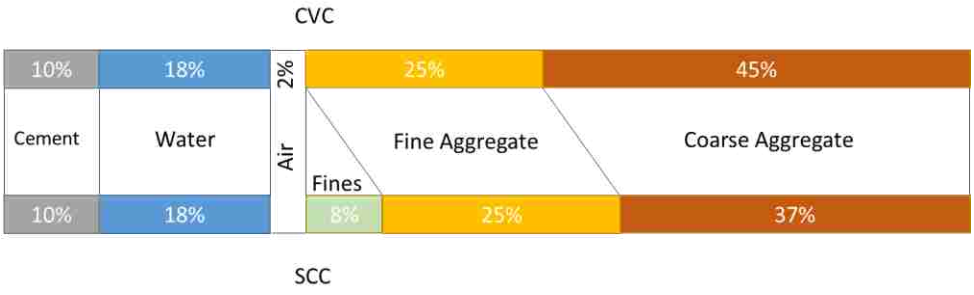

Figure 3-1 Example of materials used in CVC and SCC by volume. Adapted from [12].

The main disadvantage of SCC is the increased cost compared to CVC. However, it compensates its cost with the environmental benefits [12] (potential use of SCM, no vibration) and with the requirement of less construction workers and accelerated construction.

3.2. RHEOLOGY

Rheology is generally defined as "the science of deformation and flow of matter" [14]. In other words, it is that branch of physics that studies the interaction between force, deformation and time. Rheology is commonly used in the industry of paint, polymers, food (mayonnaise, ketchup, etc.), and others. It is also applicable for cement-based materials such as paste, mortar and concrete. With the implementation of more complex concrete types (anti-washout concrete, shotcrete, pumpable concrete, high-performance concrete with adapted rheology including SCC, etc.), rheology became a powerful tool to characterize its fresh behavior. [1] In this section, basic concepts of rheology are described including rheological models, rheometers (description, procedure and transformation equations), comparison between rheometers, and rheology of suspensions including the effect of volume fraction and viscosity amplification models.

3.2.1. Basic Relationships for Elastic Materials. Mechanical properties of concrete in hardened state are well known in the engineering and construction field. In the 17th century, Robert Hooke defined the relationship between stress and strain for solids. Hooke's law, as shown in equations 3-1 and, 3-2, is applicable for any material in the elastic range. Equation 3-1 identifies the shear modulus, as the proportionality factor between the angle of deformation and the shear stress. Equation 3-2 displays the well-

known Young's modulus, reflecting axial stress and strain. It should be noted that the shear modulus and Young's modulus can be functions of the angle of deformation or the strain. In this case, the materials are non-linear elastic (such as rubber, hardened concrete).

$$\tau = G \cdot \gamma \quad 3\text{-}1$$

$$\sigma = E \cdot \varepsilon \quad 3\text{-}2$$

Where: τ = Shear stress (Pa)

G = Shear modulus (Pa)

γ = Shear strain (-)

σ = Axial stress (Pa)

E = Young's modulus (Pa)

ε = Strain (-)

3.2.2. Basic Relationships for Fluid Materials. The following definitions were obtained from the Guide to rheological nomenclature from the National Institute of Standards and Technology "NIST" [15].

- Coefficient of viscosity or apparent viscosity: often abbreviated form as "viscosity" represents the ratio between the shear stress and shear rate. It can be easily visualized by the slope of the line connecting a point on the flow curve with the origin.
- Differential viscosity: the derivative of the shear stress with respect to shear rate.
- Plastic viscosity: when the material shows a Bingham behavior, the excess of the shear stress over the yield stress divided by the shear rate.

- Relative viscosity: Ratio of the viscosity in a suspension to the viscosity of the viscosity of the suspending medium.

3.2.2.1. Newtonian fluid.. In 1687, Isaac Newton defined the viscosity as "the resistance which arises from the lack of lubricity or slipperiness of the parts of a fluid is, other things being equal, proportional to the velocity with which the parts of the fluid are separated from one another" [16]. In rheological terms, the applied shear stress is proportional to the viscosity multiplied by the velocity gradient (shear rate) as shown in Equation 3-3

$$\tau = \eta \frac{dv}{dx} = \eta\dot{\gamma} \qquad 3\text{-}3$$

Where: τ = Shear stress (Pa)

$\dot{\gamma}$ = Shear rate (s^{-1})

$\frac{dv}{dx}$ = Velocity gradient (s^{-1})

η = Viscosity (Pa.s)

A fluid is Newtonian if it starts to flow as soon as stress is applied and if the relationship between stress and rate of deformation (i.e. the viscosity) is constant as shown in Figure 3-2 model 1. Examples of this kind of fluid include clear honey, oil, water, etc.

3.2.2.2. Non-newtonian fluids. A fluid is non-Newtonian if:

- Condition 1: the applied shear stress must overcome an initial resistance
- to start the flow. In other words, the material has to "yield" to start the flow. If the viscosity is constant after exceeding the yield stress, the fluid is a so-called Bingham material, as can be seen in Figure 3-2 model 5.

- Condition 2: if the relationship between stress and rate of deformation is not linear even if no yield stress is present (Figure 3-2 models 2 and 3). Model 2 has an increase in viscosity at higher shear rate that can be described by the power law model shown in Figure 3-2
- Condition 3: if the material shows time-dependent behavior.
- Combinations: Any combinations of different conditions above are also non-Newtonian materials.

3.2.2.3. Rheological models.. For Cement-based Materials. The rheological properties of cementitious materials are critical to concrete science. However different models can result in different values for a certain physical entity, even for the same measurement [17]. It is typically accepted that cement-based materials are Bingham materials [18, 19]. But several authors have indicated non-linear rheological behavior. In some cases, the material behaves has a shear-thickening fluid [20-21]. This can be attributed to low water/cement radio and to high shear rates applied. Yahia and Khayat observed shear-thinning behavior on high-performance concrete mixtures made with relatively low w/cm ratio (= 0.4), use of supplementary cementitious materials (SCMs) and rheology-modifying admixtures (RMAs) [22]. They also conclude that the Herschel-Bulkley model always results in the lowest value for yield stress compared to other models for shear-thinning materials, while for shear-thickening materials the highest yield stress value was systematically observed with Herschel-Bulkley. Since yield stress is obtained by extrapolating the curve to zero shear rate (impossible to measure), a fit

with an available model is required. One possible problem using the Herschel-Bulkley model, shown in Equation 3-4, is the determination of the yield stress.

$$\tau = \tau_0 + k\dot{\gamma}^n \quad 3\text{-}4$$

Where: τ = Shear stress (Pa)

$\dot{\gamma}$ = Shear rate (s-1)

τ_0 = Yield stress (Pa)

k = Consistency factor (-)

n = Consistency power index (-)

Mathematically, the value of the viscosity at zero shear rate is a concern for the Herschel-Bulkley model. The viscosity (slope of the rheogram) is a resistance to flow and for cement-based materials, most of the time, an initial stress is required to initiate the flow. If $n < 1$ in the Herschel-Bulkley model, the viscosity at zero shear rate is infinite. While if $n > 1$, the viscosity at zero shear rate is 0. The solution for this problem is to add a linear term (μ in Pa.s) to the model. Therefore, the modified Bingham model (Equation 3-5). Can provide a better description of rheological parameters [23].

$$\tau = \tau_0 + \mu\dot{\gamma} + c\dot{\gamma}^2 \quad 3\text{-}5$$

To obtain the rheological properties of a fluid, the use of a rheogram is required and the best fit to a rheological model is critical as shown in Table 3-1. Figure 3-2 shows the most common models, following the classification from ACI committee 238 [2].

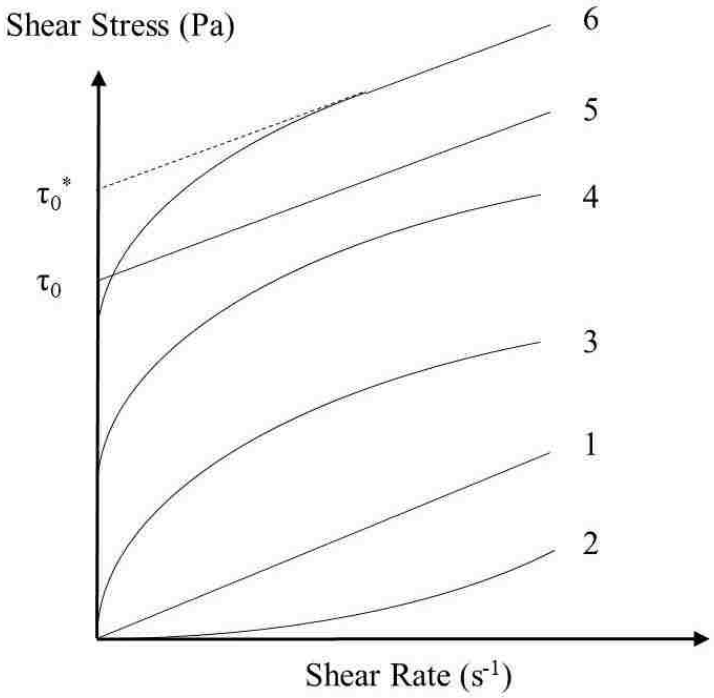

Figure 3-2 Identification of flow curves based on their characteristic shape. From ACI committee 238[68].

- Model 1 Newtonian: No shear stress required to initiate the flow, differential viscosity and apparent viscosity are independent of shear rate.
- Model 2 Shear-thickening power law: No shear stress required to initiate the flow, differential viscosity and coefficient of viscosity increase continuously with increasing shear rate.
- Model 3 Shear-thinning power law: No shear stress required to initiate the flow, differential viscosity and coefficient of viscosity decrease continuously with increasing shear rate.

- Model 4 Shear-thinning with yield response: shear stress required to initiate the flow, differential viscosity and coefficient of viscosity decrease continuously with increasing shear rate.
- Model 5 Ideal Bingham plastic: shear rate required to initiate the flow, differential viscosity is constant and is called plastic viscosity, while the coefficient of viscosity decreases continuously.
- Model 6 Non ideal Bingham plastic: Above the apparent yield stress, the coefficient of viscosity decreases continuously while the differential viscosity approaches a content value with increasing shear rate. Extrapolation of the curve from linear plastic region to the stress axis gives the apparent Bingham yield stress.

Table 3-1 Rheological models [68].

Rheological models for materials without yield stress	
Newton's Law	$\tau = \eta \frac{dv}{dx} = \eta\dot{\gamma}$
Power Law	$\tau = K\dot{\gamma}^n$
Rheological models for materials with Yield stress	
Bingham	$\tau = \tau_0 + \mu\dot{\gamma}$
Modified Bingham	$\tau = \tau_0 + \mu\dot{\gamma} + c\dot{\gamma}^2$
Herschel-Bulkley	$\tau = \tau_0 + K\dot{\gamma}^n$
Casson	$\tau = \tau_0 + \eta_\infty\dot{\gamma} + 2(\sqrt{\tau_0\eta_\infty})\sqrt{\dot{\gamma}}$

Table 3-1 Rheological models [68] (cont.).

De Kee	$\tau = \tau_0 + \mu\dot{\gamma}e^{-2\propto\dot{\gamma}}$
Yahia-Khayat	$\tau = \tau_0 + 2\ (\sqrt{\tau_o\eta_\infty})\ \sqrt{\dot{\gamma}e^{-2\propto\dot{\gamma}}}$

Where:

τ = Shear stress (Pa)

$\dot{\gamma}$ = Shear rate (s^{-1})

τ_0 = Yield stress (Pa)

K = Consistency factor (-)

n = Consistency power index (-)

μ = Coefficient of viscosity (Pa.s)

c = Second order parameter (Pa s^2)

$\propto$ = Time-dependent parameter (s)

η_∞ = Apparent viscosity at high shear rate (Pa)

3.2.3. Rheometers for Cement-Based Materials. This section describes the rheometers used for this research.

3.2.3.1. ICAR rheometer.. Description: The ICAR rheometer is, according to the manufacturer, a rugged portable instrument for measuring rheological properties of fresh concrete as shown in Figure 3-3. This instrument was developed at the International Center for Aggregate Research (ICAR).

3.2.3.2. Principle. This rheometer works under the principle of concentric cylinders for particles suspensions where the vaine representes an inner cylinder that rotates while the container stays stationary.

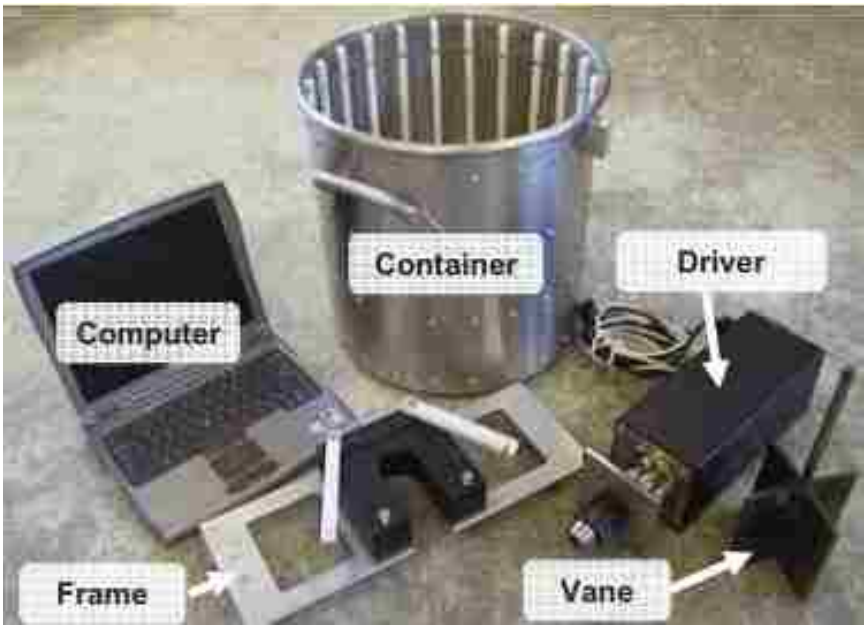

Figure 3-3 ICAR rheometer parts.

3.2.3.3. Measurement and experimental procedure. Shear is applied to concrete by the rotation of the inner cylinder, while the torque necessary to keep certain velocity is recorded. The measurements are performed by decreasing rotational velocities in a set of steps. Following the standard procedure of the software, a pre-shear time of 20 seconds occurs before the measurement starts to avoid errors due to thixotropy. A 7-step procedure is conducted where 80 points of torque are recorded in a duration of 5 seconds per step with 1.4 seconds omitted at start and 0.3 at the end of each step, as shown in Figure 3-4.

3.2.3.4. Data analysis and transformation equations. The average of torque measurements are obtained per step and from there the relationship between torque at each step and velocity (see equation 3-6) is determined. G is obtained by extrapolating

the linear equation and obtaining the intersection with the torque axis. H is obtained by determining the slope of the relationship between torque and velocity. See Figure 3-5.

$$T = G + HN \qquad 3\text{-}6$$

Where: T = Torque (Nm)

G = Intercept with the torque axis (Nm)

H = Slope of the relationship between torque and velocity (Nm.s)

N = Velocity (rps)

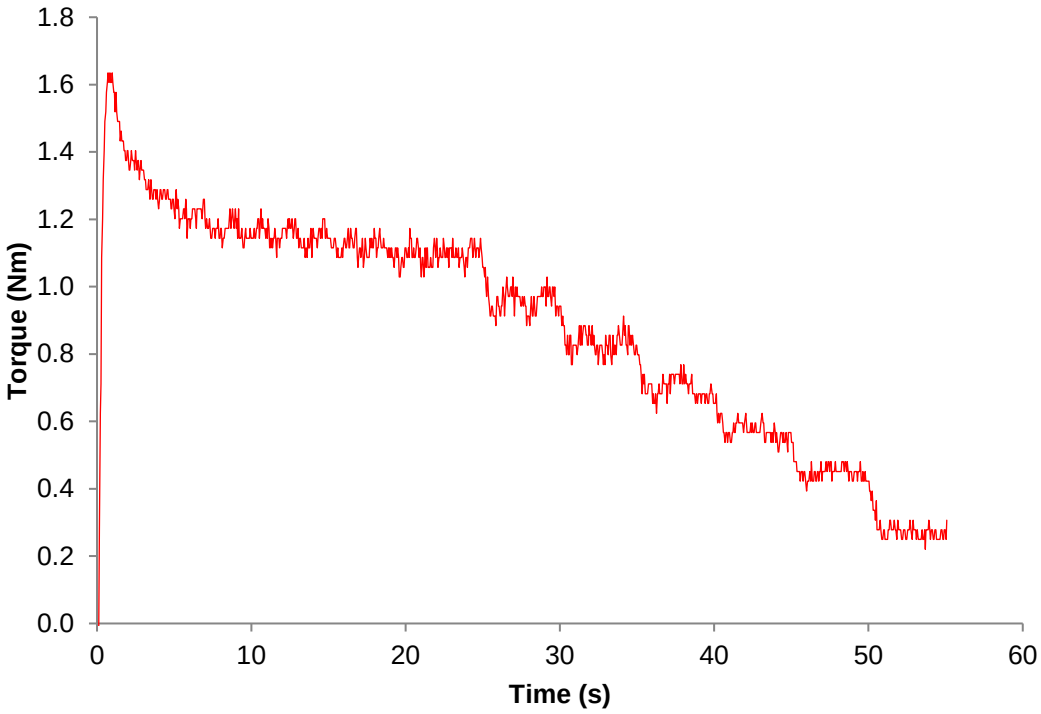

Figure 3-4 ICAR torque profile example.

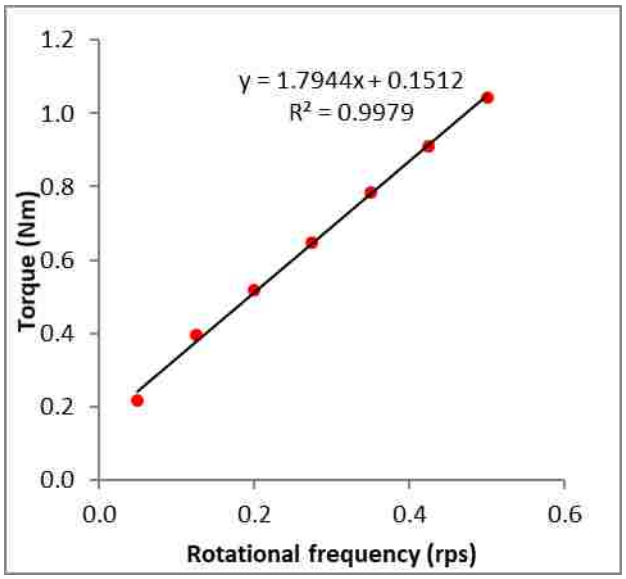

Figure 3-5 Torque vs velocity diagram.

The Reiner–Riwlin equations (see equation 3-11, further) are used to transform the relationship between torque and velocity into a relationship between shear stress and shear rate.

3.2.3.5. Contec viscometer 5. Description the Contec viscometer 5 is a non portable instrument (see Figure 3-6) for measuring the rheological properties of fresh mortar and concrete. The contec viscometer 5 has an inner cylinder divided in two parts. The upper part is used to measure torque and the lower part is used to eliminate the complex 3-D bottom flow. The system has two configurations. Further in this thesis referred as contec 5S which is used for mortar and contec 5W which is used for concrete:

- Contec 5S configuration: R_i = 65 mm and R_o = 82 mm
- Contec 5W configuration 2: R_i = 100 mm and R_o = 145 mm

3.2.3.6. Principle. This rheometer works under the principle of concentric cylinders for coarse particles suspensions where the ribbed vane representes a cylinder, which remains stationary, while the outer radius, composed by the bucket rotates. Both cylinders are equiped with vertical ribs that prevent the so-called “wall slip”.

Figure 3-6 ConTec 5 rheometer.

3.2.3.7. Measurement and experimental procedure. Shear is applied to concrete by the rotation of the outer cylinder. The measurements are performed by decreasing rotational velocities in a set of steps. As an example, Figure 3-7 shows a 10-step procedure where 50 points of torque are recorded in a duration of 5 seconds per step

with 1 second interval in between steps. A linear fit between torque and velocity was adapted as shown in Figure 3-8.

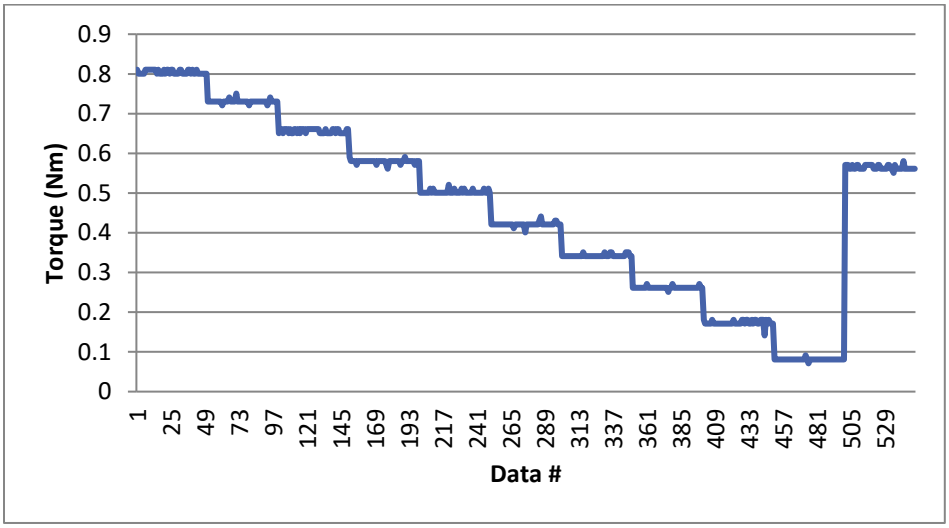

Figure 3-7 ConTec 5 velocity profile.

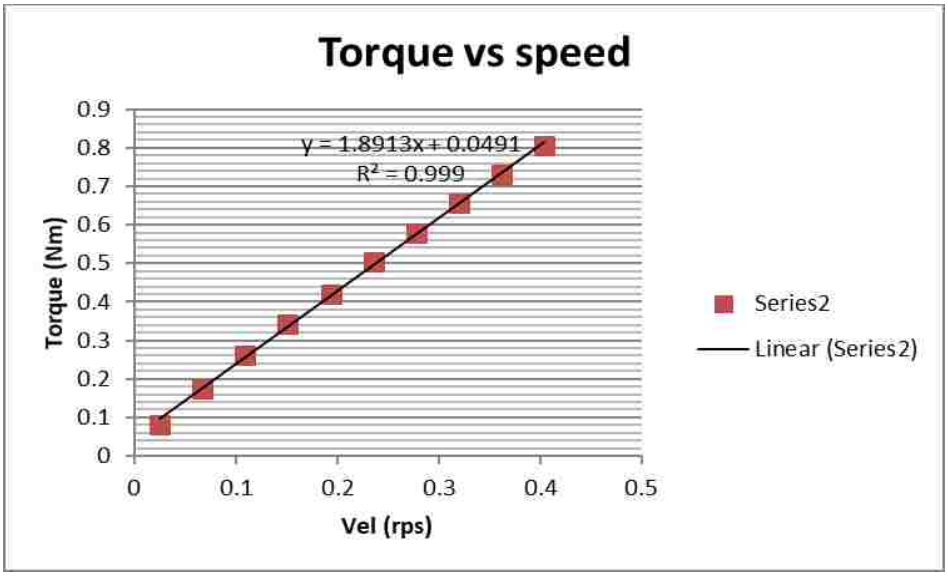

Figure 3-8 Torque vs speed measurement of the ConTec 5.

3.2.3.8. Data analysis and transformation equations. Similar procedure as the ICAR rheometer in 3.2.3.4 is followed.

3.2.3.9. Contec viscometer 6. The contec viscometer 6 (see Figure 3-9) is a smaller version of the contec viscometer 5 and suitable to measure the rheological properties of cement paste and mortar with a maximum particle diameter of 2 mm. It has only one configuration with R_o = 61.5 mm and R_i = 50 mm.

Figure 3-9 Contec 6 rheometer.

3.2.3.10. Anton Paar MCR 302 rheometer. The Anton Paar MCR 302 Rheometer (see Figure 3-10) is a non-portable temperature-controlled instrument for measuring rheological properties for all kind of materials.

3.2.3.11. Principle. This rheometer works based on the principle of concentric cylinders, although other geometries are available as well.

Figure 3-10 Anton Paar MCR 302 rheometer.

3.2.3.12. Measurement and experimental procedure. Shear is applied to cement paste by the rotation of the inner cylinder. The measurements can be performed by a linear decrease of rotational velocities or in a step wise procedure. The testing procedure in the Anton Paar rheometer is fully adjustable, in terms of shear rate range and profile. It is used in this thesis as a reference rheometer for the comparative tests, as the same pre-shear time and shear rate range of other rheometers can be imposed. Figure

3-11 shows an example of a linear procedure with 30 s of pre-shear time and data acquisition of 120 points of torque in a duration of 15 seconds. While Figure 3-12 shows the output.

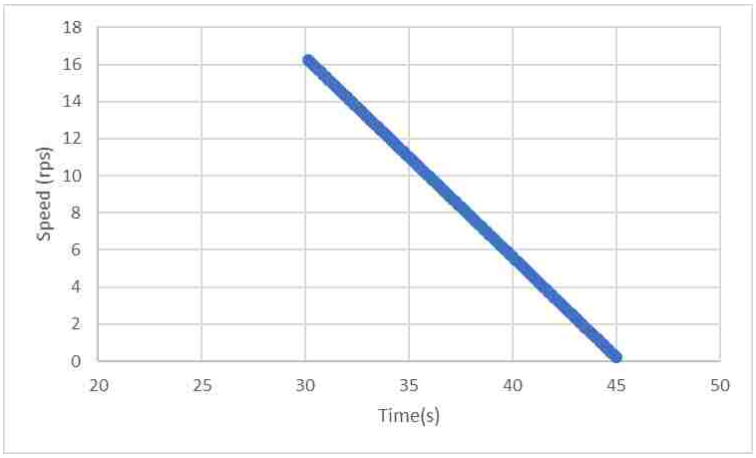

Figure 3-11 Anton Paar velocity profile.

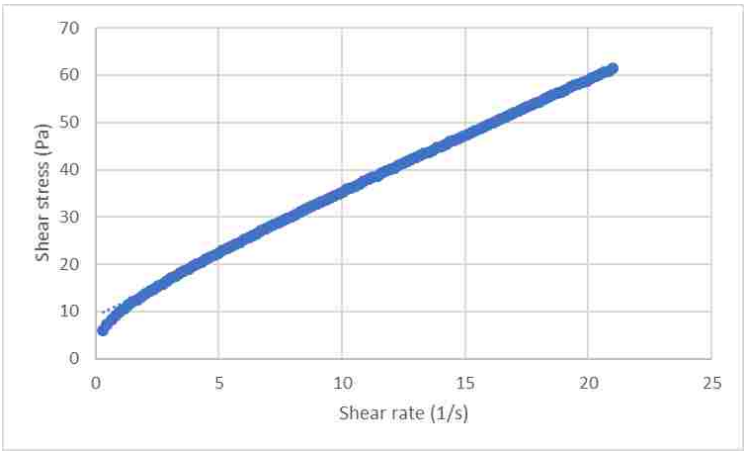

Figure 3-12 Anton Paar flow curve.

3.2.3.13. Data analysis and transformation equations. The Anton Paar software delivers directly fundamental units. After verification of their correctness, there is no need to transform torque measurements to fundamental units. The shear stress is obtained at every shear rate for each data point. In case of Bingham model, the yield stress is obtained by the extrapolation of the flow curve and intersection with the shear stress axis. Plastic viscosity is obtained by determining the slope of the flow curve.

3.2.3.14. Comparison of rheometers. Do all rheometers measure the same properties? They measure the same properties but deliver different values. The principle is the same for all rheometers: the required torque to maintain a certain speed is determined. However due to design and sensitivity factors the torque values differ from one rheometer to another.

3.2.3.15. Background. Two rheometer comparison campaigns have been done, in the beginning of the 2000s. In 2000 in Nantes, France, 5 rheometers were compared, and 12 concrete mixes were tested with slump values ranging from 90 mm to 235 mm, utilizing two types of coarse aggregate [9]. However, since SCC was becoming more and more popular, in 2003 in Cleveland, USA they decided to do another comparison in which 4 rheometers were tested. 17 concrete mixtures and five mortars were tested with a range of slump values from 121 mm to 248 mm, keeping the coarse aggregate type constant [24]. The rheometers compared were the contec BML Viscometer 3, the BTRHEOM rheometer, the IBB rheometer, the two-point workability rheometer, and the CEMAGREF-IMG rheometer.

Results from empirical measurements (slump, slump flow) show correlations with the rheological measurements as shown in Figure 3-13. As the slump/slump flow increases, the yield stress decreases.

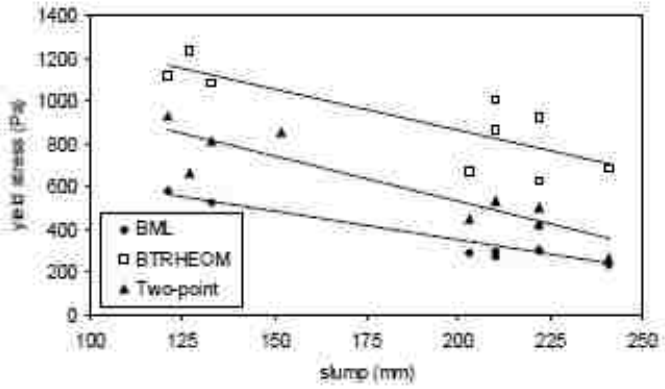

Figure 3-13 Yield stress (Pa) vs slump/slump flow (mm) [9].

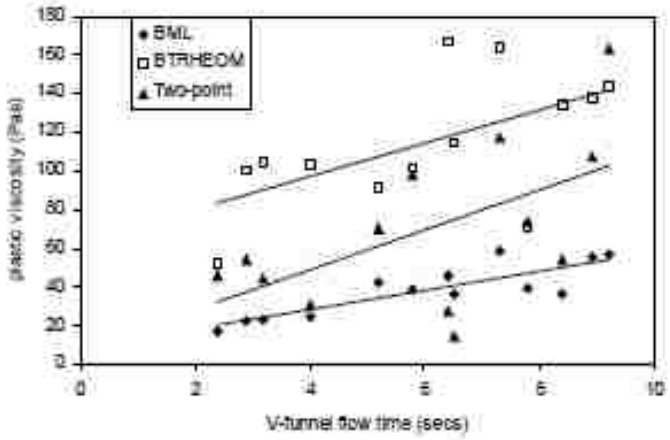

Figure 3-14 Plastic viscosity (Pa*s) vs V-funnel flow time (s) [9].

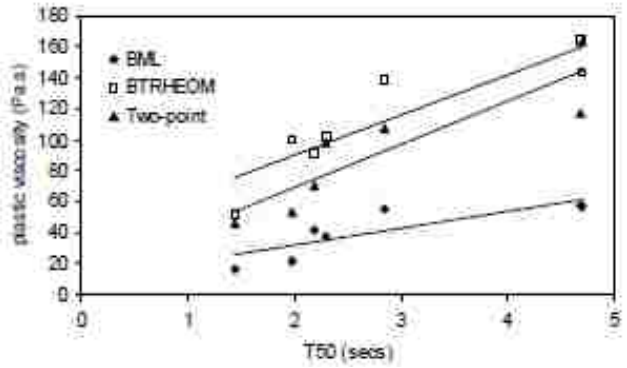

Figure 3-15 Plastic viscosity (Pa*s) vs T50 (s) [9].

Other empirical tests such as V-funnel flow time and T50 were compared with rheological parameters. However, a poor correlation between yield stress and V- funnel and T50 were shown, and a high correlation between V-funnel and T50 and plastic viscosity was observed as shown in Figure 3-14, Figure 3-15.

Regardless of the rheometer used, all rheometers show a similar trend for yield stress (Pa, Nm.s), as shown in Figure 3-16 and Figure 3-17.

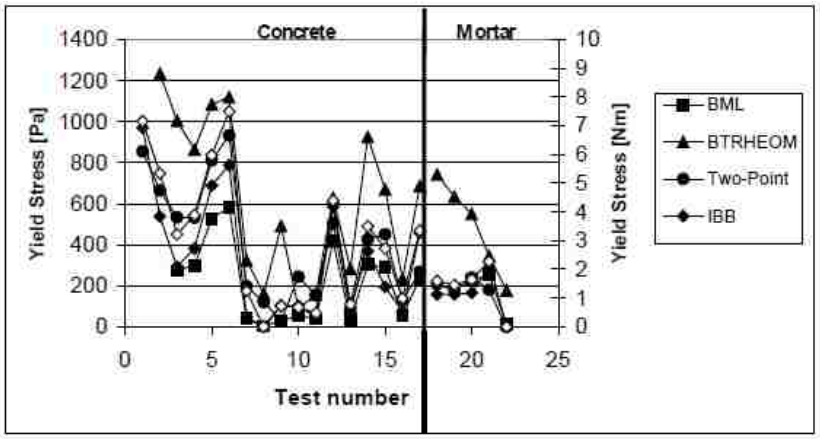

Figure 3-16 Yield stress vs test # [9].

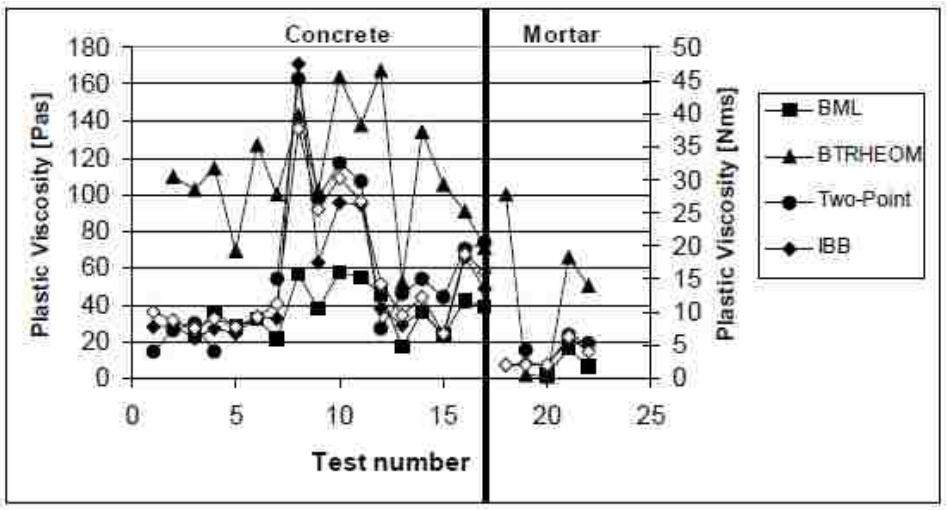

Figure 3-17 Plastic viscosity vs test # [9].

For this pumping research project, an initial attempt was made to determine the composition and thickness of the lubrication layer through rheology tests on paste, micro-mortar, mortar and concrete, all with different maximum packing density and maximum particle size. The test results in Table 3-2 show discrepancies between rheological properties measured with two different rheometers on the same materials (similar to the results described in the literature review). This has led to the incapacity of being able to predict lubrication layer composition and properties. Therefore, in the following sections (5 and 6), two solution strategies are described to overcome this issue. section 5 shows the comparison of all used rheometers employing a reproduction of the NIST reference fluid for cement paste. And section 6 shows the establishment of master curves for mortars with different particle sizes and volume fractions.

Table 3-2 First lubrication layer attempt, showing discrepancies between the measured rheological properties of the same materials in different rheometers.

Mixture	ConTec 5		ConTec 6		Anton Paar	
	Yield stress (Pa)	Plastic Viscosity (Pa s)	Yield stress (Pa)	Plastic Viscosity (Pa s)	Yield stress (Pa)	Plastic Viscosity (Pa s)
Pass 1/2"	188.1	22.2				
Pass 3/8"	234.9	18.5				
Pass No. 4*	286.5	6.2	365.7	5.3		
Pass No. 4			443.3	2.1		
Pass No. 16			348.0	0.6		
Pass No. 50			58.1	1.1	14.4	1.0
Pass No. 200*					15.7	1.1

3.2.3.16. Challenges in assessing rheological properties. Rheological measurements represent the following challenges:

- Errors due to too large particles: Cement-based materials, such as concrete and even mortar are materials that have large solid particles (i.e., aggregates), and they must have enough space to flow. To avoid blockage in the rheometer, a gap of 10 times the size of the Maximum Aggregate Size (MAS) its recommended [17], although many commercial concrete rheometers suggest a factor 3 or 4. Too large particles for the gap of the rheometer will result in large fluctuations in torque values, potential blocking of the rheometer.
- Wrong selection of rheological model: As discussed before, different models result in different values and an inadequate selection of a model can lead to a different interpretation of properties, mostly for the yield stress. In order to conduct a valid experimental program, the same model must be used for all tests.
- Errors due to time-dependent-behavior: Viscosity changes in cement-based materials can be non-time-dependent (i.e. shear thinning, shear thickening behavior), or time

dependent. In case the time-dependent changes in viscosity are reversible, the effect is defined as thixotropy. Non-reversible changes in viscosity with time are also possible. “Thixotropy is a reversible, isothermal, time-dependent decrease in viscosity when a fluid is subjected to increased shear stress or shear rate, and a gradual recovery of that said viscosity when shear rate is removed” [25].

- Mechanisms for thixotropy is caused by two aspects: flocculation and hydration [27] When a concrete mixture is at rest, cement particles flocculate with time. This flocculated structure increases the viscosity and is the result of Van der Waals attraction and Brownian motion, and, at longer term, hydration bridges [27]. The opposite phenomenon happens when a flocculated concrete mixture is subjected to shear forces. The flocs can break down [19] and viscosity can decrease. Concrete admixtures are typically used to reach desired concrete behavior. However, as a side effect, the thixotropy can be increased or decreased as shown in Table 3-3.

Errors due to thixotropic behavior and structural breakdown can play a role in the assessment of rheological properties [25]. Wallevik et al. recommended the following steps to minimize error due to thixotropy:

- Pre-shearing the sample at the highest shear presented on the test.
- Measuring right after the pre-shear period
- Plot torque vs steps and verify that equilibrium is reached.
- Use of retarders

Table 3-3 Summary of parameters influencing thixotropy from ACI 238.2T-14.

Parameter	Effect on thixotropy
HRWR	Decrease
VMA	Increase
Accelerator	Increase
Retarder	Decrease
SCM	Increase
w/p increase	Decrease
Temperature increase	Increase

The time duration of the pre-shear is critical as an excessive pre-shear can enhance undesired effects such has workability loss or particle migration [28].

Plug flow Based on the Cauchy stress principle [29] the stress for a cylinder can be calculated at a distance "r" as shown in Equation 3-7

$$\tau = \frac{T}{2\pi r^2 h} \qquad 3\text{-}7$$

One common procedure to transform torque-velocity measurements to fundamental units is the Reiner-Riwlin equation.

$$\tau_0 = \frac{\left(\frac{1}{Ri^2} - \frac{1}{R_0^2}\right)}{4\pi h \ln\left(\frac{R_0}{R_i}\right)} G \qquad \mu = \frac{\left(\frac{1}{Ri^2} - \frac{1}{R_0^2}\right)}{8\pi^2 h} H \qquad 3\text{-}8$$

For coaxial cylinder rheometers, as the radius increases, the applied stress decreases and at some point, it is possible that the shear stress becomes lower than the

yield stress of the material. If that happens the, material will not be sheared entirely, and the Reiner-Riwlin equations need to be re-evaluated.

If R_p is defined as "the distance at which applied shear stress equals the yield stress", R_s is term utilized to determine the outer boundary of the flow domain. [28] If: $R_p < R_o$, not all material is being sheared (i.e., high yield stress material); then $R_s = R_p$. If $R_p > R_o$, all material is being sheared; $R_s = R_o$, as shown in Figure 3-18.

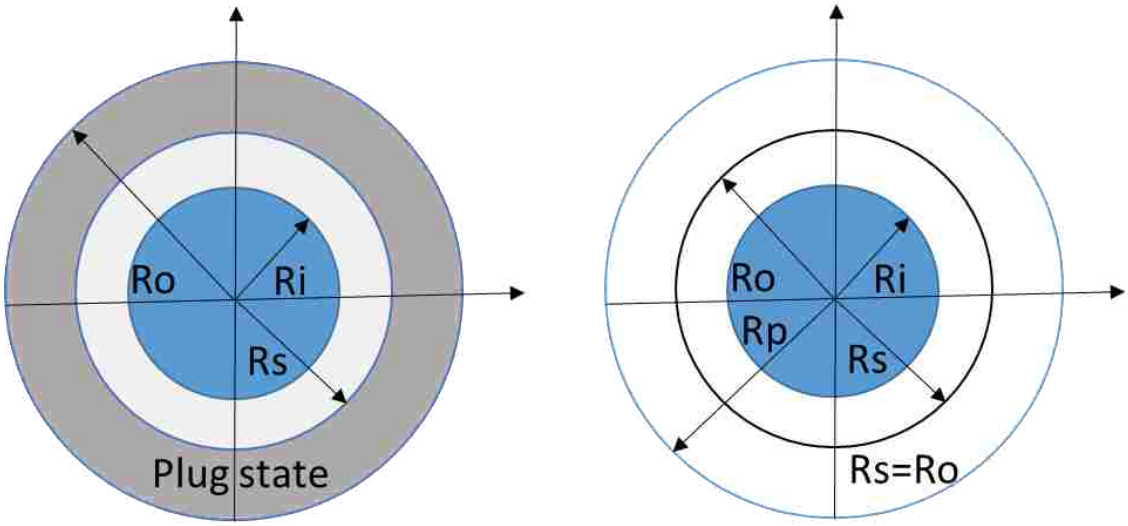

Figure 3-18 Types of flow presented inside coaxial cylinders [17].

In the case only a part of the gap is being sheared (Figure 3-18 (left)), the Reiner-Riwlin equations, with R_o being replaced by R_s are still valid, but R_s depends on an unknown yield stress value and the applied torque. To obtain the rheological properties, plug radius, yield stress and viscosity are adjusted in an iterative procedure.

3.2.4. Rheology of Suspensions. A suspension is a mixture of solid particles in a liquid medium. Concrete and mortar are considered suspensions since they are a mixture of solid particles in a liquid medium (i.e. aggregates in paste) which at the same time complicates the measurements of rheology due to the large range of particle sizes [30]. This section discusses some of the critical concepts necessary to understand the influence of particles and particle concentration on the rheological properties of cement-based materials.

- Packing density."Particle packing describes at what degree a unit volume is filled with particles, which is defined as the ratio of the solid volumes of particles to the entire volume of the suspension" [31]

$$\varphi = \frac{V_p}{V_b} \qquad 3\text{-}9$$

Where: φ = Particle packing density (-)

V_p = Solid volume of particles (cm^3)

V_b = Volume occupied by the suspension (cm^3)

Usually, maximum packing density of aggregates has a value of 0.50-0.70 [32,33] thus. Paste is required not only to fill the voids but to lubricate particles, decreasing interparticle friction.

Einstein [34] defined the relationship between the viscosity of a suspension and that of the suspending medium and the volume fraction, as follows: "the coefficient of internal friction increases by a fraction that is equal to the total volume of the spheres suspended in the unit volume" This can be translated to a simple equation 3-10.

$$\eta = \eta_s(1 + \varphi) \qquad 3\text{-}10$$

Where: η = Viscosity of the suspension (Pas)

η_s = Viscosity of the suspending medium (Pas)

φ = Volume fraction (-)

However, after an external review done by Mr. Hopf, a mathematical error was found [35]. As a result, the corrected formula is affected 2.5 times more by the total volume.

$$\eta = \eta_s(1 + 2.5\varphi) \quad 3\text{-}11$$

But Einstein's formula was limited to dilute systems($\varphi < .10$). Batchelor and Green [36] added a third term to the formula considering the interactions between distortions in the fluid field caused by neighboring particles (order φ^2) [36].

$$\eta = \eta_s(1 + 2.5\varphi + 7.6\varphi^2) \quad 3\text{-}12$$

As the volume fraction of particles increases more, the interaction between them becomes challenging. Two new terms were introduced: maximum volume fraction represents the maximum packing density which ranges from 0.64 (random close packing) to 0.74 (hexagonal close packing) for uniform spheres [37]. So and so, [38] have shown there is a critical value of volume fraction where particle concentrations reaches a transition from a suspension to granular material (0.55-0.62). Intrinsic viscosity; which has a value of 2.5 if spheres are used in the suspension [39]. But, a different value is expected for cement-based materials. The most popular equation to describe the viscosity amplification with the increase of particles in suspensions for high concentration of particles is the Krieger-Dougherty equation (Eq. 3-13)

$$\eta_R = \left(1 - \frac{\varphi}{\varphi_{max}}\right)^{-[\eta]\cdot\varphi_{max}} \quad 3\text{-}13$$

Where:

η_R= Relative viscosity (-)

φ = Volume fraction (-)

φ_{max}= Maximum volume fraction (-)

$[\eta]$= Intrinsic viscosity (Pa. s)

3.3. PUMPING CHARACTERIZATION

Rheology is used to quantify the fresh properties of concrete using fundamental quantitative units. For the pumping process, rheological properties are a powerful tool to predict how much pressure would be needed to make the concrete flow at a certain flow rate. But not only the rheological properties of bulk concrete are relevant, the rheological properties of the lubrication layer are as well, or even more, and for that, the interface properties are the key.

The following sections discuss different aspects of pumping concrete, including major flow behavior inside a pipe, type of flow presented, importance of stability, formation of the lubrication layer, the main factors affecting the lubrication layer and prediction of the pumping pressure. Major flow behavior in pipes depends on the type of flow:

3.3.1. Plug Flow. Concrete flows as a solid material separated from the pipeline by a layer with lower rheological properties (the lubrication layer). The portion that is in plug is called “bulk concrete”.

3.3.2. Degree of Saturation. The resistance to flow of concrete in a pipe depends on the shearing of the lubrication layer and the friction of the solid particles with the wall. This friction depends on how saturated the concrete mixture is. Two types of flow could occur:

- Hydraulic flow: When concrete is in a saturated state, there is enough paste to lubricate the aggregates and the magnitude of friction is negligible. As a result, the pressure evolution in the pipeline is linear as shown in Figure 3-19.

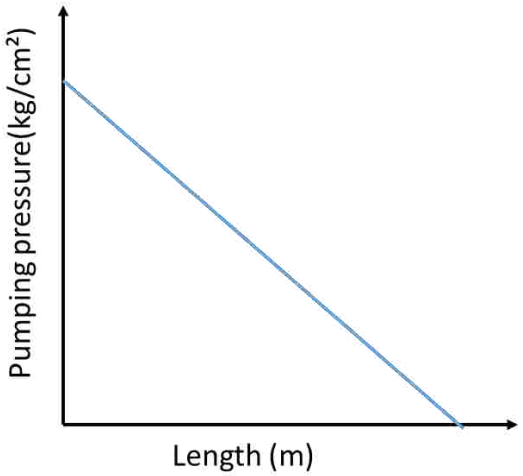

Figure 3-19 Saturated flow pressure loss from Browne and Bamforth [4].

- Frictional flow: When a concrete mixture is unsaturated, there is not enough paste to lubricate aggregates and frictional resistance increases dramatically. As a result of frictional flow the pressure loss in the pipeline is not linear as shown in Figure 3-20.

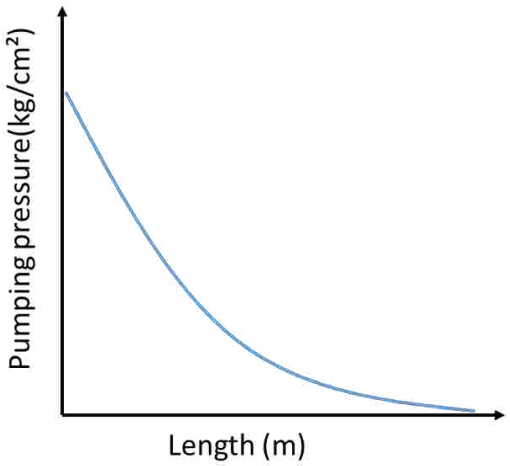

Figure 3-20 Frictional flow pressure loss from Browne and Bamforth [4].

3.3.3. Stability Under Pressure. A concrete mixture that is pumped must remain homogenous in the direction of the flow. If heterogeneity of the concrete is induced inside the pipeline a blockage can occur which can potentially damage the equipment. Blockages may be caused by the separation of water from a concrete mixture caused by a high permeability as shown Figure 3-21.

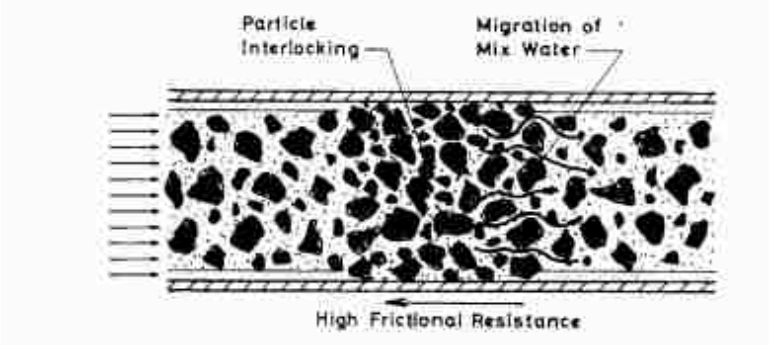

Figure 3-21 Cause of blockage inside a pipe from Browne and Bamforth [4].

As mentioned in 3.3.2 to have low resistance to flow, the concrete must be saturated to reduce the risk of blockages. However, this is not the only parameter playing a role whether a blockage will occur. Saturated concrete with high permeability can become unsaturated due to water separating from the mixture in the direction of the flow in a short amount of time. Browne & Bamforth [4] developed a pumpability diagram that serves as a practical guide to evaluate whether concrete can be pumped without risking blockages (Figure 3-22), based on two empirical tests: the slump test and the pressurized bleeding test.

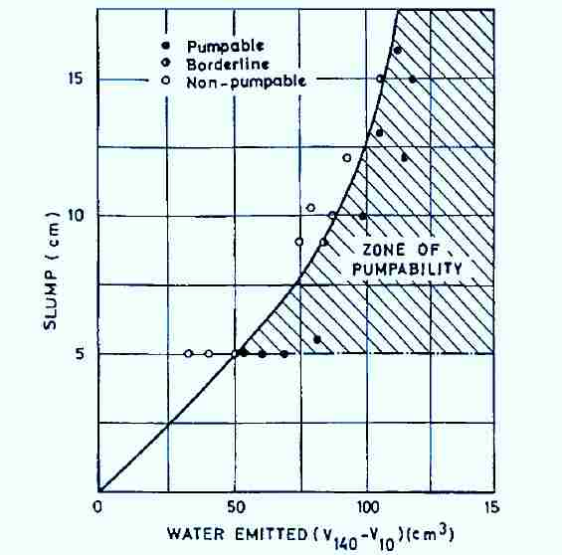

Figure 3-22 Pumpability diagram Browne and Bamforth [4].

- Effect of w/cm**.** As explained in 3.3.2 concrete can be saturated or unsaturated, depending on the w/c ratio. The degree of saturation depends on the w/cm ratio. For concrete mixtures in saturated state, the flow resistance can be represented with equation 3-14.

$$R = A + KV^n \qquad 3\text{-}14$$

Where:

A = Adhesion resistance (kg/cm^2)

K = Constant related to concrete velocity. (-)

V = Factor related to velocity(kg/cm^2)

n = Constant related to concrete velocity(-)

While for concrete mixtures in unsaturated state (0.40 < w/c in Figure 3-23) the flow resistance can be represented with equation 3-15

$$R = A + \mu P_r \qquad 3\text{-}15$$

Where:

A = Adhesion resistance (kg/cm^2)

μ = Coefficient of friction between the concrete and the pipe wall. (-)

P_r = Radial pressure (kg/cm^2)

n = Constant related to concrete velocity (-)

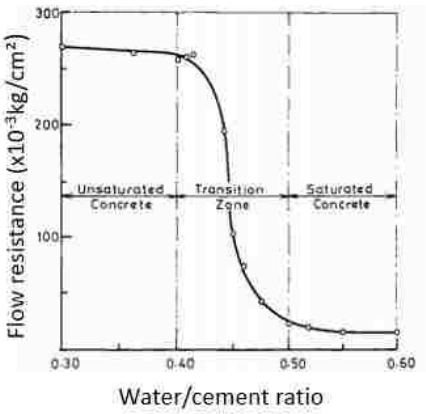

Figure 3-23 Effect of water to cement ratio on flow resistance from Browne and Bamforth [4].

3.3.4. Lubrication Layer. A layer with less volume fraction is presumed to occur during pumping.

3.3.4.1. Principle of lubrication layer. Kaplan in the early 2000s and Chapdelaine in 2006 were the first researchers to combine rheology and interface rheology to fully understand the flow behavior of concrete through a pipe. The properties of the lubrication layer (LL) can be characterized with an interface rheometer (also called a tribometer) and the properties are typically expressed by equation 3-16.

$$\tau_{surface} = \tau_{oi} + \eta_i v \qquad 3\text{-}16$$

Where:

$\tau_{surface}$ = Surface stress (Pa)

τ_{oi} = Yield stress of the LL (Pa)

η_i = Viscous constant of the LL (Pas/m)

v = Angular velocity of the LL (m/s)

By combining rheological and interfacial properties Kaplan developed a bilinear model relating pumping pressure loss vs discharge flow as shown in Figure 3-24 and Figure 3-25. As the name says, this model is divided in two parts:

- Part 1 is purely attributed to the interface properties of the lubrication layer. The shear stress induced by the pressure loss is insufficient to overcome the yield stress of the concrete. As such, no shearing occurs in the bulk concrete. Generally, this part is formed at low velocities, and concrete moves as a plug. Equation 3-17 expresses the shear stress at the wall, and equation 3-18 predicts pressure in this zone of the graph.

- Part 2 requires the interface properties of the lubrication layer and the flow properties of the concrete. There is a zone where the concrete is being sheared and that affects the flow rate. Generally, this part is formed at high velocities, the velocity is high enough that the applied shear stress closer to the central portion exceeds the yield stress initiating a viscous flow. A plug zone in the center of the pipe still forms but is reduced in diameter. Pressure prediction in this case is shown in equation 3-19.

$$\tau_w = \frac{\Delta_{ptotal}}{L} \cdot \frac{R}{2} = \Delta_p \cdot \frac{R}{2} \quad (3\text{-}17)$$

$$\Delta_p = \frac{2L}{R}\left(\frac{Q}{3600\pi R^2 k_r}\eta_{LL} + \tau_{o_{LL}}\right) \quad (3\text{-}18)$$

$$\Delta_{ptotal} = \frac{2L}{R}\left(\frac{\frac{Q}{3600\pi R^2 k_r} - \frac{R}{4\mu_p}\tau_{o_{LL}} + \frac{R}{3mu_p}\tau_o}{1 + \frac{R}{4\mu_p}\eta_{LL}}\eta_{LL} + \tau_{o_{LL}}\right) \quad (3\text{-}19)$$

Where:

τ_W = Shear stress at the wall (Pa)

τ_o = Concrete yield stress (Pa)

Δ_p = Pressure loss per meter (Pa/m)

Δ_{ptotal} = Pressure loss on the entire pipeline (Pa)

L = Length of the pipeline (m)

R = Radius of the pipeline (m)

η_{LL} = Viscous constant of the lubrication layer (Pa.s/m)

μ_p = Viscosity of concrete (Pa.s)

$\tau_{o_{LL}}$ = Yield stress of the lubrication layer (Pa)

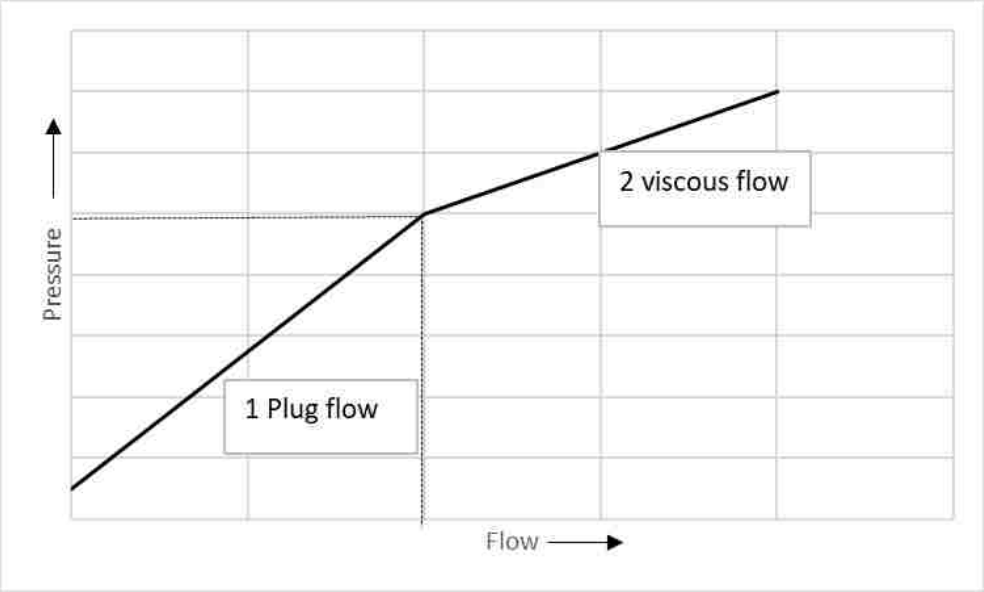

Figure 3-24 Kaplan's model Schematic representation of flow for the proposed bilinear model.

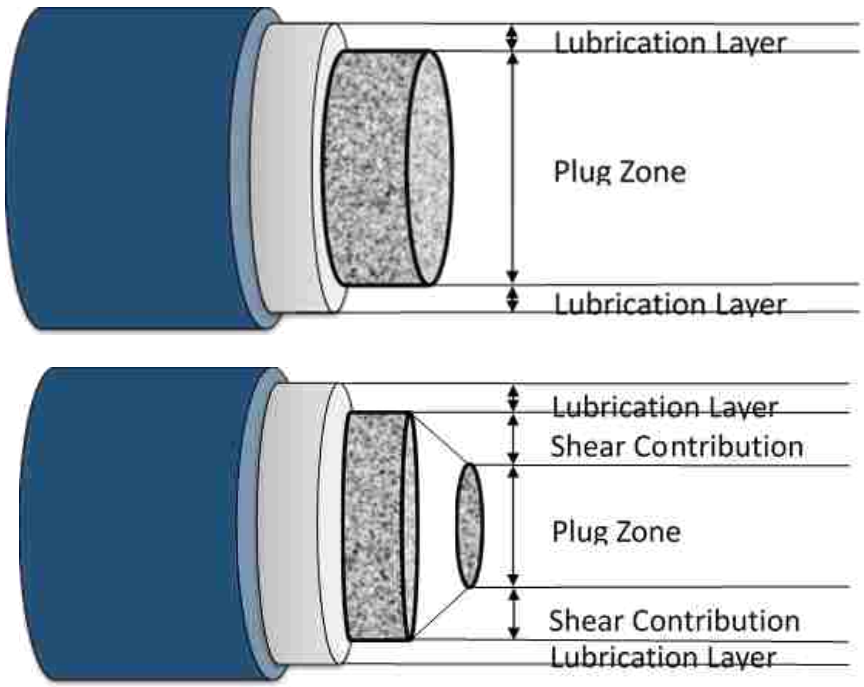

Figure 3-25 Schematic representation of the flow proposed by Kaplan part 1(above) and part 2 (below).

3.3.4.2. Formation of the lubrication layer. Several mechanisms for the formation of the lubrication layer are reported in literature [7, 40, 41]. The following mechanisms are expected to contribute to the formation of the lubrication layer:

- Wall effect: The concentration of particles tends to be lower close to the wall without external force applied on this system [42, 41]. This is applicable to the (coarse) aggregates in case of concrete, where the particle concentration is lower in the vicinity of the wall. The exclusion of particles close to the wall facilitates the formation of the lubrication layer. It is assumed that at a distance above the diameter/2 of particles, this effect does not play a role anymore, as shown in Figure 3-26(Left).

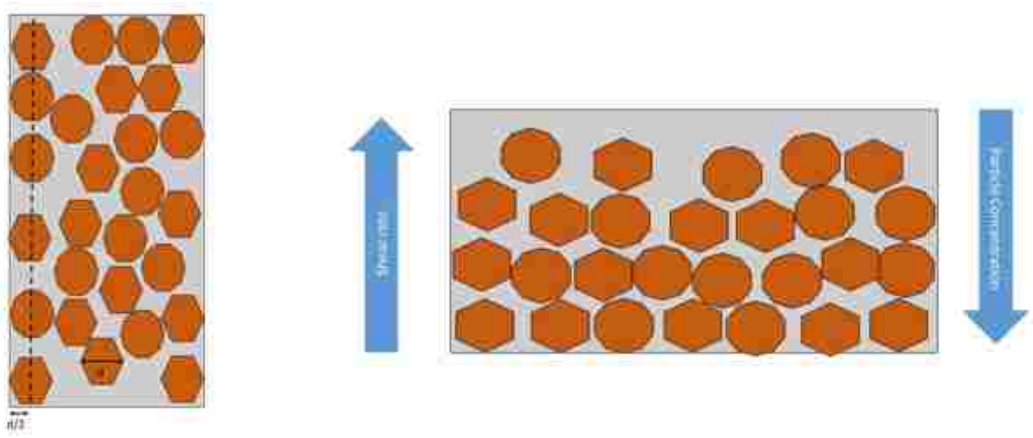

Figure 3-26 Schematic representation of wall effect (left) and particle migration (right) from Seung Hee Kwon [47].

- Shear induced particle migration: The particle concentration tends to be lower close to the wall due to the application of an external force [41, 43] (i.e. pumping) because particles migrate from a zone of high shear rate (pipe wall) to a zone with low shear

rate (center of the pipe). This leads to a heterogeneous mixture in the radial direction, as shown in Figure 3-26(right).

This phenomenon is more noted in concrete than in mortar. It is believed that increasing the coarse aggregates and the yield stress/viscosity ratio enhances the effect of particle migration [44]. This is the same phenomenon which also can lead to a wrong interpretation of rheological properties [17].

3.3.4.3. Measuring lubrication layer. Secrieru et al. [5]. performed a study that quantifies changes in rheology and the formation of the lubrication layer during pumping [5]. In this study, the portable high-pressure filter press (PHPFP) shown in Figure 3-27 was used as an indication of stability of concrete and also to estimate the thickness of the lubrication layer.

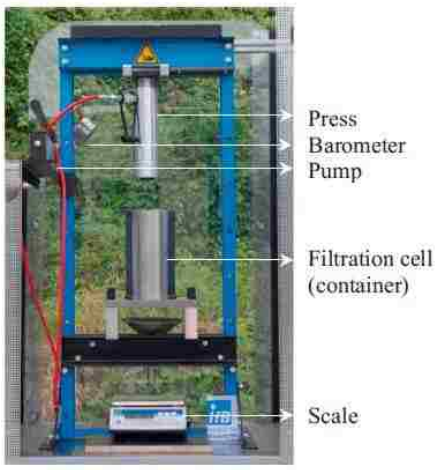

Figure 3-27 Portable high-pressure filter press. (PHPFP) [5].

According to the model shown in Figure 3-28, under similar pumping pressures (maximum 100 bar) the rheologically effective water, which is the free water that helps

concrete flow and is not required for chemical hydration or intrinsically volume, is expected to be pressed out.

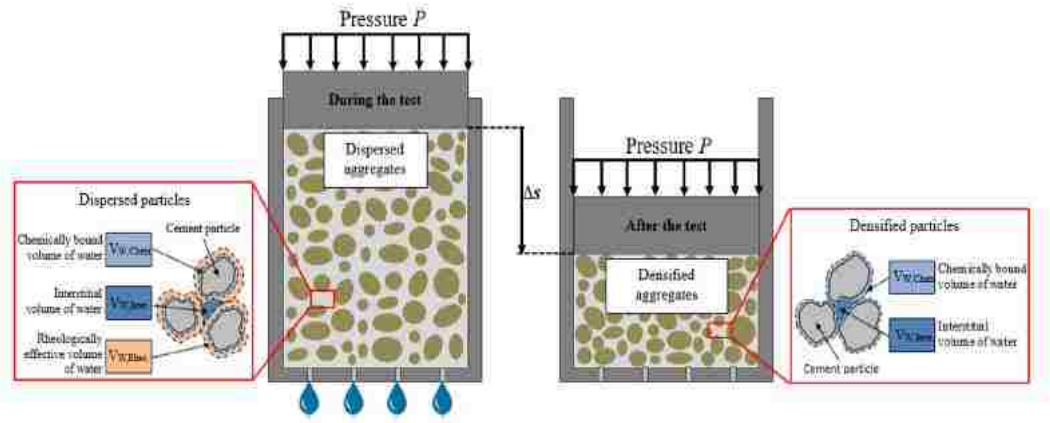

Figure 3-28 Schematic representation of filtrate extraction from concrete sample. From [5].

According to Secrieru, the entire amount of rheologically effective water is interpreted to be available for the formation of the lubrication layer. With that assumption, the relative amount of paste required to build the lubrication layer of thickness "e" can be calculated using:

$$V_{paste} = \pi[R^2 - (R - e)^2]L \qquad 3\text{-}20$$

Where:

V_{paste} = Volume of paste (m^3)

R = Pipe radius (m)

L = Length of pipeline (m)

e = Thickness of the LL (mm)

3.3.5. Prediction of Pumping Pressure. Based on the technique developed by Secrieru[5], the total amount of filtrate pressed out is related to the formation of the lubrication layer. Based on Kaplan's equations, lubrication layer properties are related to the pumping pressure. Since the volume of material available for the formation of the lubrication layer is known from the PHPFP, the theoretical thickness of the lubrication layer can be calculated. This thickness is close to what Chapdelaine observed: 1 mm [45]. This calculation makes sense since mixtures with thicker lubrication layers require less pressure to be mobilized as shown Figure 3-29.

	Mixture								
e(mm)	Gravel	M2A	M2B	M2C	M5A	M5B	M10A	M10B	SCC
BEFORE	1.31	1.65	1.48	1.91	2.15	1.74	1.13	1.18	0.85
AFTER	1.43	1.61	1.48	1.61	1.82	1.59	1.14	1.18	0.95

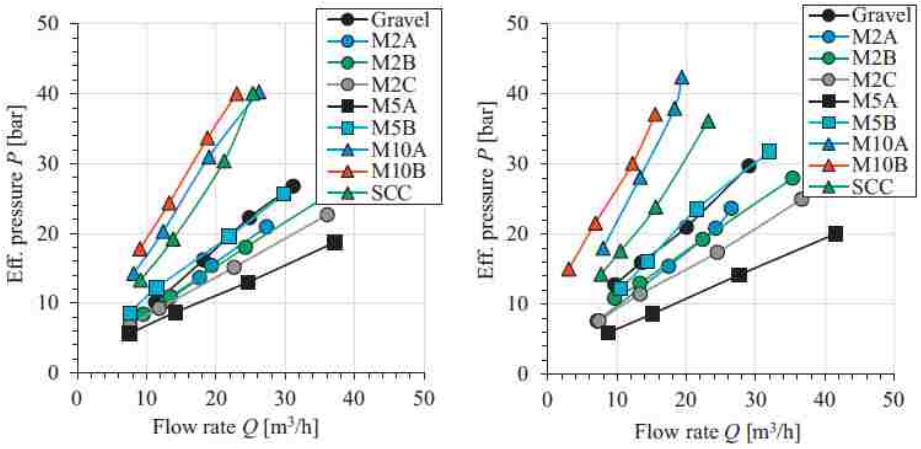

Figure 3-29 P-Q curves left at the beginning and b at the end of the pumping. [5].

3.3.6. Factors Affecting Lubrication Layer Composition and Properties. The following factors affect the composition of the lubrication layer.

3.3.6.1. Effect of paste volume. It was shown by Chapdelaine that the paste content is a factor that plays a big role in concrete pumping. It is observed that the higher the paste volume, the easier it is to pump to concrete [10]. This makes sense since paste is required not only to fill the voids in between the aggregates, but to exceed this critical value to increase workability and reduce pumping resistance [4]. However, it was shown by Burns that paste is not directly a parameter that assesses the pumpability of a mixture. He observed a mixture with 13% of air and 37% of paste being able to be pumped but a mixture with 3% of air and 42.4% of paste was not pumpable. The question is: Does air content affect the pumping behavior? And how? The concept of "real paste" was then developed by Jolin and Burns [6]. Based on the hypothesis of Dryer, shown in Figure 3-31, the air bubbles dissolve under pressure in the water. As a result, the total volume is reduced. The real paste concept "is defined as the amount of paste (%) present in concrete while under pressure in the hose, which represents the amount of paste required to create the lubrication later against the pipe wall and fill the intergranular voids." When the pressure increases, the paste is reduced to the volume of binder and water. However, the calculation of the real paste is not only decreasing the volume of air from the paste, but the volume of the entire mixture is decreased by the same volume while keeping the same solid constituents. It sounds complicated but translated to an example should be easier to understand. Assume that a concrete mix design has 5% of air and 38% of paste in a cubic meter. Under high pressure the volume of air is considered to disappear. The 1000 liters are now 950, the paste volume is reduced by 5%. Adjusting by the volume under pressure, 330 liter of paste on 950 liter of concrete, the real paste volume is 34.73%.

3.3.6.2. Effect of aggregates. The composition of the lubrication layer is not completely constant since it is dependent on multiple factors (i.e. pump position, pipe material, diameter, length, and concrete composition). During concrete pumping the maximum stress is located at the walls and particles try to escape from the "high shear zone" to the lower shear zone [41]. This migration is dependent on the particle size [47]. As a result coarse aggregates travel first to the center of the pipeline leaving paste and mortar behind suggesting that the lubrication layer is formed purely by paste. Other authors have claimed that the lubrication layer behaves as a mortar [48]. However, the composition of the lubrication layer is more complex since it is also dependent on the imposed shear rate. The layer could also be composed of micro-mortar [49]

3.3.6.3. Hose diameters/ reducers. Chapdelaine [45] classifies 2 phenomena related with the reduction of the pipes: Increase of relative paste volume: Chapdelaine observed that the thickness of the lubrication layer is constant regardless of the pipe diameter. As a result, the smaller the diameter, the more paste required to form a lubrication layer as shown in

Figure 3-30.

Increase of velocity: if the diameter is reduced, while the flow rate is constant, the velocity increases with the square of the diameter reduction.

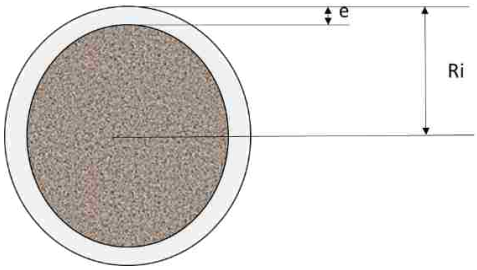

$$P = \frac{(R_1)^2 - (R_{1-e})^2}{(R_1)^2}$$

Where:
P=amount of paste
R1= pipe radius
e= lubrication layer (assumed 1 mm)

Figure 3-30 Representation of the required amount of paste to form the lubrication layer according to Chapdelaine.[45].

3.4. CHANGES IN RHEOLOGY INDUCED BY PUMPING

The following changes in rheology of concrete are affected during the high shear process experienced when pumping.

3.4.1. Changes in Air Content and Air Void Distribution. Many authors claim that a reduction of air content is the result of pumping [5]. However, this is a complex phenomenon and the mechanisms are attributed to suction and dissolution during pumping.

- Suction: This phenomenon occurs when negative pressures are applied to concrete inside the pumping mechanism, when the piston is being filled by suction (just like a syringe). This movement is suspected to cause the air bubbles inside the concrete to expand and to coalesce. If the surrounding pressure is decreased by half, the volume of the air bubbles can be double [45].
- Dissolution: When concrete is pressurized, air bubbles dissolve in the surrounding water. When concrete is out of the pipe, the pressure is back to atmospheric and the air returns. The air is more likely to return within the bubbles that did not dissolve, creating larger bubbles, and large bubbles are less stable and more likely to escape as

shown in Figure 3-31. However, in this mechanism, not only air content can be affected but also the spacing factor. Air content affects concrete rheology mainly reducing the plastic viscosity [1].

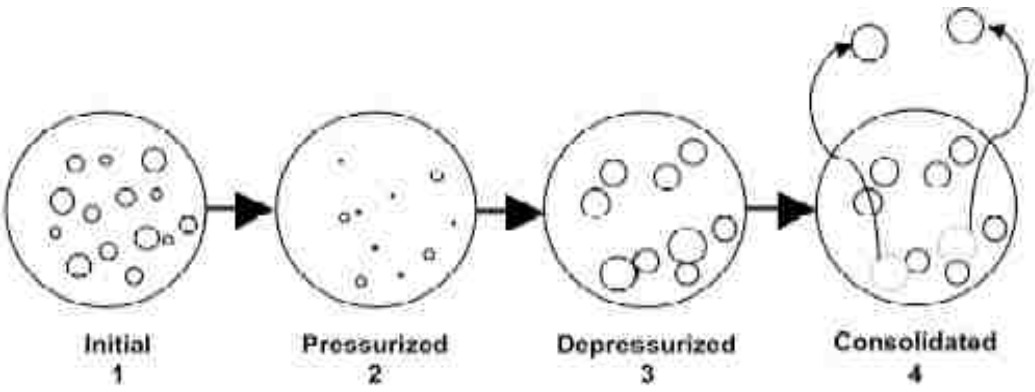

Figure 3-31Air loss during and after pumping.[6]

3.4.2. Effect of Shearing. Concrete pumping is a process that induces high shear rates into the concrete, SCC is more susceptible to be affected since a bigger portion of the concrete is being sheared. Feys et al. [50] explained that the rheological properties of SCC change induced by pumping. Why does concrete rheology change during pumping? Because the effect of shear rate, concrete pumping induces a higher shear rate than the one imposed by the mixer. That additional shear can cause additional dispersion of cement particles. As a result, increasing pumping time and flow rate decreases viscosity, while concrete yield stress does not present a uniform behavior.

4. MATERIALS AND METHODS

This section summarizes the principal properties of the materials and experimental work performed in this research. The tasks from this research include:

1. Pumping influence on fresh properties.
2. Lubrication layer composition.
3. Rheometers comparison/transformations.

4.1. PUMPING INFLUENCE ON FRESH PROPERTIES.

Overview: To evaluate the influence of pumping and pumping parameters on fresh concrete properties, a set of pumping experiments was conducted at a local ready-mix company. The fresh and hardened properties were measured in the field before and after pumping.

Specimens for hardened properties were tested in the lab while fresh properties were measured in the field. Sixteen mixtures were measured in eight different days.

Every mixture was produced following the same mix design while varying the quantity, type and brand of the chemical admixtures to achieve different fresh properties.

4.1.1. Materials and Mixtures. The following materials were used on the performed pumping campaign.

4.1.1.1. Mix design. The main purpose of this project was to create air-entrained flowable concrete which would be susceptible to freeze-thaw and scaling damage if the air-void system were inadequate. As such, the chosen water-to-cement ratio was 0.45. A paste volume of 38% was chosen as with this paste content, SCC properties could be

achieved while still maintaining adequate stability. Each mix design used the quantities shown in Table 4-1. The types and dosages of admixtures are discussed further.

Table 4-1 Mix design.

Material	Quantity (kg/m^3)
Cement	315
Fly Ash type C	105
Fine Aggregate	927
Coarse Aggregate	759
Water	189

4.1.1.2. Portland cement. A commercially available type I/II Portland cement with a density of 3160 kg/m^3 was used for the experimental part. The cement meets the requirements of ASTM C150-12 [51].

4.1.1.3. Fly ash type C. Supplementary cementitious materials (SCMs) contribute to the properties of concrete via pozzolanic or hydraulic reaction when used in conjunction with Portland cement. Fly ash is a byproduct of the combustion of pulverized coal in electric power generating plants [52]. It is typically used at dosages between 15%-40% by mass. According to ACI 232.2R-96 [53] Fly ash benefits include workability increase, reduction in bleeding, improved pumpability, extension of the setting time, improved finishability, reduction of air –entraining admixture requirement. In this work,

a fly ash type C with a density of 2930 kg/m^3 was used, at a 25 % of replacement by weight of cement.

4.1.1.4. Fine aggregates. A commercially available fine aggregate from the Missouri River was employed. The sand has a density of 2630 kg/m^3 and the absorption is 0.24%. These properties were determined according to ASTM C128 [54]. The grain size distribution was determined according to ASTM C136-14 [55] and is shown in Figure 4-1.

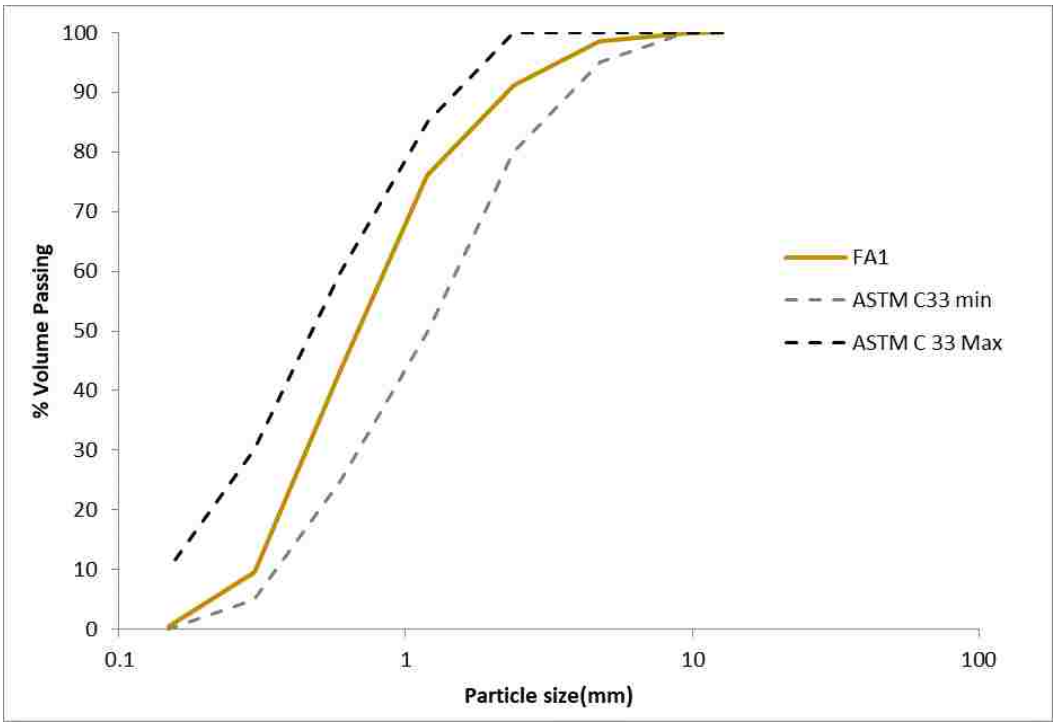

Figure 4-1 Fine aggregate (FA1) grain size distribution, including the limits stated by ASTM C33.

4.1.1.5. 3/8 in. coarse aggregates (CA1). A commercially available crushed limestone was used as a coarse aggregate with a density of 2700 kg/m^3 and an absorption of 0.66%. These properties were determined according to ASTM C127-15 [56]. Grain size distribution was determined according to ASTM C136-14 [55] and is shown in Figure 4-2.

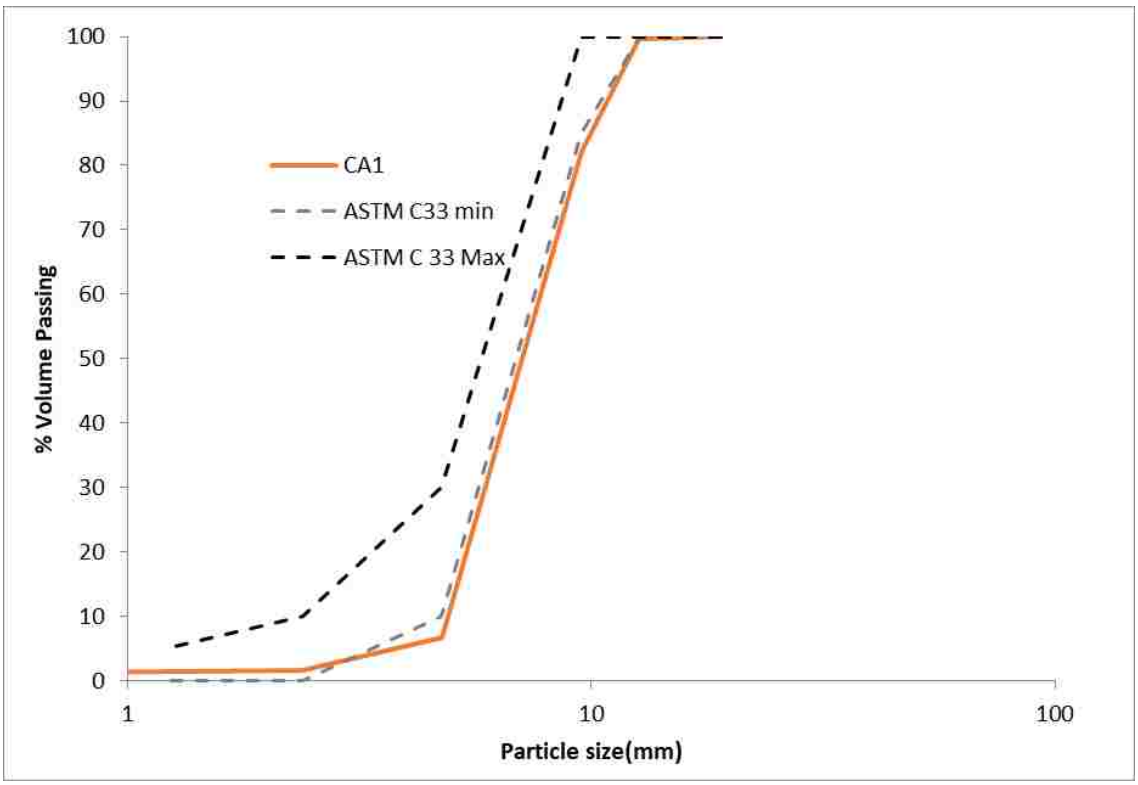

Figure 4-2 3/8 coarse aggregate grain size distribution.

4.1.1.6. Chemical admixtures. A series of chemical admixtures were used to achieve flowable concrete as shown in Table 4-2, with a target air content of around between 1 and 10% and a long workability retention (> 2hrs).

- High Range Water Reducer: A total of four HRWR Agents were used. Three were based on third generation polycarboxylate ether technology, (PCE 1, 2 and 3) meeting ASTM C 494[57], Type A and Type F and AASHTO M 194, Type A and Type F. The fourth HRWRA is a second generation poly naphthalene sulfonate (PNS 1) meeting ASTM C 494 [57], Type A and Type F AASHTO M 194 [58] as well.
- Retarder or Hydration Stabilizer: One hydration stabilizer (HS1) complying with ASTM C 494[57] Type D admixture and 1 retarder (Ret1) meeting ASTM C 494 [57], Type B & D and AASHTO M 194[58] were used to produce a more predictable and stable concrete with time.
- Workability-retaining admixture: Two workability-retaining admixtures (WR1, WR2) meeting ASTM C494/C494M [57] Type S standards were used to keep workably approximately constant over an extended amount of time.
- Air Entraining Admixtures and Defoamer: Two air entraining admixtures were used (AE1, AE2) complying with ASTM specification C 260 [59] and AASHTO Specification M 154[60] to create a well-dispersed air system and to improve freeze-thaw resistance. One de-foaming admixture (DF) complying with ASTM 494 [57] type S was employed to remove excessive air generated by the PCE HRWRA.
- Viscosity Modifying Agent: A viscosity modifying agent (VMA1) complying with ASTM C 494 [57] Type S Admixture was used to reduce the potential for bleeding and segregation of the mixtures with PNS.

Table 4-2 Admixtures quantities.

Day	Mixture	PCE 1 kg/m³	PCE 2 kg/m³	PCE 3 kg/m³	PNS1 kg/m³	RET 1 kg/m³	HS 1 kg/m³	WR 1 kg/m³	WR 2 kg/m³	AE 1 kg/m³	AE 2 kg/m³	Defoamer 1 kg/m³	VMA kg/m³
	M1	1.14				1.02		1.37		0.169			
1	M2	1.01				1.03		1.37		0.169			
	M3	0.8				0.94		1.37		0.169			
2	M4	0.58				1.03		1.03		0.169			
	M5	0				0.82		0.82		0.085			
3	M6	1.07				1.03		1.03		0.085			
	M7	1.25				1.03		1.03		0.085			
4	M8			0.48		1.03		1.03		0.085			
	M9		0.58				0.46		2.33	0.034			
5	M10		0.58				0.48		2.33	0.034			
	M11		0.47				0.5		2.51	0.037		0.75	
6	M12		0.37				0.56		2.51	0.122		0.19	
	M13		0.25				0.85		1.59	0.122		0.21	
7	M14		0.48				0.64		2.25	0.183		0.19	
	M15				7.25		1.07				0.358		5.14
8	M16				4.84		1.07				0.912		3.46

4.1.1.7. Test methodology. This section describes pumping variables and the utilized test methods to characterize fresh and hardened properties of concrete, in order to investigate the influence of pumping. Concrete mixtures with an initial slump flow below 550 mm were considered highly-workable concrete or CVC and received consolidation. Those concrete mixtures with slump flow above 550 mm were considered SCC and did not require external consolidation as shown in Figure 4-3. The consolidation energy was kept constant regardless of the slump evolution with time of each sample.

The admixture dosages where chosen in the lab to obtain the required fresh properties, based on the following criteria:

1st criterion: Slump Flow

2nd criterion: air content

3rd criterion: Workability retention.

Figure 4-3 Testing trial batches.

4.1.1.8. Field testing. A total of eight full scale pumping days were conducted in the field. The mixtures were characterized by the following empirical tests: slump/slump flow, air content (gravimetric), density, air content (pressure), T-50, stability and VSI, if applicable. During each day, two mixtures were evaluated. Every mixture has a different workability and air content due to the use of different admixture types and quantities.

The methodology to investigate the change in fresh properties was the following for every mixture: three non-pumped concrete samples were used as a reference measurement. These were evaluated before pumping, in the middle of all pumping operations and after pumping. A linear evolution over time was assumed for comparison. Up to six pumped samples were also characterized and compared to the interpolated non-pumped samples at the same time.

4.1.1.9. Variations in pumping configurations. Boom configurations “flat” horizontal position of the boom and “A” shapes were evaluated. In the A configuration, gravity may play an important role as concrete may fall under gravity in the descending part. An “A” configuration is shown in Figure 4-4.

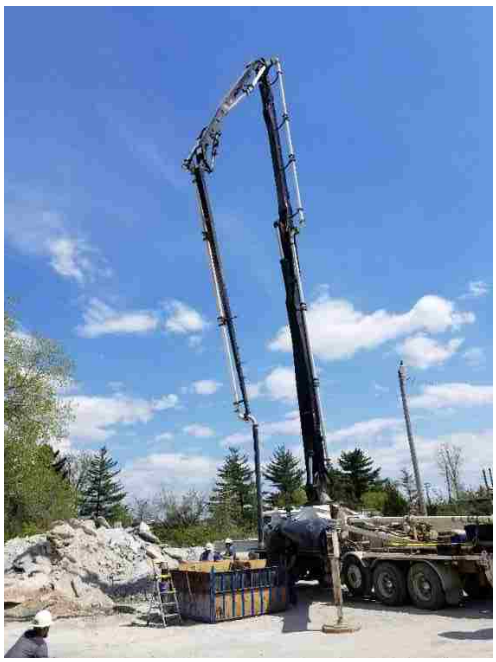

Figure 4-4 Pump on "A" configuration.

4.1.1.10. Pipe diameter. The effect of pipe diameter is explained in section 3. In the field, a reducer from 5 to 4 inches was sometimes installed at the end of the pumping boom.

4.1.1.11. Flow rate. The influence of flow rate was investigated. The flow rate was approximated by dividing the volume of a fixed number of strokes by the measured time. The flow rate was varied from 1 l/s to 33 l/s.

4.1.1.12. Submerging. In some cases, the end of the boom was kept submerged in the concrete in the formwork, mainly to investigate the effect on the air content and air-void system.

4.1.2. Tests in Field. The following tests were performed to characterize concrete behavior on field.

4.1.2.1. Slump. The slump test was performed following ASTM C143 [61] as follows:

A flat non-water absorbent plate was placed on a leveled surface. Concrete was placed in the cone in 3 layers and each layer was rodded 25 times. The excess was removed with a strike off bar and the excess was removed from the plate. The cone was lifted vertically, as shown in Figure 4-5, between 2-4 s. The cone was placed to a side as a reference and the slump from the concrete was measured.

4.1.2.2. Slump flow. The slump flow test was performed following ASTM C1611 [62] as follows:

If concrete mixture has SCC consistency: A flat non-water absorbent plate was placed on a leveled surface. Concrete was placed in the cone in a single layer with no rodding. The excess was removed with a strike off bar and the excess was removed from the plate. The cone was lifted between 1-5 s. The diameter of the spread was measured at the nearest 5 mm in 2 perpendicular directions as shown in Figure 4-6.

If concrete mixture has HWC consistency: A flat non-water absorbent plate was placed in a leveled surface. Concrete was placed in the cone in 2 layers each one with 10 rods. The excess was removed with a strike off bar and the excess was removed from the

plate. The cone was lifted between 1-5 s. The diameter of the spread was measured at the nearest 5 mm in 2 perpendicular directions as shown in Figure 4-6.

Figure 4-5 Slump flow test.

Figure 4-6 Slump flow example.

4.1.2.3. Air content: pressure method. The fresh air content determination was performed following ASTM C231 [63] as follows:

For flowable concrete, the air meter was placed on a leveled surface as shown in Figure 4-7, the interior was damped and filled in a single layer without external consolidation for SCC. For highly workable concrete, it was filled in 2 layers each receiving 10 roddings and 6 hits with the rubber mallet. While for CVC, the container was filled in 3 layers, rodded 25 times per layer, and hit 10-15 times per layer. Once the bucket was filled with concrete, the surface was finished with a standard plate. The density was determined by weighing the concrete, divided by the volume of the container. The rim of the container was cleaned, and the air meter system was locked onto the bucket. Water was added through the petcock until flow from the opposite side was observed, making sure that the air bubbles were released, after which the petcocks were closed. The air meter was then set to relative 0 and the valve was opened. The bucket was tapped with a rubber mallet while the valve was released. The air content of the concrete was recorded to the nearest 0.1% or as available.

Figure 4-7 Air content test.

4.1.2.4. Sieve stability. The sieve stability test was performed following The European Guidelines for Self-Compacting Concrete [64] as follows: A concrete sample of 5 ± 0.2 kg was poured on a #4 sieve with a pan on the bottom. The mass was recorded after 2 minutes. The sieve was then removed and the mass of material that passed through the sieve was recorded as well. The segregation value was calculated as the mass that passes the sieve divided by the total mass. The criteria of acceptance from the European guidelines of Self Consolidating Concrete are shown in Table 4-3.

Table 4-3 Stability criteria.

Stability	
Class	Segregation Resistance %
SR1	≤20
SR2	≤15

4.1.2.5. Rheological measurements. An ICAR rheometer was used for field operation. Measurements were performed on all samples (pumped and non-pumped). A seven-step procedure with a duration time of 5 seconds per step and a pre-shear time of 20 seconds was used under two different inner radius configurations: the first is the original 4 blade vane with a radius of 63.5 mm and an outer radius of 143 mm was used to determine rheological parameters. The second configuration has a Smooth cylinder with conical bottom, the cylinder measuring 127 mm in diameter and 203 mm in height was used to determine interface rheology.

4.1.2.6. Sampling. Non-pumped samples used as reference were discharged directly into a dampened wheelbarrow empirical ad fundamental tests were performed to pumped and non-pumped samples. Pumped samples were pumped into a formwork as shown in Figure 4-8.

Figure 4-8 Formwork used to discharge pumped concrete.

Concrete was collected from the formwork using 2-gallon buckets and placed into a wheelbarrow, minimizing dropping height to avoid segregation. Then the concrete mixture was transported via wheelbarrows to the testing station, as shown in Figure 4-9 (typically less than 20ft from formwork). The concrete was not pumped into buckets or wheelbarrows as this procedure may change the air-void system and fresh properties of the concrete producing non-representative changes that cannot be attributed to high volumes of concrete.

Figure 4-9 Concrete transportation using a wheel barrow.

4.2. LUBRICATION LAYER INVESTIGATION

The following materials and quantities were used to attempt to determine the thickness of the so-called “lubrication layer”.

4.2.1. Materials and Mix Design. Portland cement as detailed in 4.1.1.2, fly ash Type C as discussed in 4.1.1.3, water, HRWR (PCE1) stabilizer (1HS), and iron mountain trap rock as shown in 4.2.2 were employed for this part of the work. The mixtures design of the paste is shown in Table 4-4.

Table 4-4 Lubrication layer paste mixture design (9 liters).

Materials	Quantities (g)
Cement	9969
Fly asg	2492
Water	4984
HS1	37
PCE1	32

4.2.2. Iron Mountain Trap Rock. Iron mountain trap rock is a sand that results from crushed aggregates from Ironton, Missouri. Absorption properties are shown in Table 4-6 for each portion sieved. It was determined according to ASTM C128 [54] The grading curve was carried out according to AASHTO T11/T27 [55]. The sieve analysis is shown in Table 4-5 and in Figure 4-10.

Table 4-5 Iron mountain trap rock sieve analysis.

Sieve	Sieve size(mm)	% pass	min	max
1/2"	12.7	100	100	100
3/8"	9.51	100	100	100
No. 4	4.75	97	91	100
No. 8	2.36	68	62	74
No. 16	1.18	39	33	45
No. 30	0.6	22	15	27
No.50	0.3	10	3	15

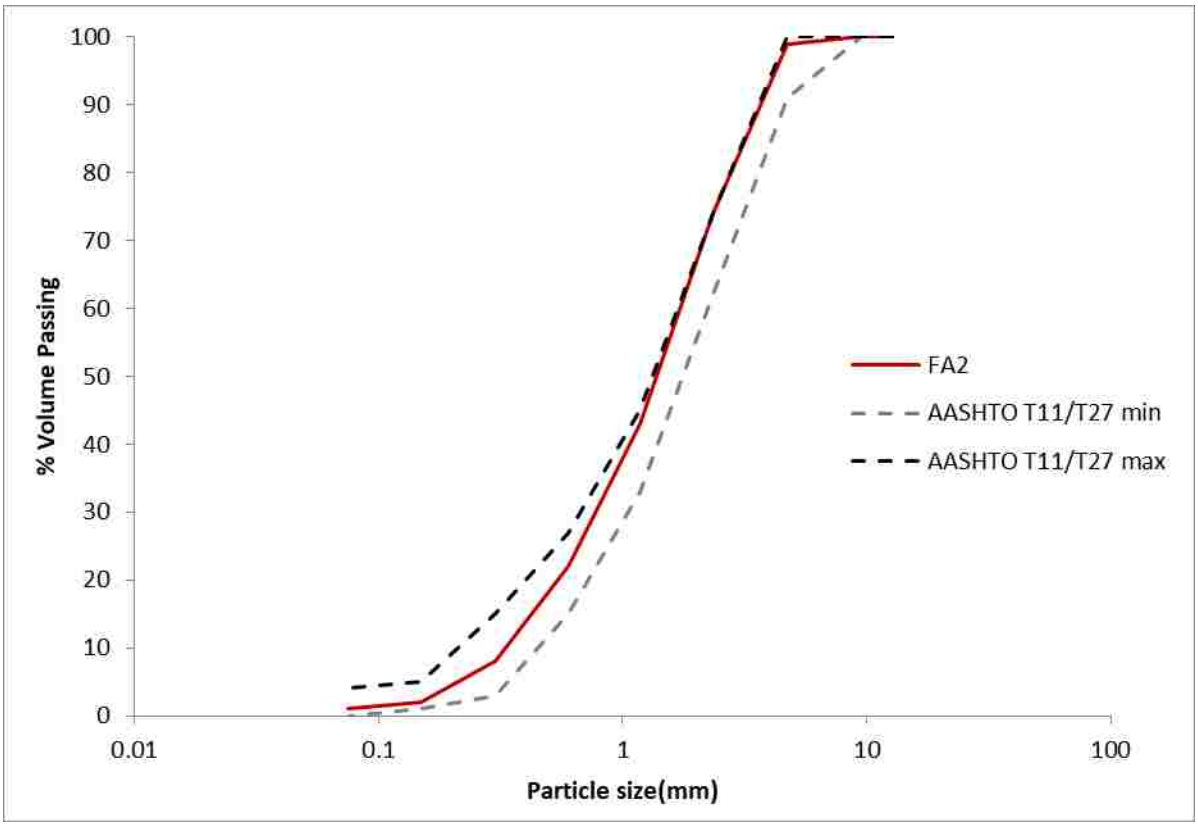

Figure 4-10 Gradation of mountain trap rock.

Table 4-6 Densities and absorption.

Mountain Trap Rock			
Pass Sieve #	SG SSD (g/cm³)	SG OD (g/cm³)	ABS (%)
8	2.58	2.55	1.27
16	2.56	2.52	1.5
30	2.56	2.52	1.77
50	2.55	2.49	2.42

4.2.3. Test Methodology. The following methodology was used to investigate the evolution in rheological properties by adding particles.

4.2.3.1. Establishment of volume fraction curves. Krieger-Dougherty-style curves were established for plastic viscosity, while for yield stress, the Chateau–Ovarlez–Trung [65] model was used for all portions of the sand with different maximum particle sizes. The Iron Mountain trap rock gradation was divided into four portions by sieving. Sand that passes sieves #8, #16, #30, #50 was considered for the analysis. The volume fraction was varied from 20-50 % using the mix design shown in Table 4-8 depending on the validity of the rheological measurements.

$$\tau_{0,r} = \frac{\tau_0}{\tau_{0,s}} = \sqrt{(1-\phi)\cdot\left(1-{\phi}/{\phi_m}\right)^{-\eta\cdot\phi_m}} \qquad 4\text{-}1$$

Where: $\tau_{0,r}$= Relative yield stress (-)

φ = Volume fraction (-)

φ_m= Maximum volume fraction for friction (-)

$[\eta]$= Intrinsic viscosity (-)

Testing: Seven measurements where planned in the ConTec Viscometer 6 rheometer per sieved portion. The testing protocol can be seen in Figure 4-11 and the procedure was performed as follows:

1. Nine liters of paste were mixed in the high shear mixer with the mix design shown in Table 4-1. First, cement and fly ash were added to the mixer. Approximately 90% of the water was added followed by 2 minutes of mixing at its maximum speed. After that, PCE1 was added with the rest of the water and mixed again for 2 minutes at maximum speed. Ret1 was finally added and the paste was mixed again for 1 minute at maximum speed (Table 4-7).

2. A representative sample of approx. 1 liter was taken and tested in the ConTec 6 Rheometer to use it as a base.
3. After measuring the rheology of the paste. The paste was returned to the mixer and mixed for 1 minute at maximum speed to avoid the error of reading the effect of thixotropy.
4. Paste was weighted and the pre-weight volume fraction of sand was added as shown in Figure 4-13. It should be noted that the Iron Mountain Trap Rock was added on oven dry conditions at room temperature and the water required to achieve SSD was added.
5. The mortar was mixed by hand until homogeneity was visually achieved. The mixing was performed by hand to ensure that the maximum shear rate in the paste caused by the mixer was not exceeded, as this was deemed one of the shortcomings of the measurements previously discussed.
6. The rheological properties of the mortar were measured in the contec 6, and the time was recorded.
7. Discard the sample.
8. Take a new sample of paste of approximately 1liter from the mixer, mix for 1 minute to minimize thixotropy and repeat step 4-7 with different volume fractions of sand.
9. Lastly, a final measurement of the paste in the contec viscometer 6 was executed. A linear evolution of the rheological properties with time was assumed.

Figure 4-11 Methodology flow diagram.

The contec viscometer 6 procedure used was a seven-step procedure with 20 points per step. Each step was maintained for 1.5 seconds and the transition between steps was 0.5 seconds. The maximum rotational velocity was 0.707 rps and the minimum was 0.030 rps, as shown in Figure 4-12. The pre-shear was 10 seconds at a velocity of 0.35 rps, which includes the descent of the inner cylinder into the material.

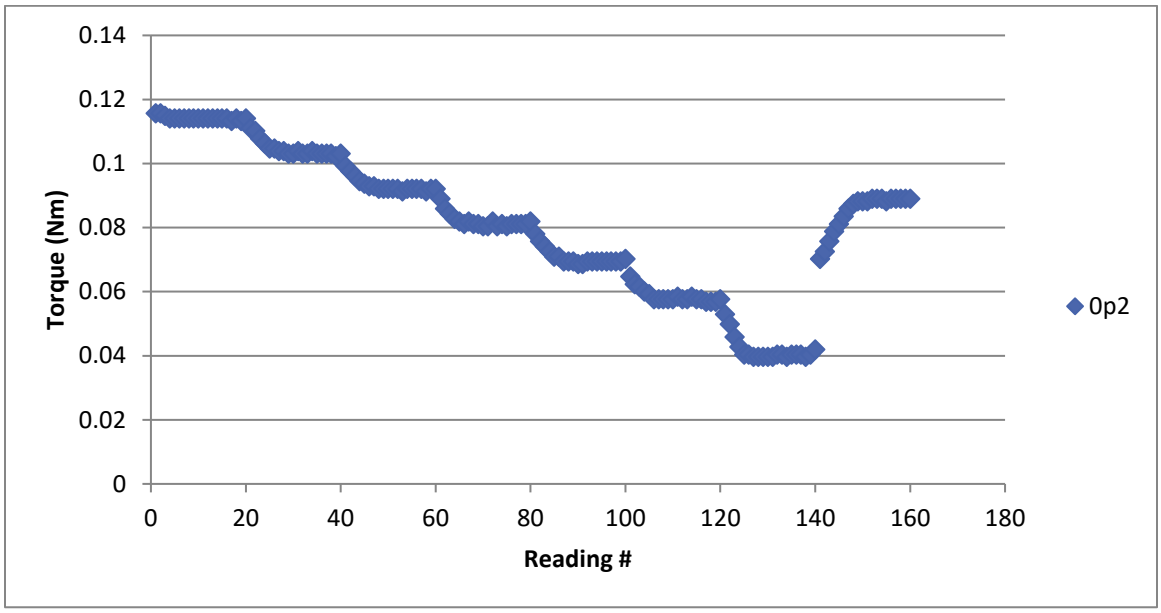

Figure 4-12 Contec 6 torque steps.

Table 4-7 Paste mixing procedure.

Activity	Time(min)	Time Cummulative(min)
Add 90% of the water	-	-
Mix	2	2
Add Superplastizicer	0.5	2.5
Mix	2	4.5
Add Stabilzer	0.5	5
Mix	1	6

note that superplasticizer and stabilizers were not added at the same that due to the incompatibility advised and validated by the producers and sellers of the chemical admixtures.

Figure 4-13 Batched weights of the sand and equivalent water to bring the sand to SSD condition.

Table 4-8 Weight of paste and sand required before measurement.

Volume(%)	Mass of Sand (g)	Mass of paste(g)
20	633.6	1873.3
30	950.4	1639.1
40	1267.2	1405.0
45	1425.6	1287.9
50	1584.0	1170.8

Two measurements were performed on the paste: one before addition of volume fractions and one after the set of experiments. This is done to observe the evolution of paste over time, and to correctly calculate the amplification of yield stress and viscosity due to the presence of the aggregates. The time evolutions of yield stress and viscosity are shown in Figure 4-14, Figure 4-15, respectively.

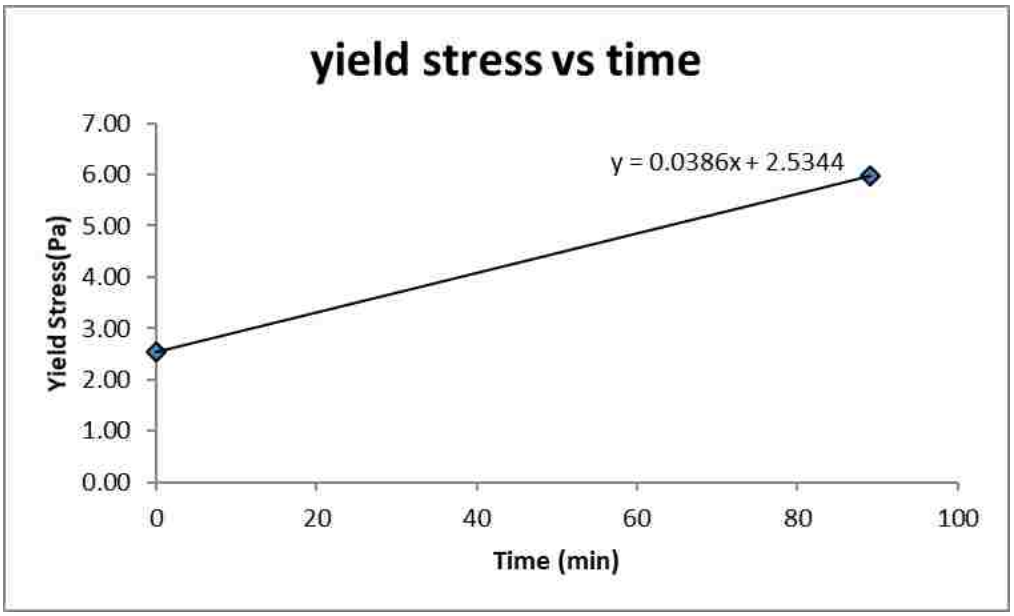

Figure 4-14 Yield stress evolution of paste used on portion that passes sieve #8.

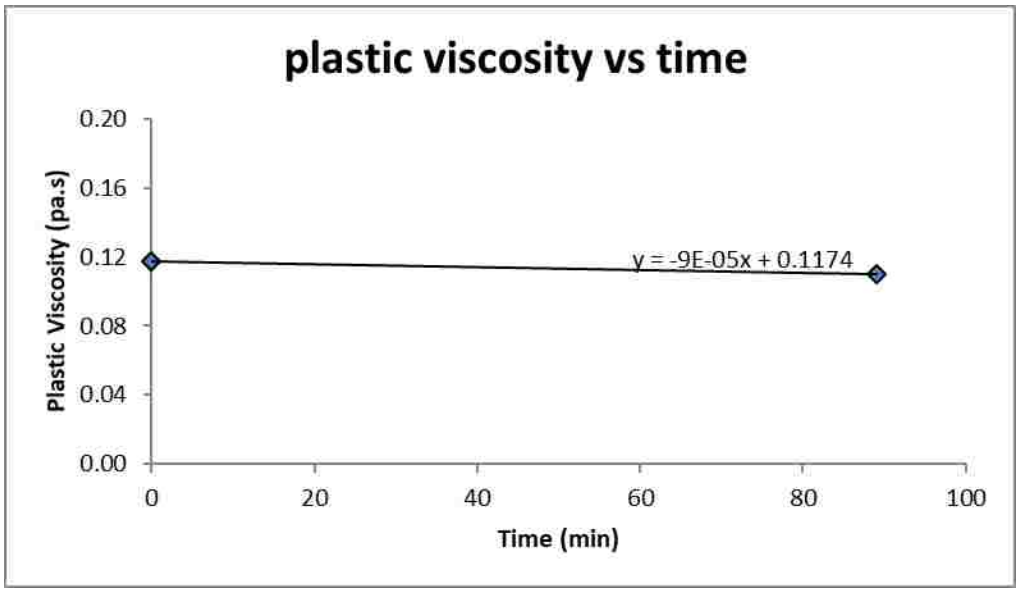

Figure 4-15 Plastic viscosity evolution of paste used on portion that passes sieve #8.

The volume fractions of sand in the mortars were increased in increments of 10%. i.e. (20%, 30%, 40%, 50%). However, this was changed due to the formation of plug

flow and “walls of mortar”, due to frictional behavior that invalidate the test, as shown in Figure 4-16. In this case intermediate percentages were added (I.e. 35%, 45%) to obtain more complete data.

Figure 4-16 Discarded sample of a sample in pure plug flow due to high yield stress. This measurement was on the sand portion that passes sieve #50 at 42.5% of volume fraction.

Typically, five measurements were taken for mortar per sand portion. However, the mortar with the portion that passes # 50 has only 4 data points due to uncertainty of the 5th. Table 4-9 shows for which volume fraction of sand, dependent on their particle size, rheological measurements were performed.

Table 4-9 Tests realized per sieved portion. (Gray indicates performed test).

passes sieve #	volume fraction(%)	20	30	35	40	42.5	45	47.5	50
8									
16									
30									
50									

4.2.3.2. Tests for determination of lubrication layer thicknesses. To do so, paste rheology, mortar rheology, bulk concrete and interfacial zone rheological properties must be known. And that can only be achieved by using several rheometers. The following mix design was used.

The proportions were fixed as follows:

1. 38% by volume of paste.
2. 34.7% by volume of iron mountain trap rock as fine aggregate.
3. 27.3% by volume of 3/8 as coarse aggregate.
4. PCE 1 was used at a dosage of 2gr/kg of cementitious material.
5. Ret1 was used at a dosage of 4gr/kg of cementitious material

While 3 different paste compositions were used

1. Water/cement of 0.35
2. Water/cement of 0.40
3. Water/cementitious of 0.40 using fly ash as 20% of replacement by volume.

The test protocol is explained in Table 4-10.

Table 4-10 Rheometer procedure.

rheometer	pre-shear time (s)	steps	points per step	Velocity (rps)	
				min	max
Contec 6	10	7	20	0.0300	0.7070
Contec 5W	10	7	20	0.0300	0.7070
ICAR	20	7	95	0.0500	0.5000
Anton Paar	180	1	125	0.0001	1.2900

- Measuring concrete: Concrete rheology was measured using contec viscometer 5 rheometer with the bucket used for concrete further referred in this thesis as "contec 5W" dimensions are listed in Table 4-12. While the rheology of the interface zone was measured with the ICAR rheometer using a smooth cylinder to simulate the inside of a pipe also known as "tribometer head".
- Measuring mortar: Mortar measurements where performed using the contec 6 as explained in 4.2.3.
- Measuring paste measurements where measured using the Anton Paar MCR 302. A shear rate decrease in a linear manner was used.

4.3. RHEOMETER COMPARISON

Materials and Mix Design: The mix design follows the suggested composition of the reference NIST material for cement paste. Corn syrup (see Figure 4-17), distilled water and limestone were used as shown in Table 4-11. The only difference with the reference material from NIST is that it is not calibrated.

Table 4-11 Reference material proportions.

Reference material	
Material	Quantity (g)
Corn syrup	18631
Distilled water	5884.5
Limestone	42680.7

Figure 4-17 Corn syrup sample.

Each rheometer works under the principle of concentric cylinders the interior radius, outer radius and gap are shown in Table 4-12.

Table 4-12 Rheometers configurations.

Rheometer	Ri(mm)	Ro(mm)	Gap(mm)
Contec 5S	65	82	17
Contec 5W	100	145	45
ICAR	63.5	143	79.5
Contec 6	50	61.5	11.5
Anton Paar MCR 302	13.33	14.46	1.13

5. RHEOMETER COMPARISON

This section summarizes a rheometer comparison performed with 4 available rheometers at Missouri S&T. Transformation formula between the rheometers were obtained as a result.

5.1. EXPERIMENTAL WORK

The following work was performed inside a lab:

5.1.1. Methodology. To understand the correlation between the rheometers the following were compared:

- Contec viscometer 5 small configuration (mortar)
- Contec viscometer 5 wide configuration (concrete)
- Contec viscometer 6 (mortar up to 2 mm NMS)
- ICAR rheometer (concrete)
- Anton Paar MCR 302 (reference) (cement paste)

A reference material composed of corn syrup, limestone filler and water were utilized to obtain a material with a yield stress.

The rheological properties of the reference material were measured on the 4 rheometers. The testing procedures are described in section 4, and they were executed at three different temperatures: room temperature ≈ 20.5 °C, hot temperature (31-34.5 °C), and cold temperature (1-3 °C).

For every temperature, the samples were covered to avoid evaporation or any kind of alteration of the sample, and all removable parts of the rheometers were subjected to the same temperature to avoid temperature gradients, as show in Figure 5-1.

Figure 5-1 Reference material in cold configuration.

The Bingham model was used for the comparison between rheometers. One of the main differences between rheometers involves the design, including vane or cylinder shape of the inner cylinder and size of the inner and outer radius, determining the gap.

5.1.2. Results and Discussion. In order to compare all rheometers, the Anton Paar rheometer was chosen as a reference, as it could mimic exactly all temperatures measured in all other rheometers.

The Anton Paar MCR 302 also offered the flexibility of matching the shear rate range with each of the other rheometers. In the following figures, the values obtained

with the Anton Paar rheometer are displayed on the X axis, while the Y axis shows the values of the other rheometers. The slope is an indicator of how close a certain rheometer is to the Anton Paar is, while the correlation coefficient shows how "good" the correlation is.

5.1.2.1. Yield stress comparison. As shown in Figure 5-2, the ConTec 6 (slope = 0.82) has the highest slope value compared to the Anton Paar and also has the highest correlation factor (R^2 = 0.98) indicating that the ConTec Viscometer 6 delivers slightly different values repeatedly compared to the Anton Paar MCR 302. Comparing the yield stress in the ConTec 5s with the Anton Paar delivers a slope of 0.72 and an R^2 = 0.74. The ConTec 5w shows an even lower slope of (0.52), but the correlation factor is low (R^2=.15).

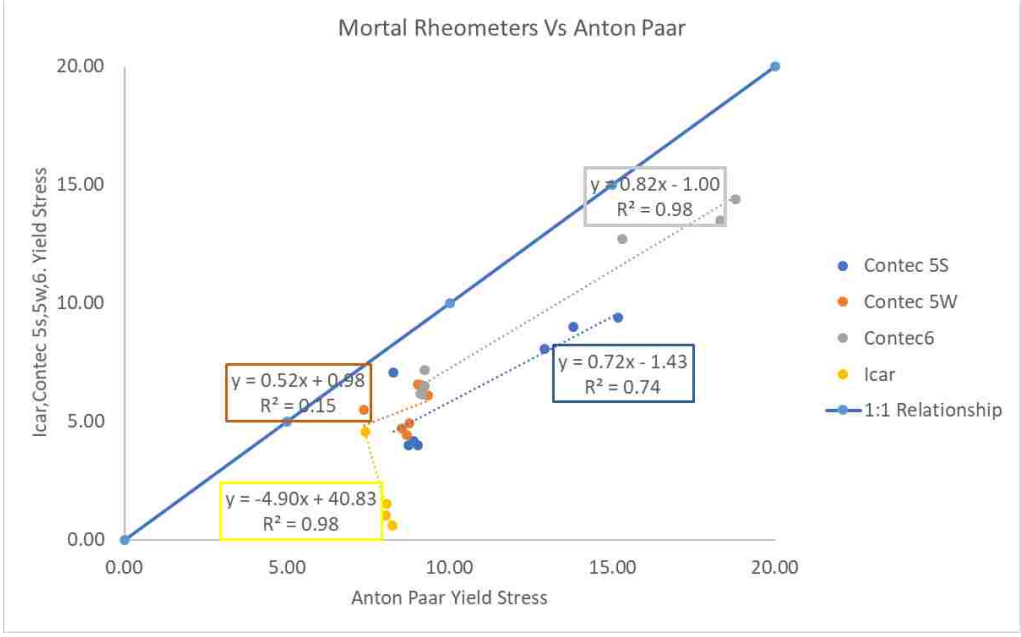

Figure 5-2 Yield stress comparison.

Despite the high correlation coefficient, the ICAR yield stress measurements are completely off from the Anton Paar measurements and there could be multiple causes for this behavior.

The cold measurements are not included, since the cold measurements resulted a high plastic viscosity and a negative yield stress from the Bingham model, which is physically impossible.

- Material Behavior. As shown in Table 5-1 shear thinning behavior is more noted at lower shear rate ranges (higher absolute values of c/μ). And the ICAR works with the lowest shear rate ranges of all tested rheometers.
- ICAR Precision**.** As shown in Figure 5-10 the ICAR rheometer has big "noise" for a measurement, which is in the order of 0.5 Nm, with some peaks up to 0.15 Nm.
- Plug Flow. As the gap increases the risk of not shearing the entire sample increases. And the ICAR rheometer has the biggest gap of all tested rheometers as shown in Table 4-12.

5.1.2.2. Plastic viscosity comparison. As shown in Figure 5-3, the contec 6, contec 5s and contec 5w have the same slope when comparing to the Anton Paar rheometer (0.64) and measure thus the same viscosity values. The ICAR rheometer seems to measure viscosity almost identical to the Anton Paar rheometer, specially values of plastic viscosity bellow 5pa.s. All viscosity regressions have excellent correlation coefficients.

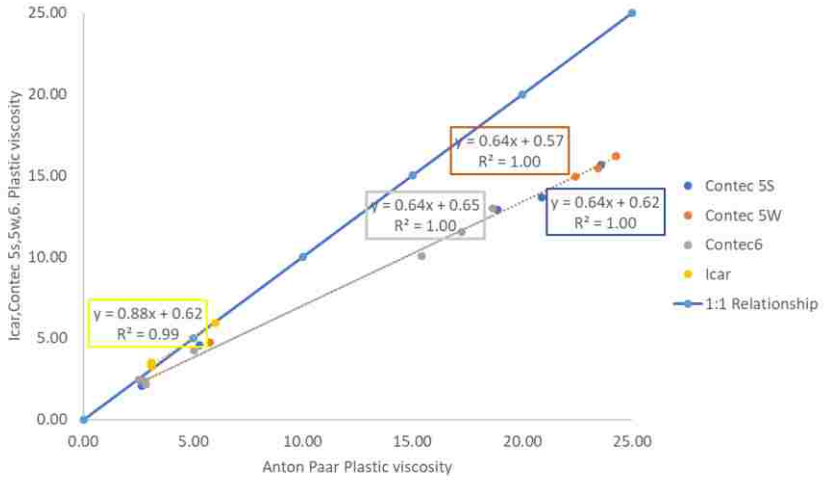

Figure 5-3 Plastic viscosity comparison.

However, for the ICAR rheometer, the cold measurements were excluded due to a negative yield stress value. When artificially setting the yield stress value at zero for the cold measurements, the ICAR rheometer viscosity seems to be in between the Anton Paar and the ConTec viscometer values, still with an excellent correlation (Figure 5-4).

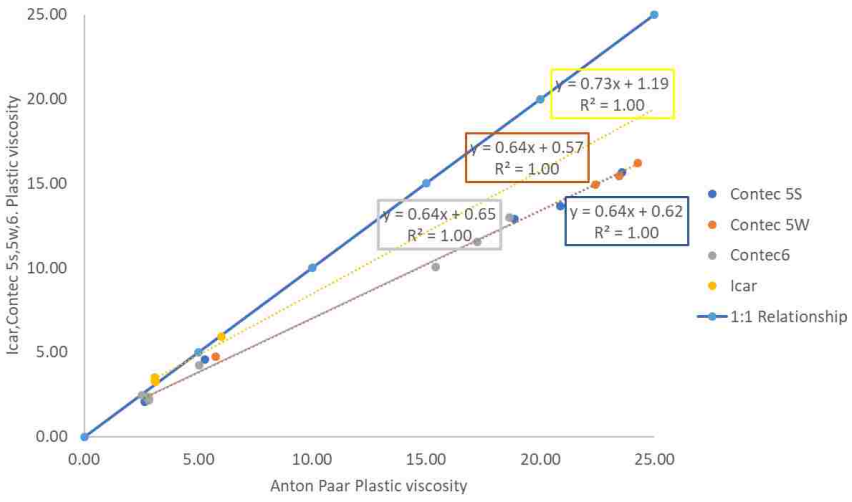

Figure 5-4 Plastic viscosity comparison.

5.1.2.3. Temperature influence. It was shown by Ferraris [9] that even if rheometers have different readings, they overall have the same tendency in increases or decreases of rheological properties. In this set of experiments this was induced by means of temperature changes: as the temperature increases, rheological properties decrease and vice-versa. And both yield stress and plastic viscosity "seem" to have similar tendency as shown in Figure 5-5 and Figure 5-6 . However, it is not straightforward to compare all rheometers in foundamental units with each other, because every rheometer has a different design and works at a different shear rate range, which especially seems to affect the yield stress estimation.

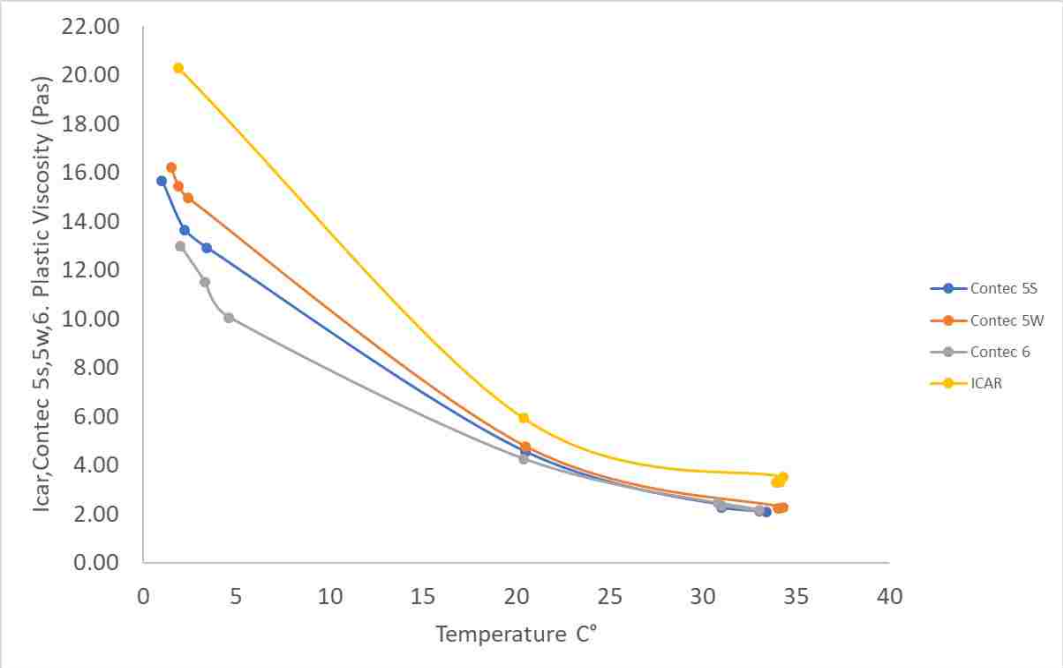

Figure 5-5 Temperature influence on plastic viscosity.

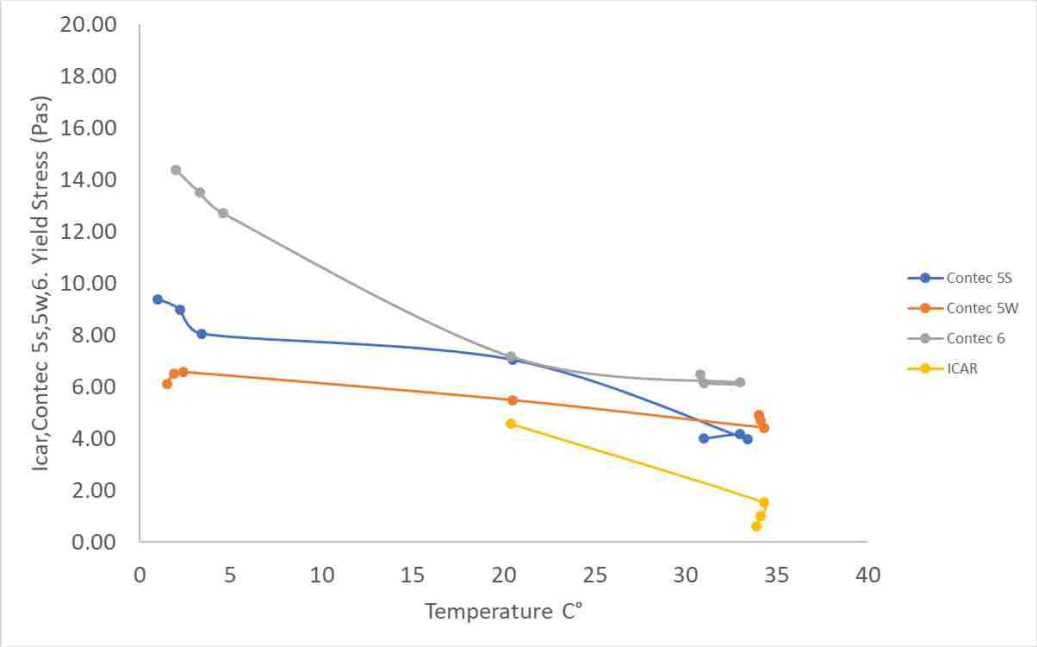

Figure 5-6 Temperature influence on yield stress.

5.1.2.4. Material behavior. Ideally, if the material is the same, the rheometers should measure the same values fundamental values. However, it seems that the way they behave is dependent on the shear rate applied (shear thinning behavior), as shown in Figure 5-7. As the maximum shear rate applied decreases, shear thinning behavior becomes more pronounced. Comparing the reference fluid in the Anton Paar for the shear rate ranges corresponding to the contec 5W (Figure 5-7) and contec 6 (Figure 5-8), the ratio between c and μ as an indicator of non-linearlity, if is higher in absolute values if the shear rate range is lower (-.015 vs -.006) as the material shows more curvature when it comes close to zero shear rate.

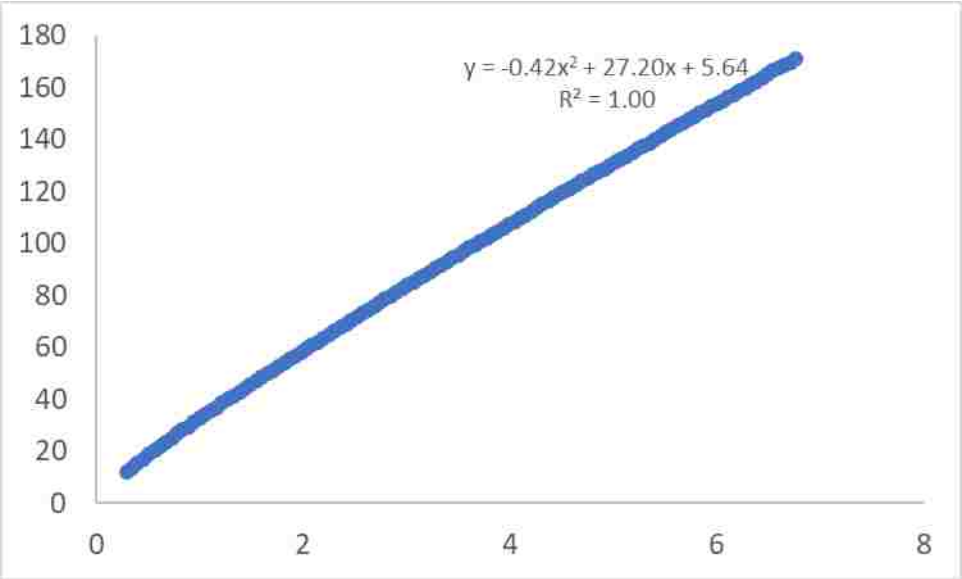

Figure 5-7 Anton Paar flow curve for the shear rate range of the contec 5W at cold temperature.

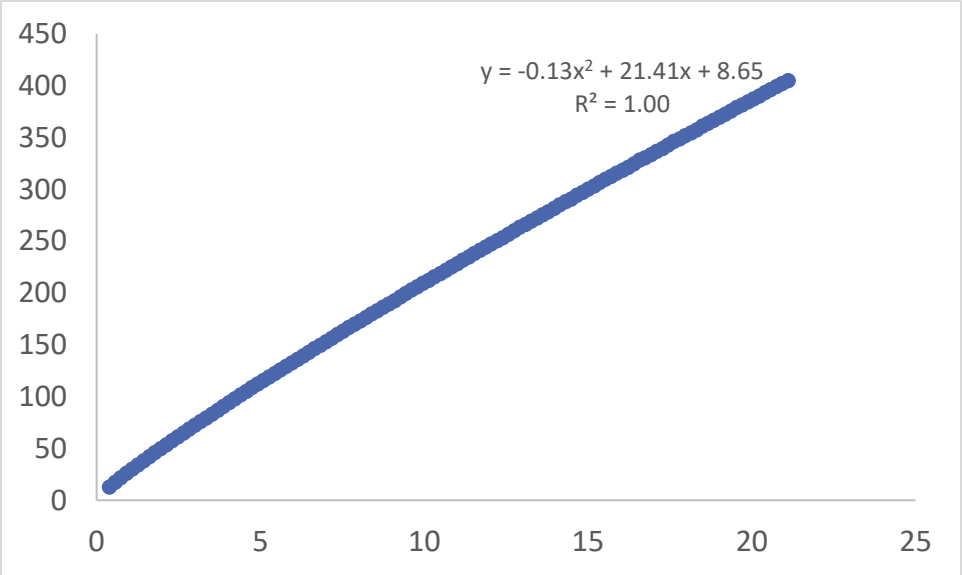

Figure 5-8 Anton Paar flow curve for the shear rate range of the contec 6 at cold temperature.

As the shear rate range increases, the measured yield stress increases as a result of extrapolation, and the plastic viscosity decreases. A clear example is shown in Table 5-1 from the Anton Paar readings. At low shear rate ranges (from .65 to 3.90 s^{-1}) the ratio of c/μ is high in absolute value. Oppositely, when the shear rate range is high (from .41 to 21.31 s^{-1}) the ratio of c/μ is low. What is potentially indicating that the material can have a multi-behavior? As seen in Figure 5-9 at shear rates above approx. 6 s^{-1} the material has a "linear" evolution with shear rate.

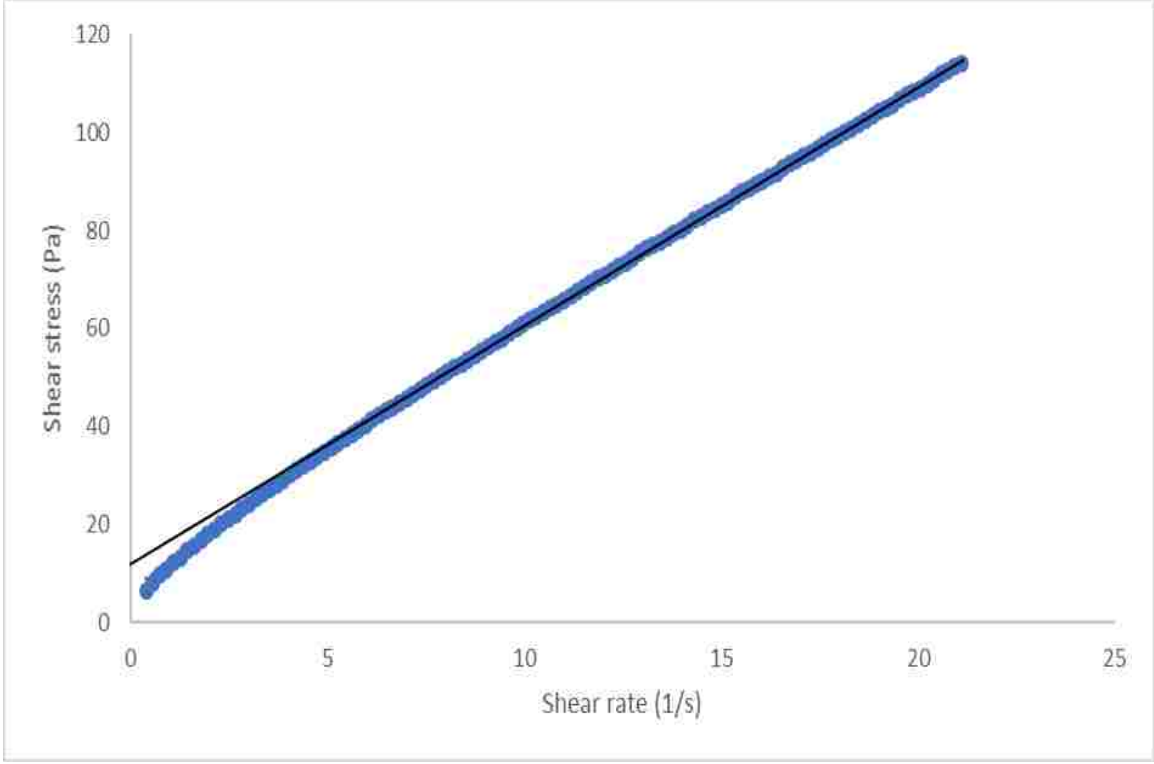

Figure 5-9 Multi-behavior of reference material measured in Anton Paar (shear rate to match contec 6, room temperature).

Table 5-1 Rheological variations with shear rate range.

SHEAR RATE (1/s)		TO MATCH	Rheological properties		temperature C°	c/μ
FROM	TO		YS(Pa)	PV(Pa.s)		
3.9	0.65	ICAR	7.41	6.02	20.40	-0.132
6.77	0.3	Contec5w	7.37	5.76	20.50	-0.061
13.16	0.43	Contec5S	8.27	5.29	20.50	-0.038
21.13	0.41	Contec6	9.25	5.04	20.40	-0.022

5.1.2.5. ICAR rheometer does not show adequate data. One possible reason is the precision of the ICAR. Even if the "noise" for the readings was high, a good fit to a linear equation was obtained (Figure 5-10, Figure 5-11). Due to a high plastic viscosity, a negative reading of the yield stress was obtained which is physically impossible.

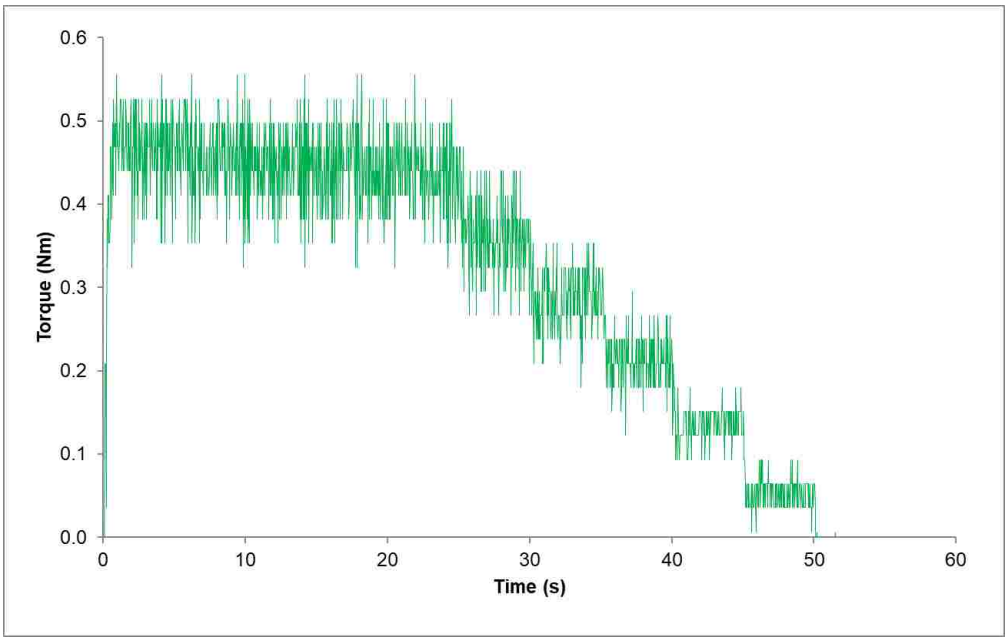

Figure 5-10 Torque vs time 7 step configuration for ICAR.

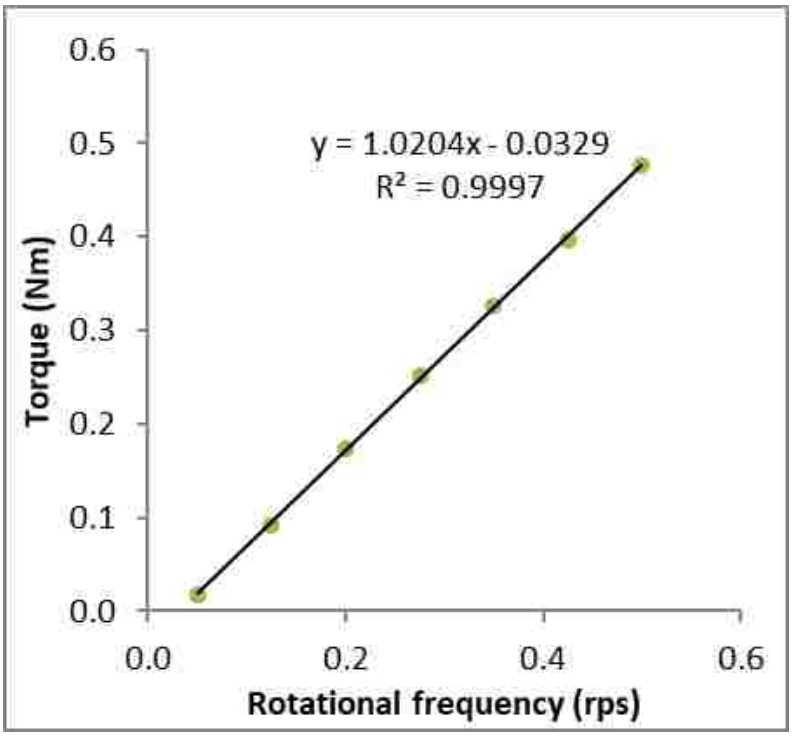

Figure 5-11 Torque vs speed from ICAR.

5.2. RHEOMETERS TRANSFORMATION EQUATIONS

An initial attempt to find direct equations to transform the data from one rheometer to another was performed. However, small differences were found since the material is shear dependent and all rheometers work at a different shear rate range. The system works as follows: a linear equation y = mx+b in imposed where y = output (rheometer Y), m and b are constants and x = input (rheometer X). These constants were obtained by fitting a linear equation between the values of plastic viscosity and yield stress for each rheometer. Table 5-2 (in yellow) demonstrates an example where inversing the equation delivered a slightly different value for the relationship between contec 6 and ICAR rheometers. As shown in

Table 5-2 Direct transformation attempt.

Plastic Viscosities(pa/s)			
ICAR to Anton Paar			
Output	m	Input	b
19.99788	1.3748	15.7366	-1.6368
ICAR to Contec 6			
Output	m	Input	b
11.3962	0.5382	20	0.6322
ICAR to contec 5S			
Output	m	Input	b
13.9118	0.6985	20	-0.0582
Anton paar to Contec 5W			
Output	m	Input	b
15.58769	0.7807	20	-0.02631

Plastic Viscosities(pa/s)			
Contec 6 to Anton Paar			
Output	m	Input	b
19.94902	1.5589	13.418	-0.9683
Contec 6 to ICAR			
Output	m	Input	b
19.69666	1.7957	11.3962	-0.7675
CONTEC 6 to contec 5S			
Output	m	Input	b
25.6379	1.2859	20	-0.0801
Contec6 to Contec 5W			
Output	m	Input	b
27.3824	1.4172	20	-0.9616

A way to avoid this issue is to utilize a “2 step transformation”. Where first the “Input” rheometer measurement is transformed to the Anton Paar (both in the same shear rate range) and then from the Anton Paar to desired rheometer “Output” (both in the same shear rate range as well).

5.2.1. Plastic Viscosity Transformation Equations. by comparing plastic viscosities measured within the rheometers and the rheological properties from the Anton Paar that work at the same shear rate range. The following equations were developed to compare within rheoeters. Utilizing the rheomers in the “x” axis and the anton paar in the “y” axis as shown in Figure 5-12 and Figure 5-13.

STEP 1			
Plastic Viscosities(pa/s)			
Anton paar to ICAR			
Output	m	Input	b
	0.7271		1.1946
Anton paar to Contec 6			
Output	m	Input	b
	0.6384		0.65
Anton paar to contec 5			
Output	m	Input	b
	0.6381		0.617
Anton paar to Contec 5W			
Output	m	Input	b
	0.6408		0.5747

Figure 5-12 Transformation equations step 1.

Step 2			
Plastic Viscosities(pa/s)			
ICAR to Anton paar			
Output	m	Input	b
	1.3748		-1.6368
Contec 6 to Anton paar			
Output	m	Input	b
	1.5589		-0.963
contec 5 to Anton paar			
Output	m	Input	b
	1.5633		-0.9372
Anton paar to Contec 5W			
Output	m	Input	b
	1.5587		-0.8816

Figure 5-13 Transformation equations step 2.

5.2.2. Yield Stress Transformation Equations. Unfortunately, after trial and error yield stress transformations in these experiments are not applicable for ICAR rheometer see Figure 5-14 and Figure 5-15. Since negative values of yield stress where

frequently found every time a transformation that involves the ICAR was performed. The transformation procedure is exactly the same as mentioned in 5.2.1. As such, since the values of the yield stress of the measurements at room temperature in the ICAR rheometer were in the same range as in the ConTec 5W, the yield stress for the ICAR is assumed to follow the yield stress of the ConTec 5W.

Step 1			
Yield Stress (Pa)			
Anton paar to Contec 6			
Output	m	Input	b
	0.8241		0.9992
Anton paar to contec 5			
Output	m	Input	b
	0.724		-1.4267
Anton paar to Contec 5W			
Output	m	Input	b
	0.5223		0.9837

Figure 5-14 Yield stress transformation equations Step 1.

step 2			
Yield Stress (Pa)			
Contec 6 to Anton Paar			
Output	m	Input	b
	1.1836		1.4963
contec 5 to Anton paar			
Output	m	Input	b
	1.0224		4.3096
Contec 5W to Anton paar			
Output	m	Input	b
	0.2798		7.1482

Figure 5-15 Yield stress transformation equations Step 2.

6. LUBRICATION LAYER

This section summarizes an attempt to understand the composition of the lubrication layer. The methodology was previously explained in 4.2.3.

6.1. KRIEGER-DOUGHERTY-STYLE CURVES

For each of the pastes and the mortars prepared for this task, a sample was measured quickly in the contec 6 rheometer to determine yield stress and plastic viscosity, one last measurement was performed at the end and a linear evolution over time to be used as a base. The procedure does not include an extensive pre-shear and is using shorter steps than what is typical. This was chosen, in combination with hand-mixing the sand, to minimize the exposure of the paste to higher shear rates compared to the shear rate from the mixer. As discussed in conjunction with Table 3-1, not controlling the shear rate in the paste can deliver non-expected results.

Relative plastic viscosity is plotted as a function of sand volume fraction as shown in Figure 6-1. Following Krieger Dougherty style curves while measurement was valid. This was determined by dividing the plastic viscosity of the mortar by the interpolated plastic viscosity of the paste at the time that the test was performed. This is performed assuming that the plastic viscosity of the paste evolves linearly as shown in Figure 4-15.

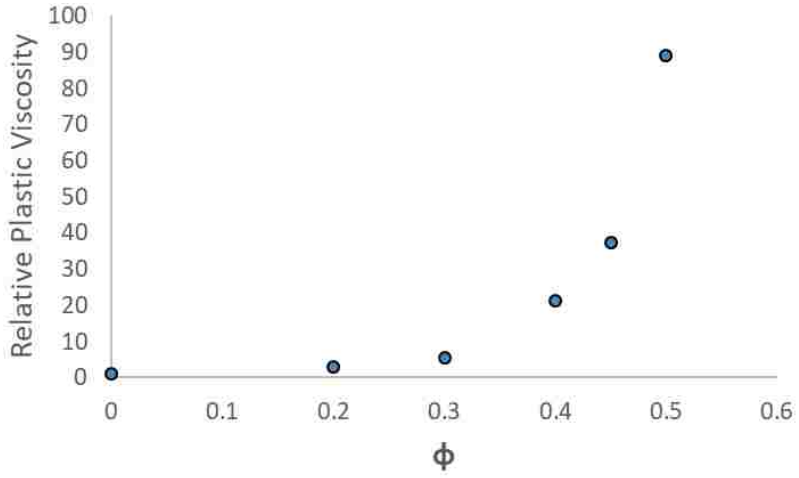

Figure 6-1 Relative plastic viscosity vs volume fraction on the sand portion that passes sieve #8.

The relative yield stress is determined in the same fashion using the Chateau–Ovarlez–Trung model. As shown in Figure 6-2

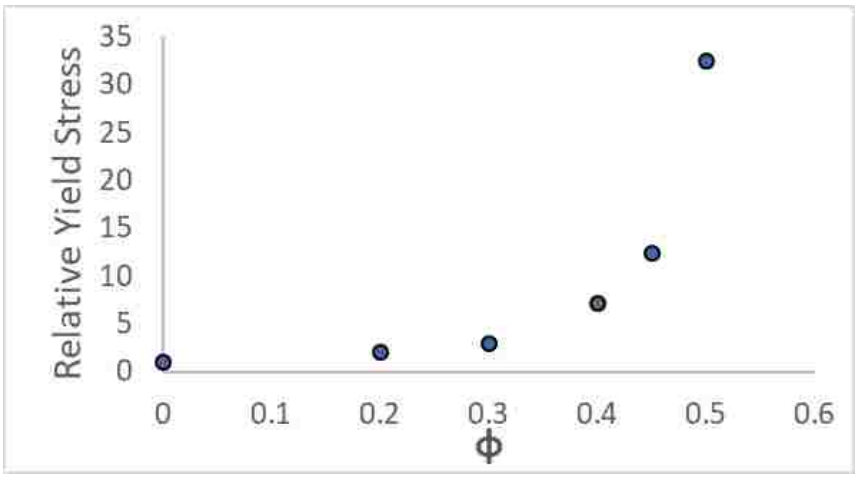

Figure 6-2. Relative yield stress vs volume fraction on the sand portion that passes sieve #8.

The same analysis was performed for every portion sieved (#8, #16, #30, and #50). As shown in Figure 6-3 and Figure 6-4, relative yield stress and plastic viscosity increases dramatically at lower volume fraction ranges as the average particle size decreases.

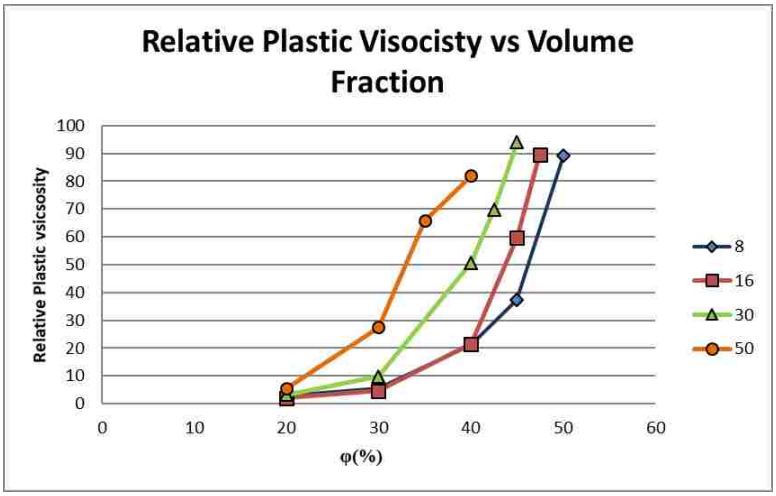

Figure 6-3 Comparison of plastic viscosity amplification with volume fraction.

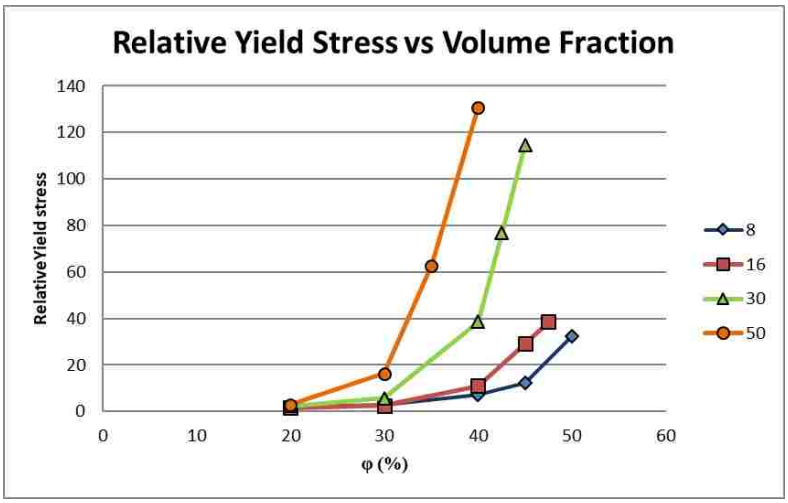

Figure 6-4 Comparison of yield stress amplification with volume fraction.

6.2. DETERMINATION OF INTRINSIC VISCOSITY AND φm

In order to determine the intrinsic viscosity, φm (volume necessary to reach friction) and φmax, an iterative procedure was utilized to minimize the differences between measured rheological properties(shown in green) and calculated rheological properties(shown in white on Table 6-1). Since relative plastic viscosity and relative yield stress were known (measured), volume fraction was set, calculated relative viscosities were calculated using the Krieger-Dougherty equation as shown in Table 6-2 and Figure 6-6, while the relative yield stress used the Chateau–Ovarlez–Trung model as shown in Table 6-1 and Figure 6-5. A summary of obtained results with each parameter is shown in Table 6-3.

Table 6-1 Example of determination of φm and intrinsic viscosity using Chateau–Ovarlez–Trung model.

Portion Sieved by #8			**OUTPUT**
		φ_m	0.565079844
INPUT		intr. V	6.273550231
φ	Relative Yield Stress (Pa)	Calculated Yield Stress (Pa)	SQ difference
0	1	1	0
0.2	2.037	1.940	0.00227843
0.3	2.968	3.201	0.006130708
0.4	7.201	6.860	0.00223849
0.45	12.437	12.451	1.22816E-06
0.5	32.462	32.606	1.96662E-05
			0.011

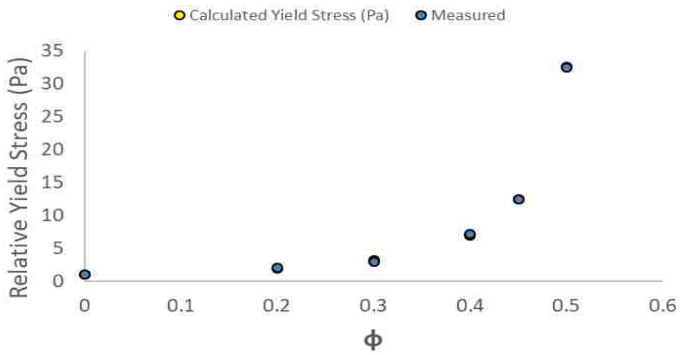

Figure 6-5 Relative yield stress evolution with volume fraction.

Table 6-2 Example of determination of φmax and intrinsic viscosity using Krieger-Dougherty equation.

Portion Sieved by #8			OUTPUT
		phimax	0.627965177
INPUT		intr. V	4.532274174
φ	Relative Plastic (Pa.s)	Calculated K-D (Pa.s)	SQ difference
0	1	1	0
0.2	2.927	2.978204978	0.000304709
0.3	5.590	6.351992988	0.018557841
0.4	21.211	17.88460644	0.024598385
0.45	37.316	36.18524683	0.000918383
0.5	89.081	92.51615548	0.001486672
			0.046

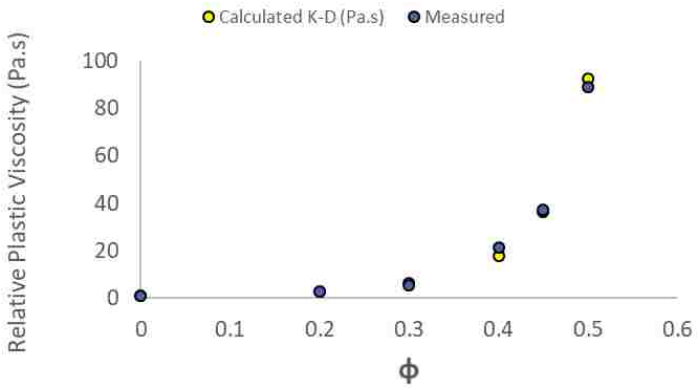

Figure 6-6 Relative plastic viscosity evolution with volume fraction.

Table 6-3 Summary of parameters per sieved portion.

Portion Sieved by.	Yield stress		Plastic viscosity	
	φm	Intrinsic viscosity	φmax	Intrinsic viscosity
8	0.565	6.274	0.628	4.532
16	0.511	6.011	0.579	4.519
30	0.501	9.019	0.591	5.509
50	0.455	12.378	0.494	7.051

It was observed that, as the average particle size decreases the volume required to cause friction decreases, the maximum volume fraction decreases, and the intrinsic viscosity increases. Intrinsic viscosities have values from 4.532-12.378 while literature has reported values from 5-6 for cement-based materials.

6.3. ESTIMATION OF THICKNESS OF EACH THEORETICAL LAYER

The approach to the estimation of the thickness of the lubrication layer was performed by comparing the evolution from paste through concrete by adding particles and performing rheological/tribological measurements as follows:

Measure the rheological properties of paste: using the Anton Paar rheometer. Analyze the grain size distribution from Table 4-5 and estimate the volume fraction that passes through each sieve. (i.e Mix design has 10 liters of paste and 10 liters of sand. 10% of the sand passes sieve #30 (1 liter). The volume fraction of sand is 1 /11 (10 from paste + 1 from sand); this procedure is applied to all available sieves.

Measure the rheological properties of concrete (using ConTec 5W concrete configuration), then measure interface rheology of the concrete (using ICAR).

Use the transformation equations between rheometers developed in section 5 to transform paste and concrete measurements to the ICAR rheometer. Note: For paste values, based on Figure 5-3, no transformation is required since for values lower than 5 Pa.s, as the correlation between ICAR and Anton Paar is close to 1:1. But, the extrapolation in such low values will result in an exaggerated plastic viscosity as a 5-10 times higher than the measurement by other rhemoeters which makes an extra big change. And since shear thinning behavior of the material and such different shear rate ranges of rheometers where used, yield stress transformations where decided not to be used.

Based on previous measurements, the rheological properties of each mortar layer can be calculated since volume fraction and paste rheology is known.

A theoretical model with 7 layers was developed, starting with paste, mortar of different particle sizes and concrete at the end as shown in Figure 6-8. In a hypothetical interface rheometer, with known rheological properties of each layer and for each torque value measured, the velocity difference within each layer can be calculated. Summing all velocities over all layers delivers the velocity difference between inner and outer cylinder. Now, the optimal thickness of each layer can be calculated to get as close as possible to each T-N point from the interface rheometer, as shown in Figure 6-7. In these calculations, if a layer was fully in plug flow, there was no contribution to velocity. If the layer was partially in plug flow, the layer's velocity was adjusted to take this into consideration. Calculations are shown in Table 6-4.

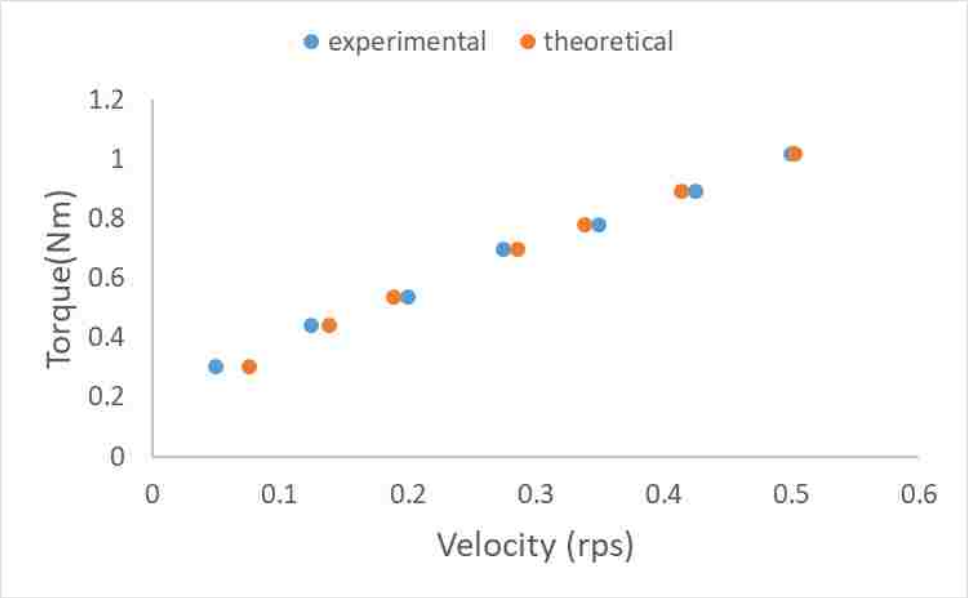

Figure 6-7 Torque vs rotational velocity profile.

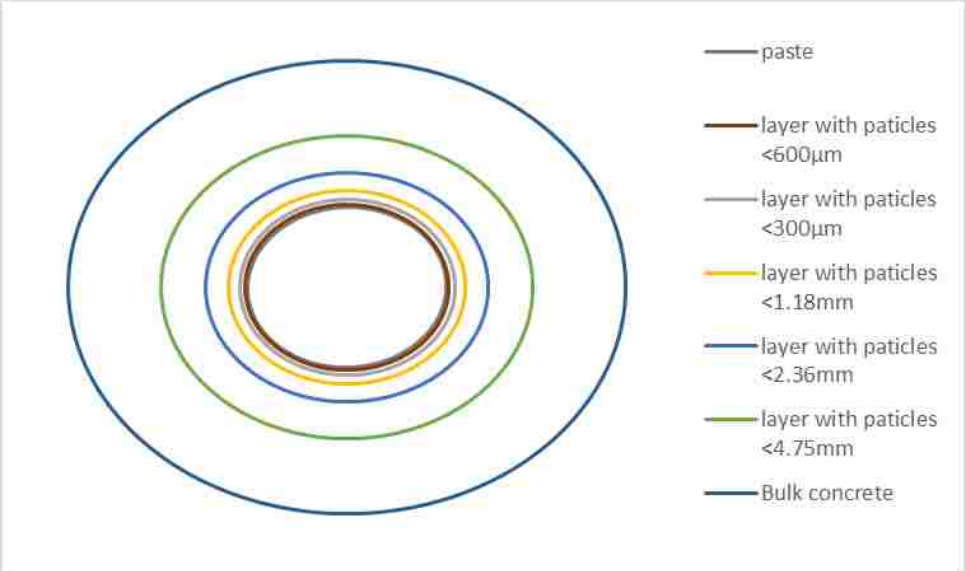

Figure 6-8 Theoretical thicknesses of each layer in the lubrication layer.

Table 6-4 Example 1. Calculations performed to obtain thicknesses of each layer. Torque and velocity of tribometer (yellow), rheological properties of each layer (red) and determination of optimal thickness in (light blue).

Step 1. Measured properties									
			Ri	Ri+2	Ri+3	Ri+4	Ri+5	Ri+6	Ri+7
Torque (Nm)	Velocity	YS (Pa)	0.720	1.253	1.620	1.874	4.181	12.389	39.659
		PV (Pa.s)	0.130	0.256	0.377	0.632	1.877	6.629	33.477
0.897	0.500	Rp	0.996	0.755	0.664	0.617	0.413	0.240	0.134
0.784	0.424		0.931	0.706	0.621	0.577	0.386	0.224	0.125
0.614	0.350		0.824	0.624	0.549	0.511	0.342	0.199	0.111
0.487	0.275		0.733	0.556	0.489	0.455	0.304	0.177	0.099
0.370	0.200		0.640	0.485	0.426	0.397	0.265	0.154	0.086
0.216	0.125		0.489	0.371	0.326	0.303	0.203	0.118	0.066
0.081	0.050		0.299	0.227	0.199	0.185	0.124	0.072	0.040
		Step2. Determination of plug flow at Inner Radius							
		plug flow	0.063	0.063	0.063	0.063	0.063	0.063	0.063
		at Ri?	0.063	0.063	0.063	0.063	0.063	0.063	0.063
			0.063	0.063	0.063	0.063	0.063	0.063	0.063
			0.063	0.063	0.063	0.063	0.063	0.063	0.063
			0.063	0.063	0.063	0.063	0.063	0.063	0.063
			0.063	0.063	0.063	0.063	0.063	0.063	0.063
			0.063	0.063	0.063	0.063	0.063	0.063	0.000
		Step 3. Determination of plug flow at Outer Radius							
N/A	N/A	plug flow	0.063	0.063	0.063	0.063	0.063	0.063	0.134
		at Ro	0.063	0.063	0.063	0.063	0.063	0.063	0.125
			0.063	0.063	0.063	0.063	0.063	0.063	0.111
			0.063	0.063	0.063	0.063	0.063	0.063	0.099
			0.063	0.063	0.063	0.063	0.063	0.063	0.086
			0.063	0.063	0.063	0.063	0.063	0.063	0.066
			0.063	0.063	0.063	0.063	0.063	0.063	0.000
		Step 4. Contribution to speed of each layer							
		Ri	Ri+2	Ri+3	Ri+4	Ri+5	Ri+6	Ri+7	Sum of Velocities (rps)
0.897	0.500	0.342	0.000	0.000	0.000	0.000	0.000	0.195	0.536
0.784	0.424	0.299	0.000	0.000	0.000	0.000	0.000	0.153	0.452
0.614	0.350	0.233	0.000	0.000	0.000	0.000	0.000	0.094	0.327
0.487	0.275	0.185	0.000	0.000	0.000	0.000	0.000	0.055	0.239
0.370	0.200	0.140	0.000	0.000	0.000	0.000	0.000	0.024	0.164
0.216	0.125	0.081	0.000	0.000	0.000	0.000	0.000	0.001	0.082
0.081	0.050	0.030	0.000	0.000	0.000	0.000	0.000	0.000	0.030
		Step5. Optimal thickness (m)							
N/A	N/A	0	0.0625	0.062596	0.062596	0.062596	0.062596	0.062596	0.143
		0.0625	0.062596	0.062596	0.062596	0.062596	0.062596	0.062596	0.143
		N/A	9.60394E-05	0	0	0	0	0	N/A

6.4. RESULTS

After the analysis, two possible scenarios where contemplated: scenario 1 with multiple layers as shown in Figure 6-8. And scenario 2 where only one layer is formed within the lubrication layer. From scenario 1 Table 6-5, illogical values of each layer thickness were obtained for all mixtures (i.e. mixture 0.40 layer formed of particles that pass sieve #30 with a maximum particle size of 600 μm has a calculated "thickness" of 9 μm).

Scenario 2 assumed only one layer within the lubrication layer formed of purely paste. As a result, the mix design with 0.35 w/c resulted in a lubrication layer of 96 μm thick, the 0.4 w/c mixture flowed with a paste layer of 123 μm and the 0.40 w/c mixture with fly ash had a 33 μm thick paste layer as shown in Table 6-6. These values are at least one order of magnitude smaller than what other authors reported [45], this discrepancy can probably be attributed to several errors in the characterization: from the measurement of rheological properties in each rheometer, the potential for particle migration lowering the rheological properties of the concrete, the amplification factors established with the K-D style curves, the comparison of the rheometers, etc.the proposed technique is not suitable to calculate the lubrication layer composition and thickness.

Table 6-5 Scenario 1 radius of each layer within the lubrication layer.

layer formed of	paste	#50	#30	#16	#8	#4	concrete
max particle size (m)	0.000075	0.0003	0.0006	0.00118	0.00236	0.00475	0.0095
W/C	Ri	Ri+2	Ri+3	Ri+4	Ri+5	Ri+6	Ri+7
0.35 radius (m)	0.062500	0.062596	0.062596	0.062596	0.062596	0.062597	0.062597
0.40 radius (m)	0.062500	0.062500	0.062500	0.062509	0.062510	0.062510	0.071743
.40 FA radius (m)	0.062500	0.062500	0.062536	0.062570	0.062584	0.062594	0.062594

Table 6-6 Scenario 2 radius of each layer within the lubrication layer.

layer formed of	paste	#50	#30	#16	#8	#4	concrete
max particle size(m)	0.000075	0.0003	0.0006	0.0018	0.00236	0.00475	0.0095
W/C	Ri	Ri+2	Ri+3	Ri+4	Ri+5	Ri+6	Ri+7
0.35 radius (m)	0.062500	0.062596	0.062596	0.062596	0.062596	0.062596	0.062596
0.40 radius (m)	0.062500	0.062623	0.062623	0.062623	0.062623	0.062623	0.062623
.40 FA radius (m)	0.062500	0.062533	0.062533	0.062533	0.062533	0.062533	0.062534

7. PUMPING CAMPAIGN

This section presents and discusses the results obtained through the experimental pumping campaign previously described in section 4. Properties discussed are oriented on the changes (Δs) before and after pumping to focus on the pumping influence. Differences analyzed include plastic viscosity, yield stress, air content, sieve stability, slump/slump flow and "I_{trib}" as an indication of interface flow resistance.

Pumping is a process that induces high shearing into concrete that can produce unknown changes, especially if the shear stress applied when pumping is higher than the shear stress applied when mixing [50].

The shear stress in a circular pipe evolves linearly from zero at the center and maximum at the wall. The type of flow inside a pipe depends on 2 parameters: shear stress (related to the pressure loss) and the yield stress which is a property of the concrete mixture. If the mixture has a CVC behavior, it is more likely to have a "plug flow" (phase 1 Kaplan's model) and it is believed that only the lubrication layer near the wall is being sheared. In the case of SCC, since the yield stress is low, it is believed that shearing occurs inside the pipe (phase 2 Kaplan's model), where not only the lubrication layer near the wall is affected, but part of the bulk concrete as well.

7.1. ANALYSIS STRATEGY

All changes in properties where reported relative to the non-pumped samples directly from the truck, concrete evolution over time was assumed as follows:

If the middle test value was not between before and after test; use bilinear (Figure 7-1)

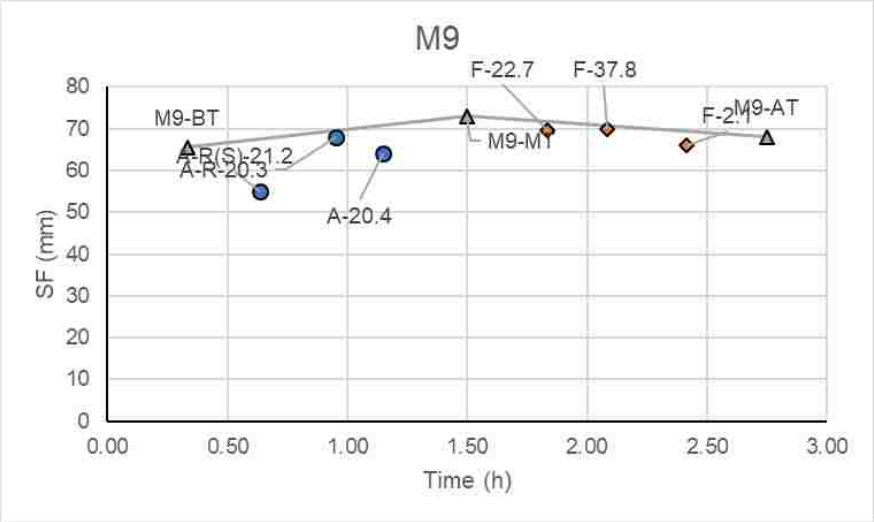

Figure 7-1 Slump flow bilinear example.

If the middle test is between before and after and within 25 % of a difference with before or after; use bilinear. (Figure 7-2)

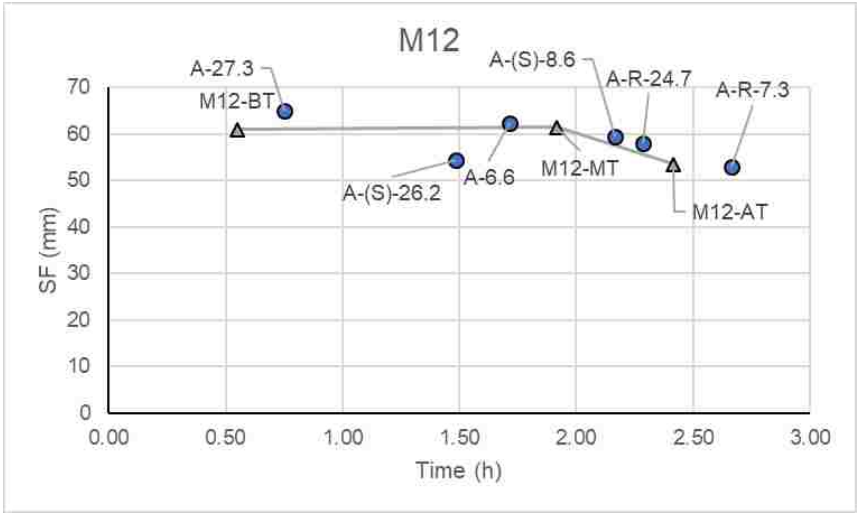

Figure 7-2 Slump flow bilinear example.

If the middle test value is between before and after test, and has at least 25% of difference with any end, use linear. (Figure 7-3)

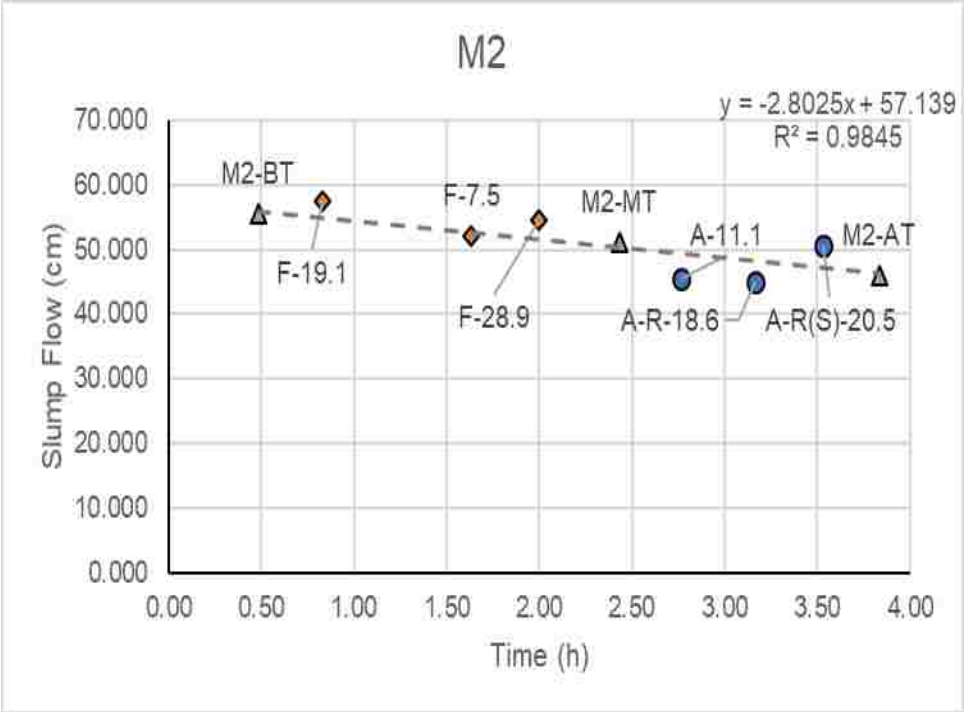

Figure 7-3 Slump flow linear example.

From Table 7-1, tolerance is defined as: 25% of the difference between before and after measurements; max value (red) = before measurement – tolerance. While min value (red) = after reading + tolerance. Middle test value (yellow) must be between max and minimum to be considered linear.

Table 7-1 Example of determination of the evolution of concrete over time.

equation	ID	Slump/Slump flow (cm)	Tolerance (cm)	max	min	Result
1	M1-BT	59.0	N/A	N/A	N/A	N/A
	M1-AT	51.5				
2	M2-BT	55.5	2.4	53.1	48.4	Linear
	M2-MT	51.0				
	M2-AT	46.0				
3	M3-BT	48.0	1.0	47.0	45.0	Bilinear
	M3-MT	52.0				
	M3-AT	44.0				
4	M4-BT	49.0	1.3	47.8	45.3	Bilinear
	M4-MT	45.0				
	M4-AT	44.0				
5	M5-BT	13.0	2.5	10.5	5.5	Bilinear
	M5-MT	3.5				
	M5-AT	3.0				
6	M6-BT	57.5	2.6	54.9	49.6	Bilinear
	M6-MT	48.5				
	M6-AT	47.0				
7	M7-BT	79.0	1.9	77.1	73.4	Bilinear
	M7-MT	70.5				
	M7-AT	71.5				
8	M8-BT	71.0	2.6	68.4	63.1	Linear
	M8-MT	67.0				
	M8-AT	60.5				
9	M9-BT	65.5	0.6	64.9	68.6	Bilinear
	M9-MT	73.0				
	M9-AT	68.0				
10	M10-BT	79.0	5.1	73.9	63.6	Linear
	M10-MT	65.0				
	M10-AT	58.5				
11	M11-BT	69.0	3.4	65.6	58.9	Bilinear
	M11-MT	74.0				
	M11-AT	55.5				
12	M12-BT	61.0	1.9	59.1	55.4	Bilinear
	M12-MT	61.0				
	M12-AT	53.5				
13	M13-BT	44.5	1.6	42.9	39.6	Bilinear
	M13-MT	45.0				
	M13-AT	38.0				
14	M14-BT	68.5	3.6	64.9	57.6	Bilinear
	M14-MT	67.0				
	M14-AT	54.0				
15	M15-BT	78.0	0.8	77.3	75.8	Bilinear
	M15-MT	79.0				
	M15-AT	75.0				
16	M16-BT	69.0	2.0	67.0	79.0	Bilinear
	M16-MT	71.0				
	M16-AT	77.0				

Flow rate categories were assigned according to available data. “Slow” pumping flow was assigned to those mixtures pumped with a flow rate below 8 l/s. “Medium” pumping flow was assigned to those mixtures pumped between 8 l/s and 25 l/s and “fast” pumping flow was assigned to those mixtures pumped above 25 l/s.

7.2. INFLUENCE OF PUMPING PARAMETERS ON ΔI_{trib}.

I_{trib} term represents the slope of the T-N diagram obtained using the interface rheometer. It is an indicator of the resistance to flow between the smooth cylinder and the concrete. An attempt to correlate the change of I_{trib} with pumping parameters and mix design, was performed. Interface properties, such as yield stress and viscous constant were hard to derive seen some of the issues encountered with determining the rheological properties of the concrete on-site.

ΔI_{trib}, which is the change in I_{trib} caused by pumping, initially appears to be independent of the flow rate, as shown in Figure 7-4. This does not correlate with other authors [50]. However, there are 4 parameters at the same time playing a role. As a result, a cloud is shown. The solution to this problem is to individualize each parameter and observe its own influence. For that, the mixtures where compared with mixtures within the same flow rate and separated in 2 groups M1-M10 and M11-16. For the first group, pumping in A configuration was done only at medium speed (which was taken as a reference), while for the second group, the A configuration was used at fast and slow speeds (used as reference as well), but no pumping was done in flat configuration.

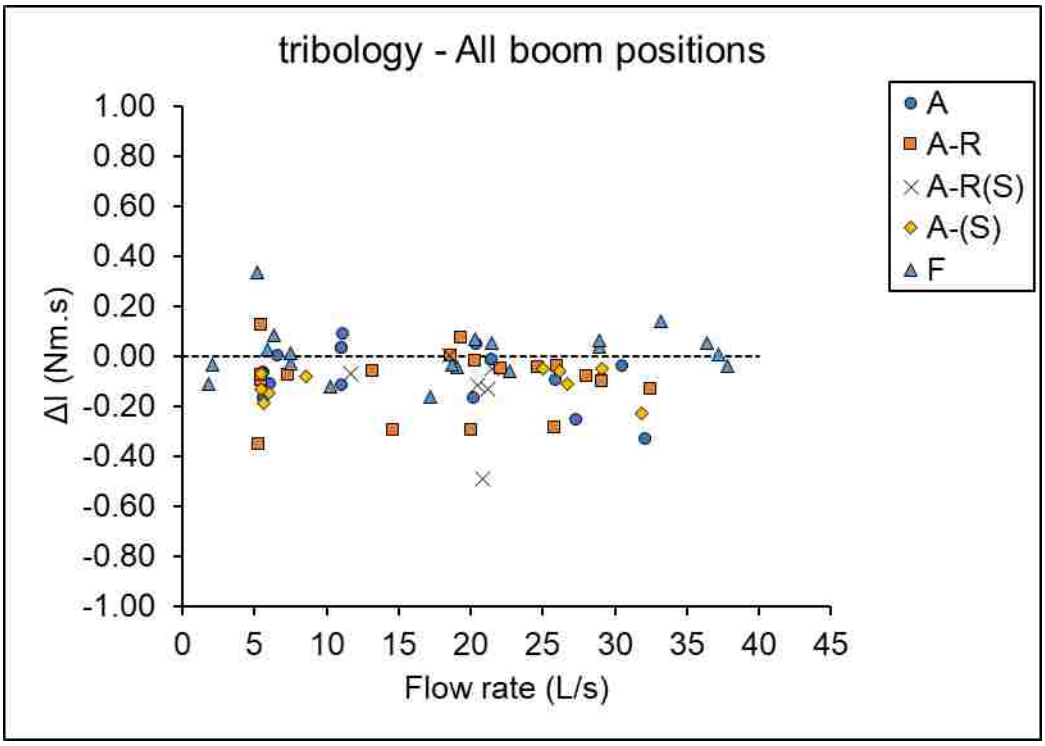

Figure 7-4 Change in I_{Trib} vs flow rate.

7.2.1. Influence of Reducer and Submerging the Boom for Mixtures M1-M10.

ΔItrib changes for the reducer (A-R) and submerging the boom with the reducer (A-R-S) were compared to ΔItrib changes in the same boom position without submerging and without reducer (A) are shown in Figure 7-5

The results explain that the resistance to flow in the interface rheometer decreases more when a reducer is utilized, compared to the standard A configuration. This is expected since a reducer will increase the velocity, increasing the shearing in concrete. This can potentially result in an increased cement dispersion. Additionally, it seems that the effect is amplified when submerging the hose. However, this was not observed for mixture M8.

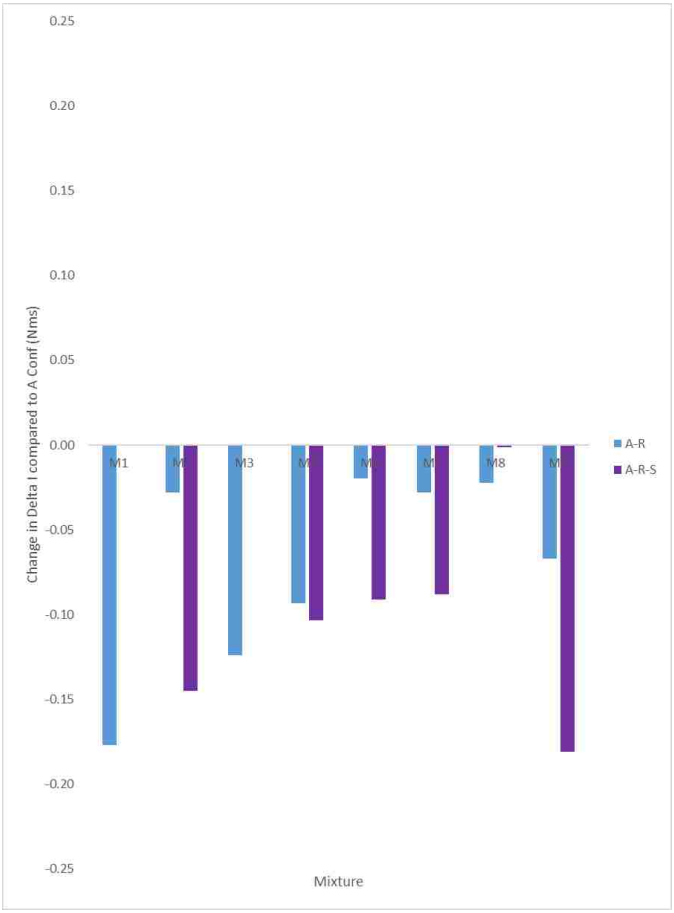

Figure 7-5 ΔI_{trib} changes from A-R and A-R-S compared to A configuration.

7.2.2. Influence of Boom Position for Mixtures M1-M10. ΔI_{trib} changes in F configuration were compared to ΔI_{trib} changes in "A" boom position and are shown in Figure 7-6. Concrete likely experiences a different pressure when it is pumped horizontally in "F" boom position. However, this change in pressure compared to the A configuration is not straightforward, as it should be dependent on how much the downward pipe in the A configuration is filled. From the tested data, no uniform conclusion can be reported.

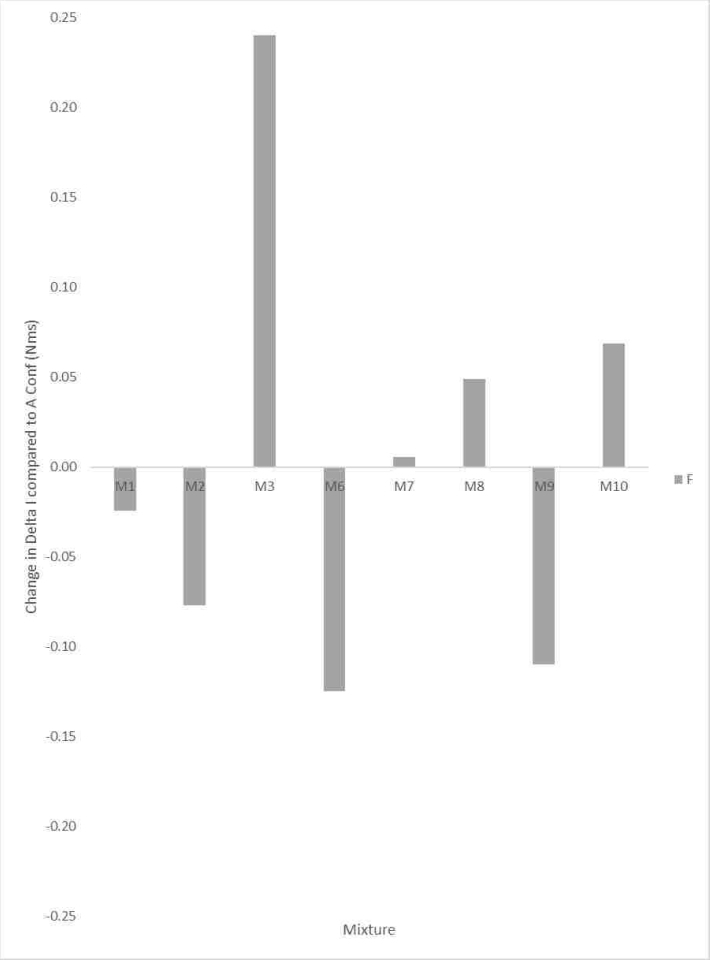

Figure 7-6 ΔI_{trib} changes from "F" configuration compared to A configuration.

7.2.3. Influence of Flow Rate in Flat Position for Mixtures M1-M10. The effect of varying the flow rate on ΔI_{trib} in the F configuration is shown in Figure 7-7. A reduction of ΔI_{trib} was expected when decreasing the flow rate while keeping geometry constant, as that would be accompanied by a decrease in velocity and the shear rate in the concrete. But on the other hand, increased velocity can increase temperature which is known to increasing cement hydration. Unfortunately, tested data led to no uniform

conclusion. It seems that the concrete increases in flow resistance due to pumping in more cases than it sees a decrease.

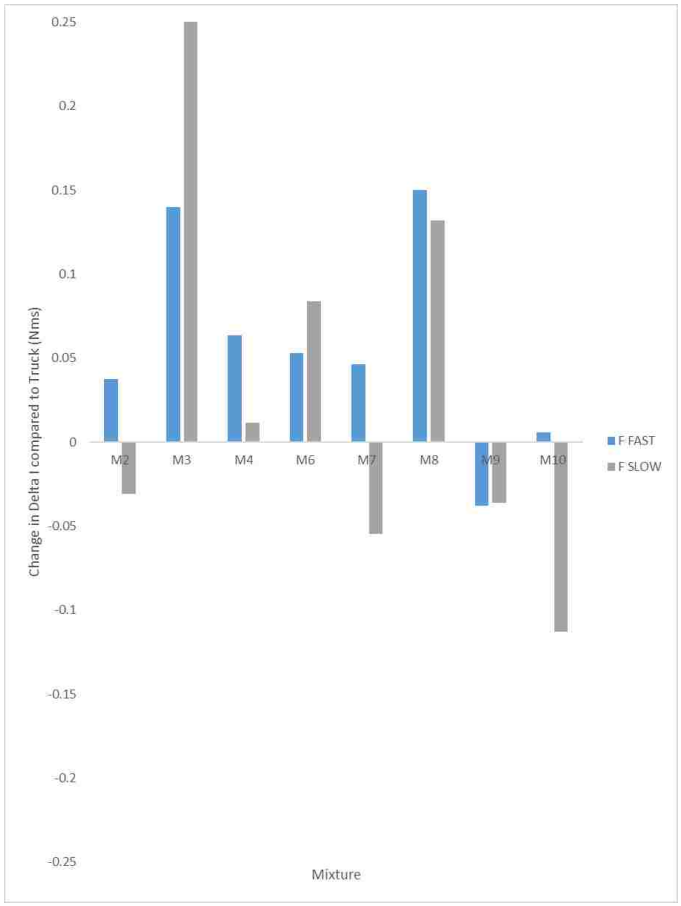

Figure 7-7 ΔI_{trib} changes from "F" configuration: fast vs slow flow rate.

7.2.4. Influence of Reducer and Submerging the Boom for Mixtures M11-M16. The influence of reducer and reducer while submerged was determined in the same fashion as 7.2.1.

The difference is that only medium flow rate was evaluated for mixtures M1-M10, while the A configuration was tested in slow and fast flow rate for mixtures M11-M16.

"A" configuration with a reducer and "A" configuration with a reducer plus submerged in fast pumping category are shown in Figure 7-8. When concrete is pumped in fast flow rate, the effect of a reducer increased the change in ΔI_{trib} for mixtures M12-M15 and decreased it for M11 and M16. The effect of submerging the hose can increase or decrease ΔI_{trib} in an unpredictable manner, although it seems to reduce the observed changes. For slow pumping, the effect of a reducer decreased the change in ΔI_{trib} for mixtures M12 and M13 and increased it for M14 and M15. The effect of submerging the hose can increase or decrease ΔI_{trib} in an unpredictable manner as shown in Figure 7-9.

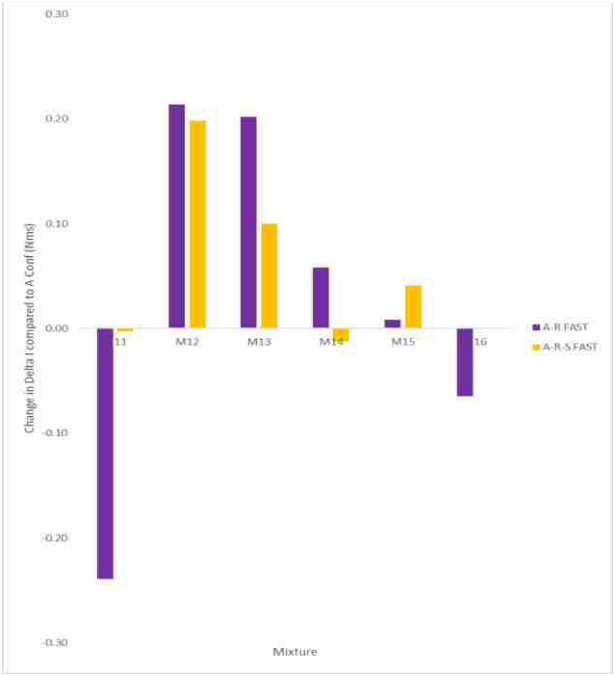

Figure 7-8 ΔI_{trib} changes from A-R and A-R-S configuration in fast flow rate.

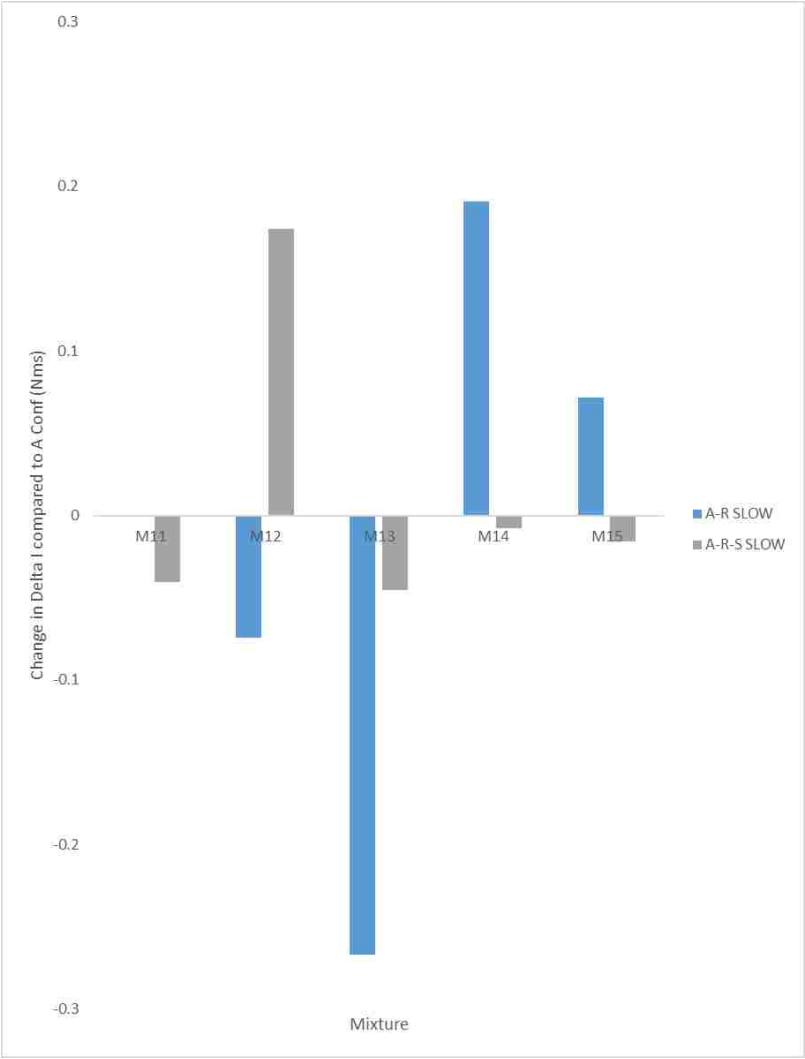

Figure 7-9 ΔI_{trib} changes from A-R and A-R-S configuration in slow flow rate.

7.2.5. Influence of Flow Rate in "A" Boom Position for Mixtures M11-M16.

The influence of flow rate was obtained by comparing the ΔI_{trib} to the truck (before pumping). Influence of flow rate without any reducer is shown in Figure 7-10. Pumping fast increased the changes for mixtures M12-M14 while the changes decreased for M11 and M15. Overall ΔI_{trib} decreased for all mixtures in A configuration as shown Figure 7-11, but the effect of flow rate, reducers and submerging the hose remains unclear.

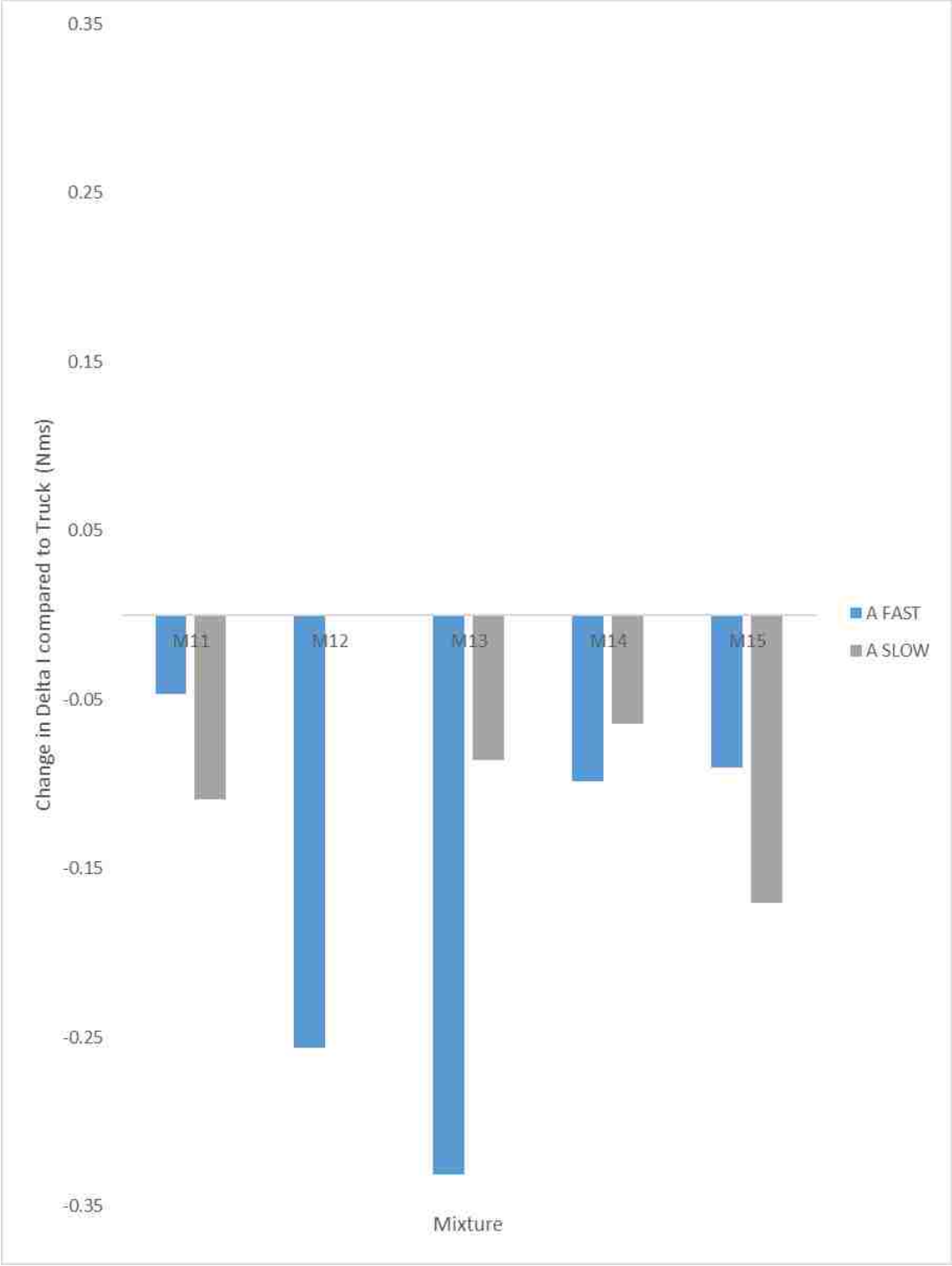

Figure 7-10 ΔI_{trib} changes from "A" configuration in slow vs fast flow rate.

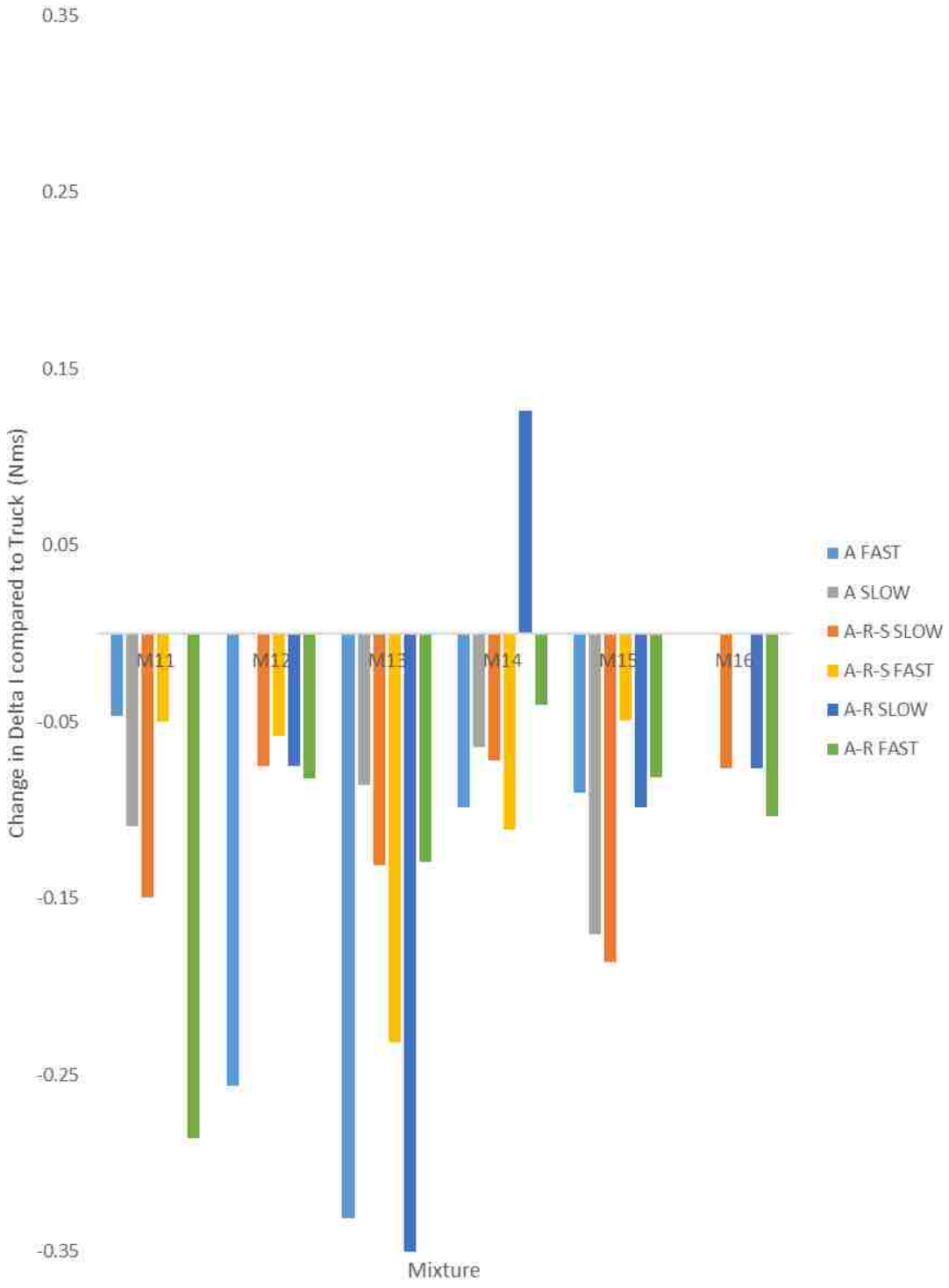

Figure 7-11 ΔI_{trib} changes from all "A" configurations from truck.

7.2.6. Correlation With Rheological Properties For All Mixtures. ΔI_{trib} did show correlation with Δyield stress, as the Δyield stress decreases compared to control test, ΔI_{trib} becomes negative as shown in Figure 7-12.

This contradicts findings from Secrieru et al. [5] who explained that pumping increases yield stress and decreases plastic viscosity from bulk concrete and lubrication layer.

Unfortunately, plastic viscosity changes have a magnitude between -5 to 5 Pa/s (see Figure 7-13) which does not give a very accurate indication of the effect on plastic viscosity, since magnitude of the measurement is similar to the precision of typical concrete viscosity measurements.

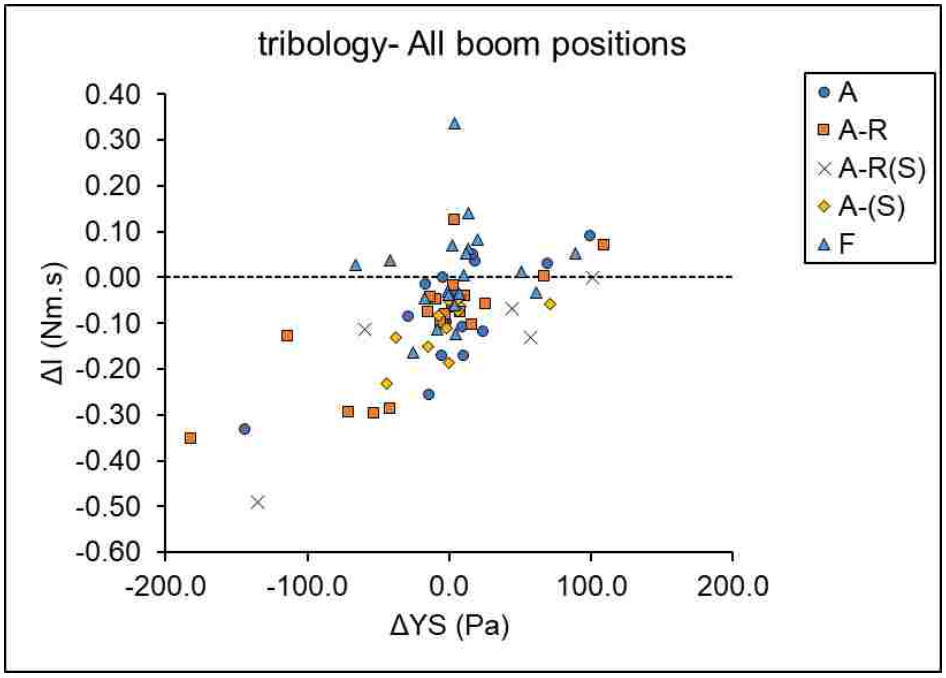

Figure7-12 Change in I_{Trib} vs change in yield stress.

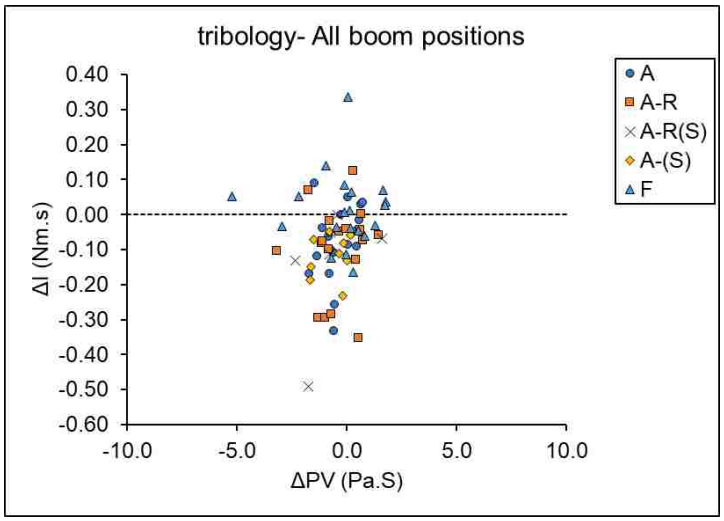

Figure 7-13 Change in I_{Trib} vs change in plastic viscosity.

7.2.7. Correlation With Fresh Concrete Properties. ΔI_{trib} could have a correlation with ΔAir, as when ΔAir increases ΔI_{trib} should decrease. However this is not observed in Figure 7-14 which indicates that the changes in tribology are not dominated by the air content. This correlates with experiments from Secrieru [5] where not all mixtures who gained air due to pumping got a reduction of viscosity parameter of lubrication layer.

An increase in yield stress and decrease in plastic viscosity due to pumping was in bulk concrete was reported from Secrieru [5]. In these experiments as the Δyield stress increases the viscosity coefficient that relates to the lubrication layer ΔItrib increases. This explains that for the evaluated mixtures, Itrib is not negligibly influenced by the yield stress. Figure 7-15 shows the relationship between ΔITrib and Δslump flow. Overall, as the Δslump flow increases ΔITrib decreases and vice versa which correlates with Δyield stress influence from Figure7-12

The change in SSI sieve stability index should correlate with plastic viscosity of bulk concrete. Unfortunately, plastic viscosity parameters are not available for reasons previously explained. ΔSSI does not correlate with ΔI changes, which may reaffirm that the plastic viscosity changes are less or not affected by pumping as shown in Figure7-16

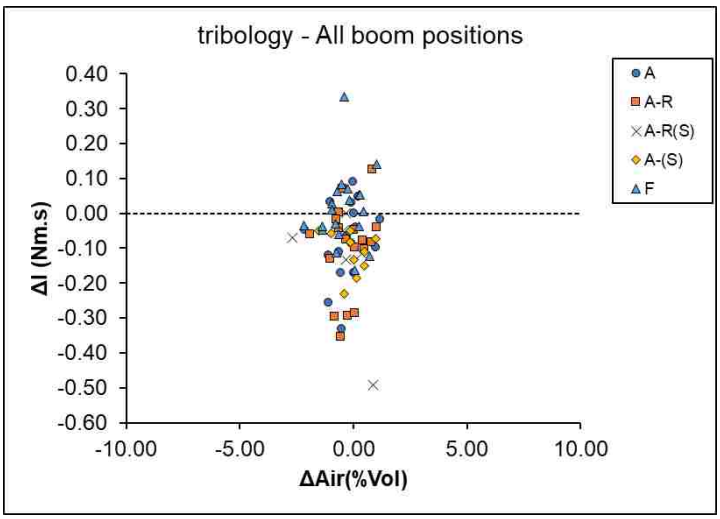

Figure 7-14 Change in I_{Trib} vs change in air content.

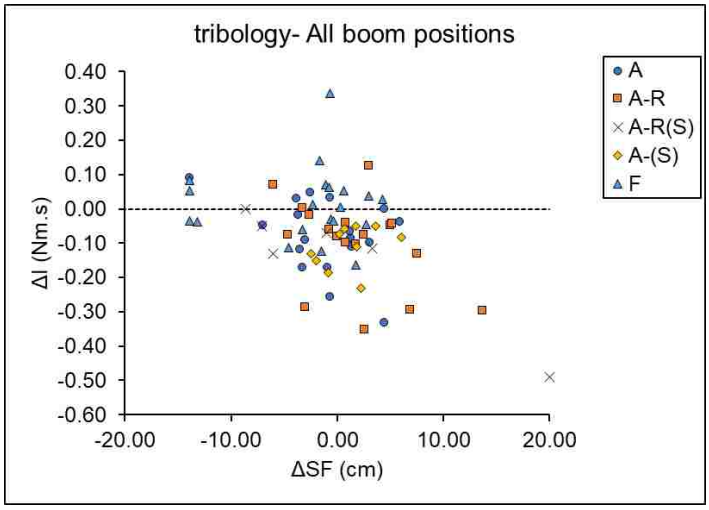

Figure 7-15 Change in I_{Trib} vs change in slump flow.

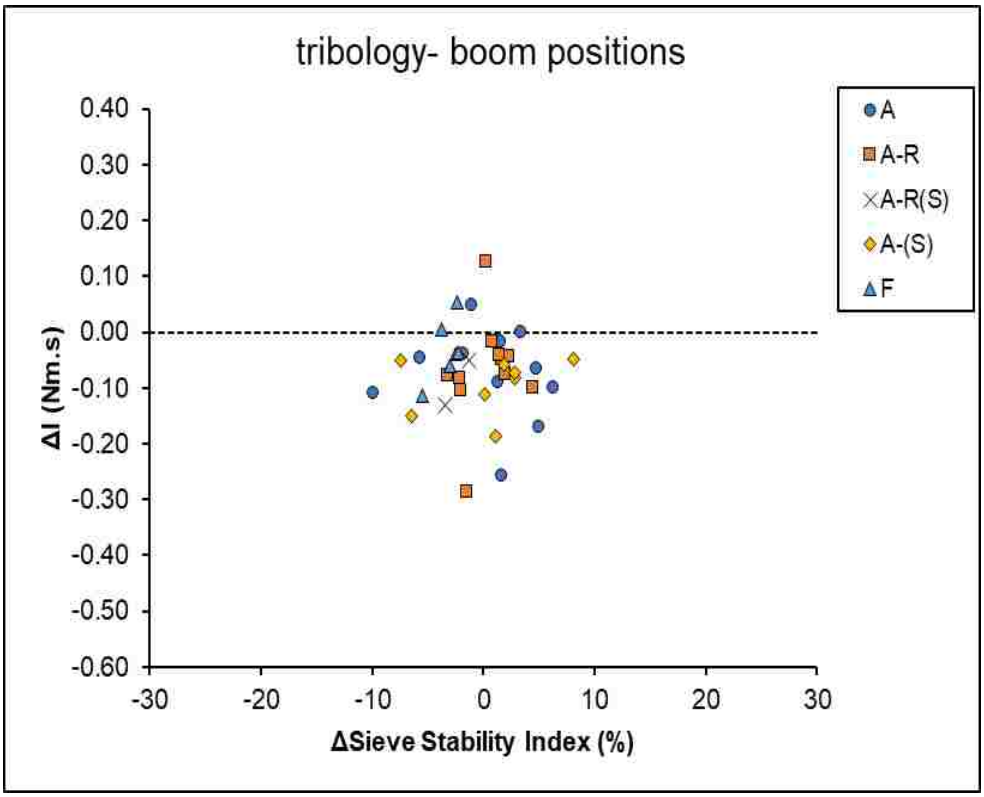

Figure7-16 Change in I_{Trib} vs change in sieve stability index (SSI).

Based on some of the observations in the previous graphs, the average of changes was determined per mixture and divided per boom configuration. It was found that average ΔI_{Trib} was always similar or "more negative" for the A configuration compared to the flat configuration. This gives an indication that the A configuration reduces rheology of the interface more than the flat boom position, as shown in Table 7-2. That can be attributed to the fact that when pumping in A configuration potentially the portion that is dropping may be dropping purely by gravity and that can produce higher shear rates compared to regular flat configuration.

Table 7-2 Change in I_{trib} per boom position F vs A.

Test ID	Boom	Flow rate		I term (Nm.s)			AVERAGE ΔI (Nm.s)		
	position	(l/s)	Time	Test	Truck	ΔI (Nm.s)	BOTH	A	F
M1-A(R)-14.6	A-R	14.6	0.93	0.500	0.796	-0.30			
M1-A-11.1	A	11.1	1.33	0.713	0.832	-0.12		-0.21	
M1-F-10.3	F	10.3	1.97	0.767	0.890	-0.12			
M1-F-17.2	F	17.2	2.35	0.761	0.925	-0.16	-0.18		-0.14
M2-F-19.1	F	19.1	0.83	0.712	0.733	-0.02			
M2-F-7.5	F	7.5	1.63	0.751	0.847	-0.10			
M2-F-28.9	F	28.9	2.00	0.831	0.899	-0.07			-0.06
M2-A-11.1	A	11.1	2.77	0.942	1.009	-0.07			
M2-A(R)-18.6	A-R	18.6	3.15	1.041	1.063	-0.02			
M2-A(RS)-20.5	A-R(S)	20.5	3.53	1.041	1.118	-0.08	-0.06	-0.06	
M3-A(R)-20.8	A-R(S)	20.8	0.55	0.577	1.081	-0.50			
M3-A(R)-20.0	A-R	20.0	0.90	0.799	1.072	-0.27			
M3-A-20.2	A	20.2	1.12	0.938	1.066	-0.13		-0.30	
M3-F-20.3	F	20.3	2.03	1.147	1.041	0.11			
M3-F-33.2	F	33.2	2.32	1.190	1.034	0.16			
M3-F-5.2	F	5.2	2.70	1.349	1.023	0.33	-0.05		0.20
M4-F-5.9	F	5.9	0.32	0.992	0.930	0.05			
M4-F-7.5	F	7.5	0.47	0.975	0.960	-0.02			
M4-F-28.9	F	28.9	0.95	1.025	1.057	-0.04			0.00
M4-A-11.1	A	11.1	1.60	1.104	1.188	-0.08			
M4-A(R)-13.2	A-R	13.2	2.02	1.173	1.271	-0.13			
M4-A(RS)-11.7	A-R(S)	11.7	2.53	1.364	1.375	-0.02	-0.04	-0.08	
M6-F-18.68	F	18.68	0.8	1.38	1.416	-0.033			
M6-F-36.38	F	36.38	1.1	1.57	1.478	0.089			
M6-F-6.37	F	6.37	1.4	1.67	1.525	0.146			0.07
M6-A-11.143	A	11.143	2.0	1.78	1.628	0.138			
M6-A(R)-19.35	A-R	19.35	2.4	1.79	1.699	0.095			
M6-A(RS)-18.535	A-R(S)	18.535	2.7	1.75	1.761	-0.012	0.071	0.07	
M7-A-RS-19.11	A-R(S)	19.1	0.70	0.540	0.581	-0.04			
M7-A-R-22.58	A-R	22.6	1.10	0.540	0.561	-0.03			
M7-A-21.28	A	21.3	1.28	0.540	0.551	-0.01		-0.03	
M7-F-21.09	F	21.1	1.87	0.555	0.522	0.03			
M7-F-38.01	F	38.0	2.13	0.582	0.509	0.07			
M7-F-1.05	F	1.1	2.75	0.545	0.478	0.07	0.02		0.06
M8-F-1.4	F	1.4	0.75	0.625	0.501	0.14			
M8-F-35.56	F	35.6	1.00	0.739	0.556	0.18			
M8-F-21.84	F	21.8	1.20	0.707	0.599	0.09			0.14
M8-A-20.92	A	20.9	1.75	0.754	0.718	0.01			
M8-A-RS-21.09	A-R(S)	21.1	2.03	0.762	0.780	-0.03			
M8-A-R-20.41	A-R	20.4	2.52	0.771	0.885	-0.16	0.04	-0.06	
M9-A-R(S)-21.2	A-R(S)	21.2	0.63	0.436	0.568	-0.14			
M9-A-R-20.3	A-R	20.3	0.95	0.543	0.589	-0.05			
M9-A-20.4	A	20.4	1.15	0.600	0.603	-0.01		-0.06	
M9-F-22.7	F	22.7	1.83	0.552	0.649	-0.10			
M9-F-37.8	F	37.8	2.08	0.613	0.666	-0.05			
M9-F-2.1	F	2.1	2.42	0.667	0.688	-0.02	-0.06		-0.06
M10-F-1.8	F	1.8	0.83	0.388	0.501	-0.12			
M10-F-37.2	F	37.2	1.20	0.517	0.547	-0.02			
M10-F-21.5	F	21.5	1.33	0.575	0.564	0.01			-0.04
M10-A-21.5	A	21.5	2.00	0.598	0.648	-0.05			
M10-A-R-22.1	A-R	22.1	2.33	0.620	0.691	-0.06			
M10-A-R(S)-21.5	A-R(S)	21.5	2.42	0.659	0.701	-0.05	-0.05	-0.05	

7.3. INFLUENCE OF PUMPING ON AIR CONTENT

Hover stated in 1995 “Air content can go up, down or stay relatively constant”. An attempt to correlate the influence of pumping parameters and change in air was performed. Changes in air content were obtained in the same fashion as discussed for I_{trib} in section 7.2. Mixtures M7 and M8 had a high risk of segregation and additional mixing was performed in field to avoid it. As a result, more air was entrapped due to additional mixing. But that entrapped air tended to disappear fully after pumping as shown in Figure 7-17.

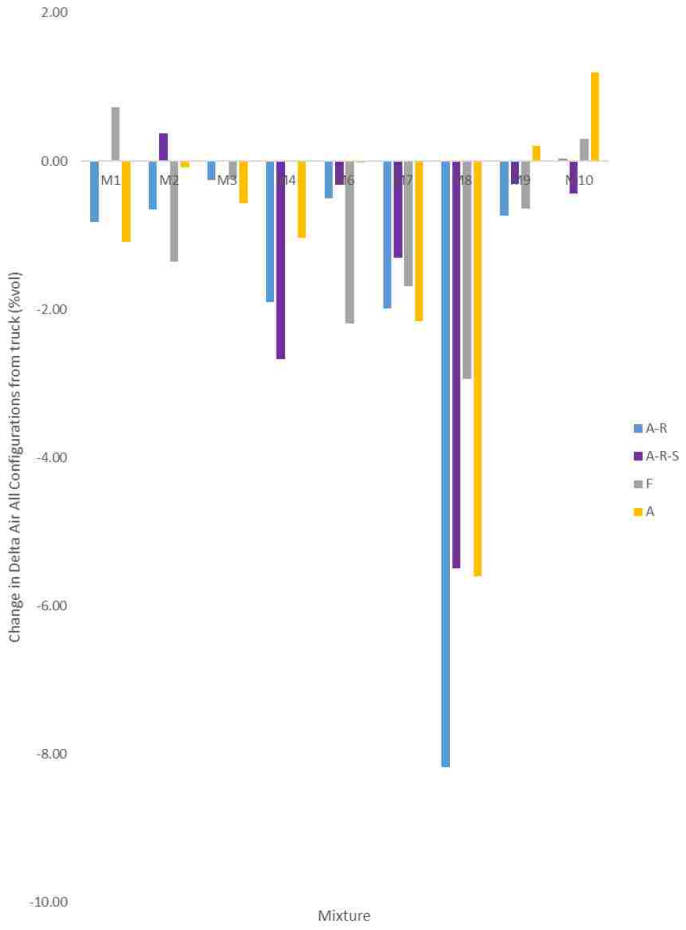

Figure 7-17 ΔAir changes from all configurations from truck.

7.3.1. Influence of Reducer and Reducer While Submerged for Mixtures M1-M10. Determined in the same fashion as 7.2.1: the use of a reducer decreased the change in air content for mixtures M2, M4, M6, and M8-M10, while for M1, M3 and M7, it increased the change in air content (Figure 7-18). Pumping while the hose is submerged does not induce consistent changes to the mixtures' air content.

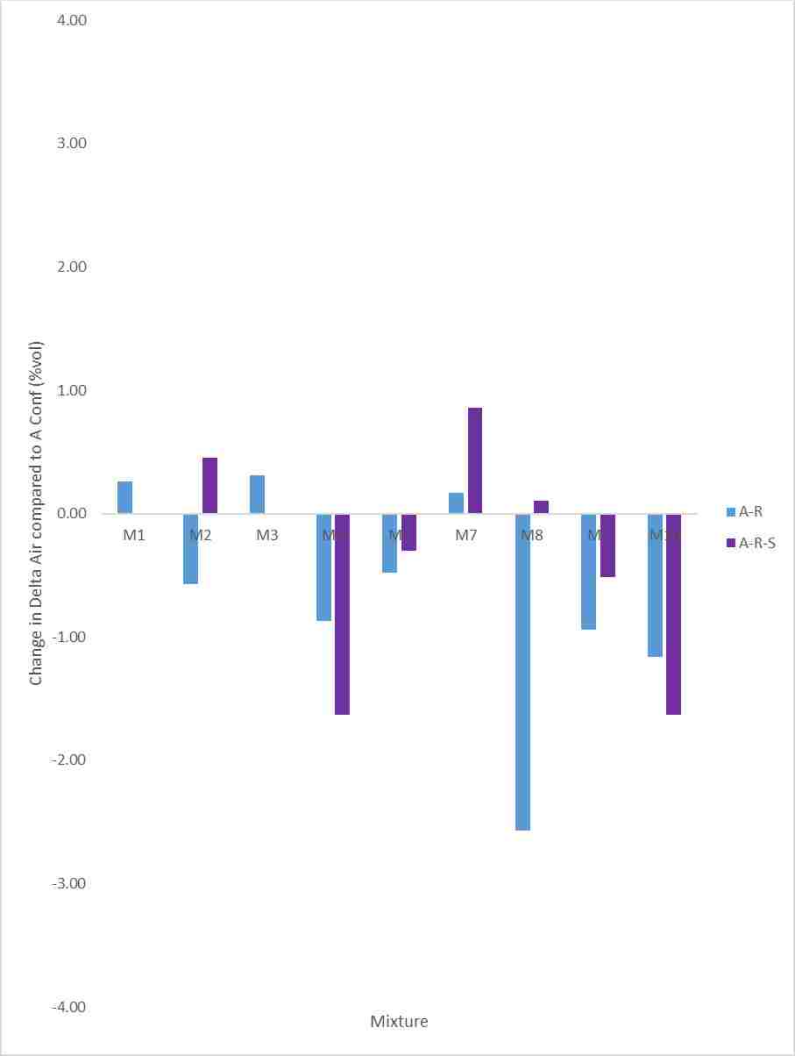

Figure 7-18 ΔAir changes from A-R and A-R-S compared to A configuration.

7.3.2. Influence of Boom Position for Mixtures M1-M10. In mixtures M1, M3, M7 and M8, an increase in air content change (higher increase or lower decrease) was observed in flat configuration compared to those pumped in A configuration, while for M2, M6, M9 the opposite was observed, as shown in Figure 7-19.

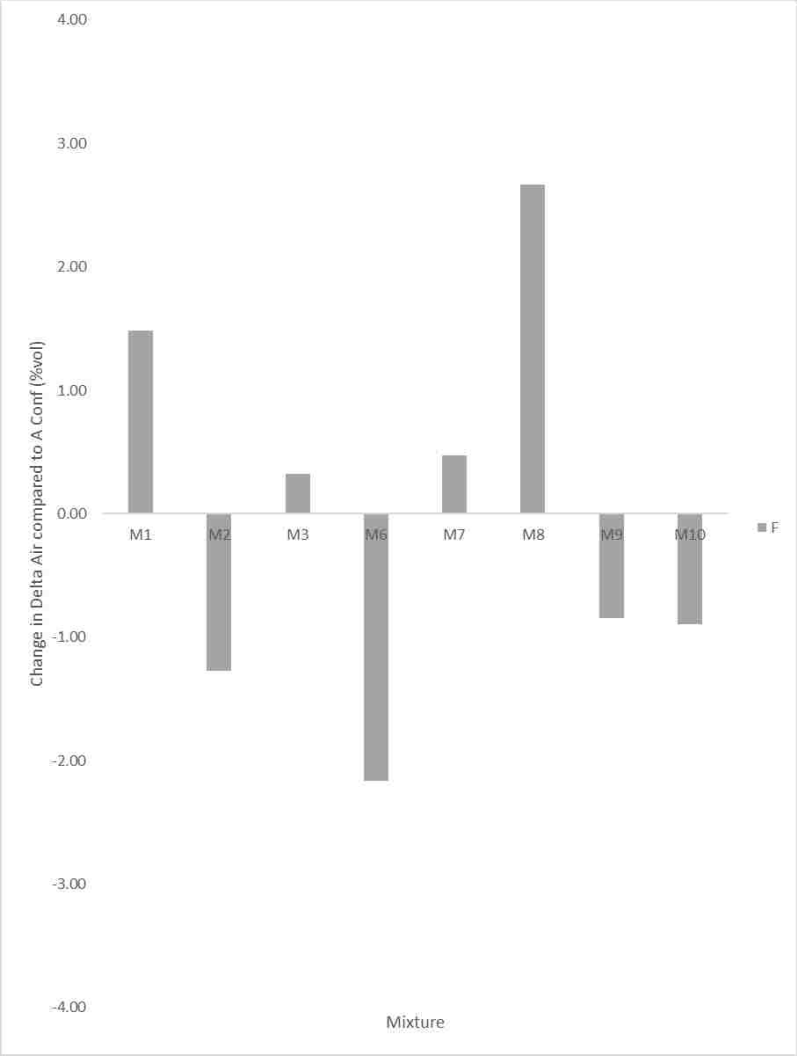

Figure 7-19 ΔAir changes from "F" configuration compared to A configuration.

7.3.3. Influence of Flow Rate in Flat Position for Mixtures M1-M10. Flat position at "slow" and "fast" flow rates was compared to flat configuration at "medium" flow rate. It was observed that from available data fast configuration always results in an increase in ΔAir, which is beneficial. While at slow flow rate, no uniform conclusion can be obtained as shown in Figure 7-20.

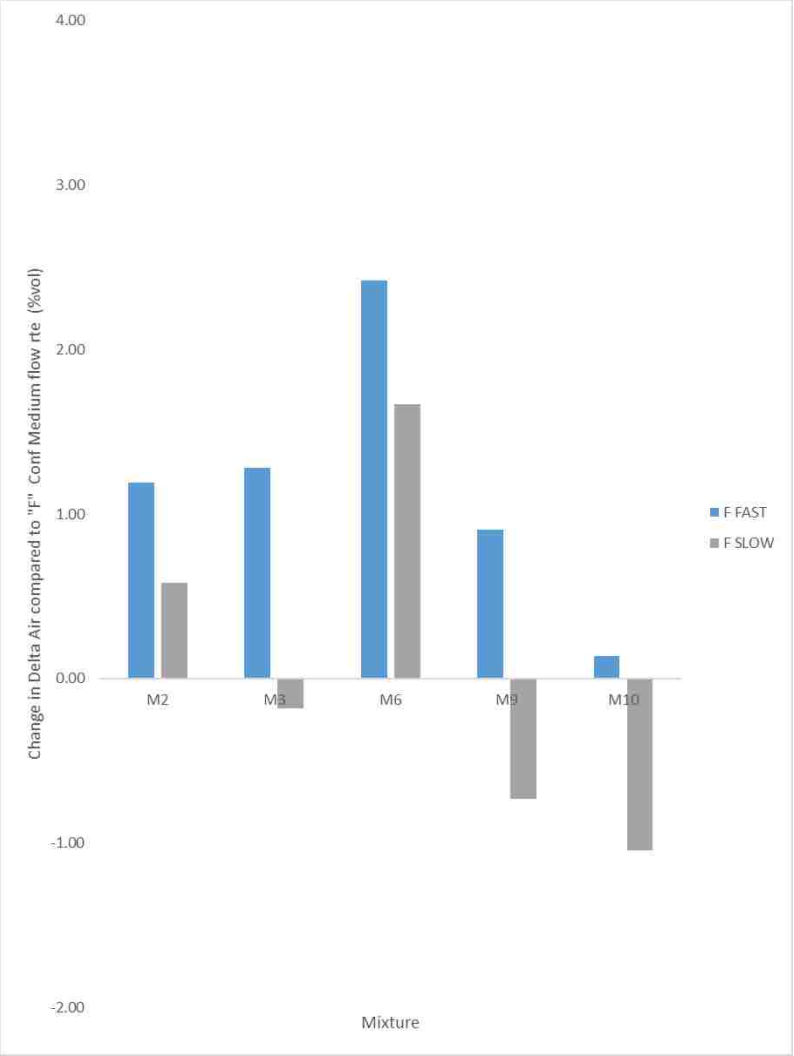

Figure 7-20 ΔAir from "F" configuration in slow and fast flow rate compared to A configuration in medium flow rate.

7.3.4. Influence of Reducer and Submerging for Mixtures M11-M16. "A" configuration with a reducer and "A" configuration with a reducer and submerged in fast pumping category are shown in Figure 7-21. When concrete is pumped in fast flow rate the effect of a reducer increased the change in ΔAir for all mixtures except for M13. The effect of submerged changed the ΔAir. While in slow pumping category, the effect of a reducer increased the change in ΔAir for mixtures M11-M15. The effect of a submerged hose can increase or decrease ΔAir in an unpredictable manner as shown in Figure 7-22.

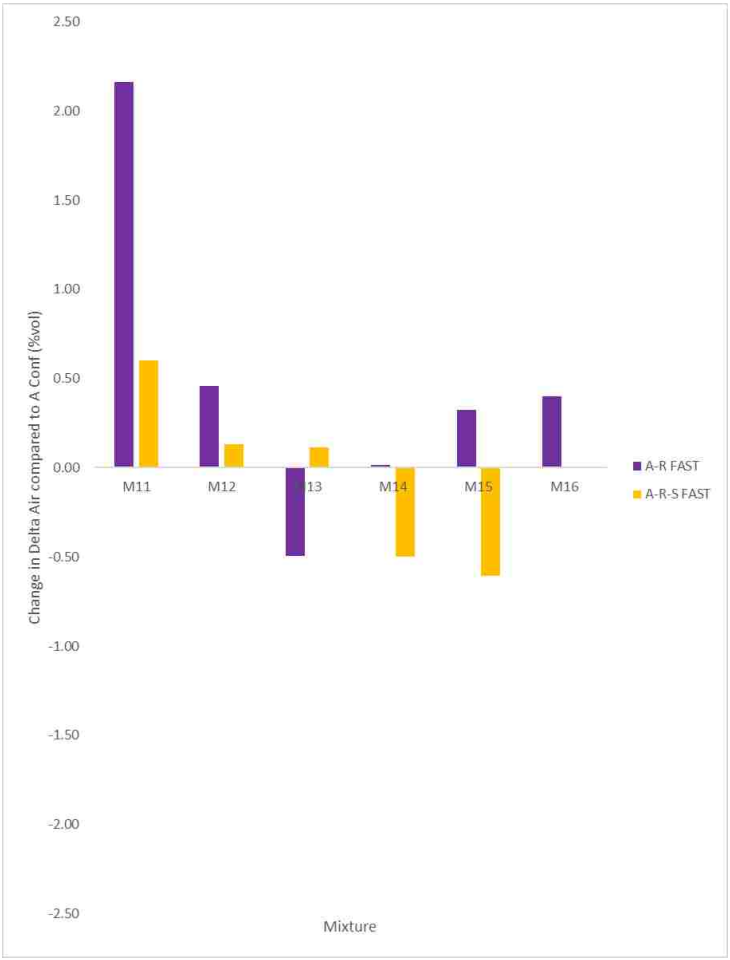

Figure 7-21 ΔAir changes from A-R and A-R-S configuration in fast flow rate.

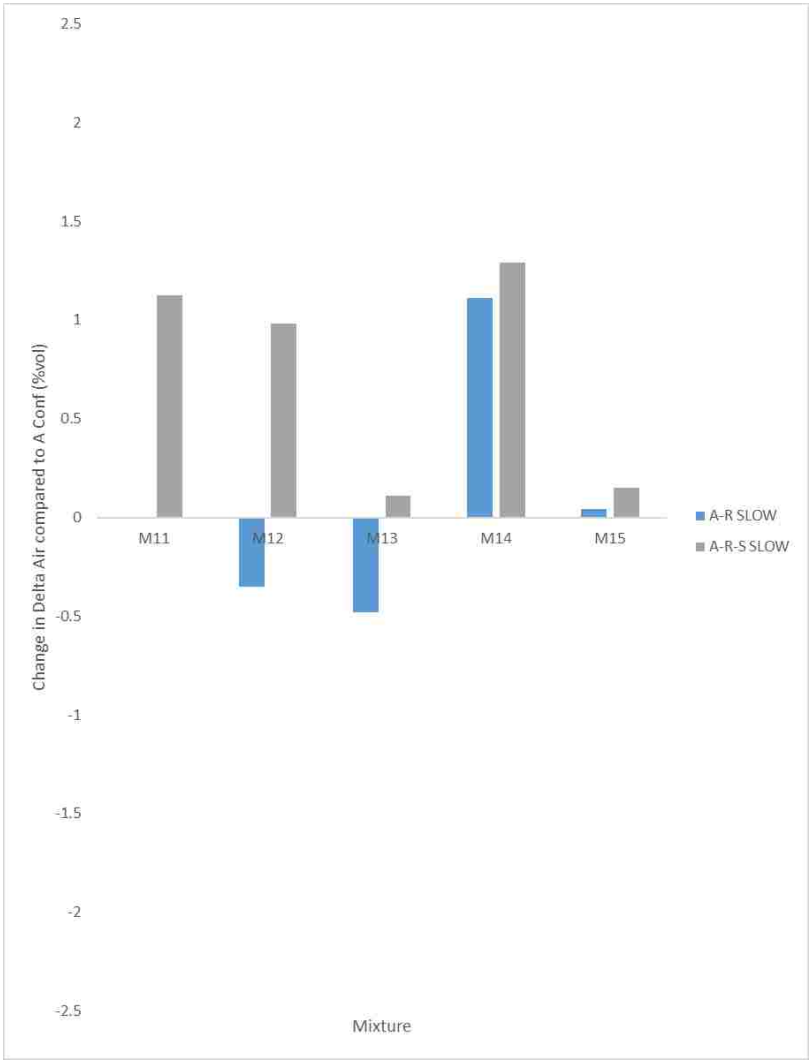

Figure 7-22 ΔAir from A-R and A-R-S configuration in slow flow rate.

7.3.5. Influence of Flow Rate in "A" Boom Position. The influence of flow rate without any reducer is shown in Figure 7-23. Increasing flow rate increased air for mixtures M14 and M15 while it decreased for M11- M13. Slow pumping decreased the air content for M11, M13, and M14.

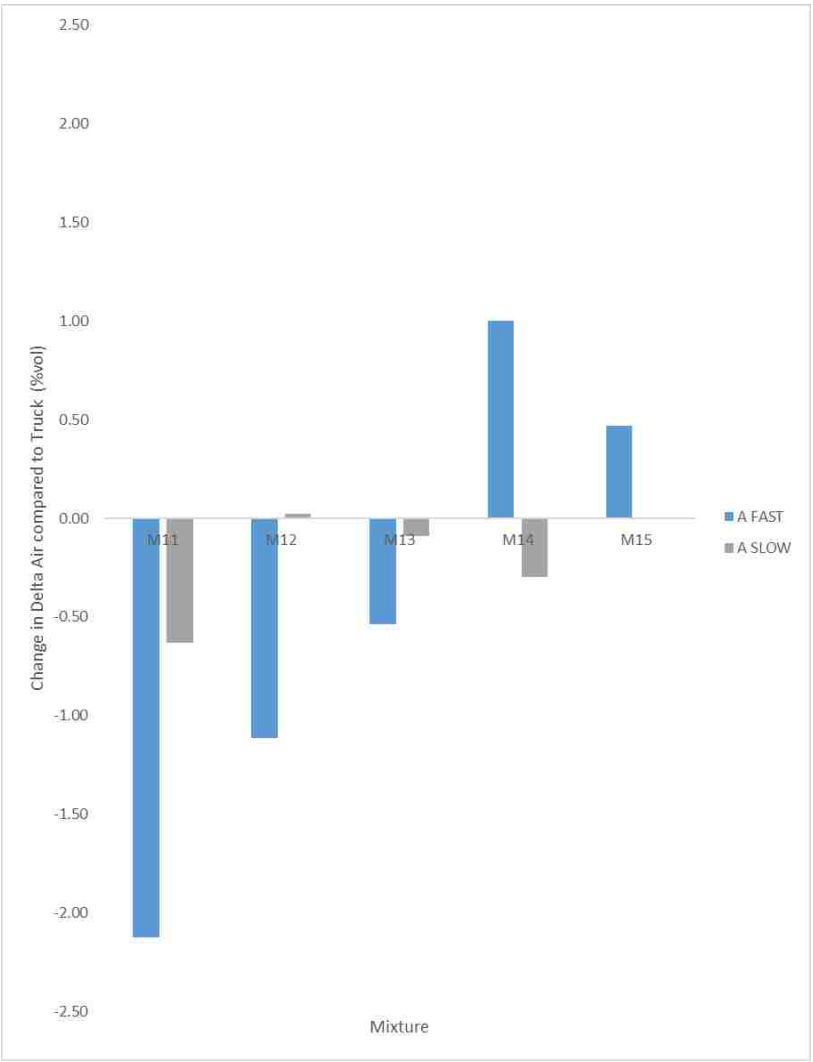

Figure 7-23 ΔAir in A configuration compared to the truck in slow and fast flow rate.

7.3.6. ΔAir Compared to Other Parameters. Figure 7-24 and Figure 7-25 show the changes in air content due to pumping and their influence on slump flow and yield stress. No correlation has been found between changes in air and changes in slump flow/ yield stress. According to literature [1], an increase or decrease in air content should affect mainly plastic viscosity but also yield stress. A positive change in sieve stability index ΔSSI due to pumping indicates loss in stability. Generally a decrease in

stability might result in a decrease in air content. But from Figure 7-26, this is not happening in all cases. Most likely, other effects changing the air content and the stability might just be minor, negligible factors. An increase in air content generally results in a decrease in plastic viscosity [1 ,5]. However, plastic viscosity measurements were discarded as previously explained.

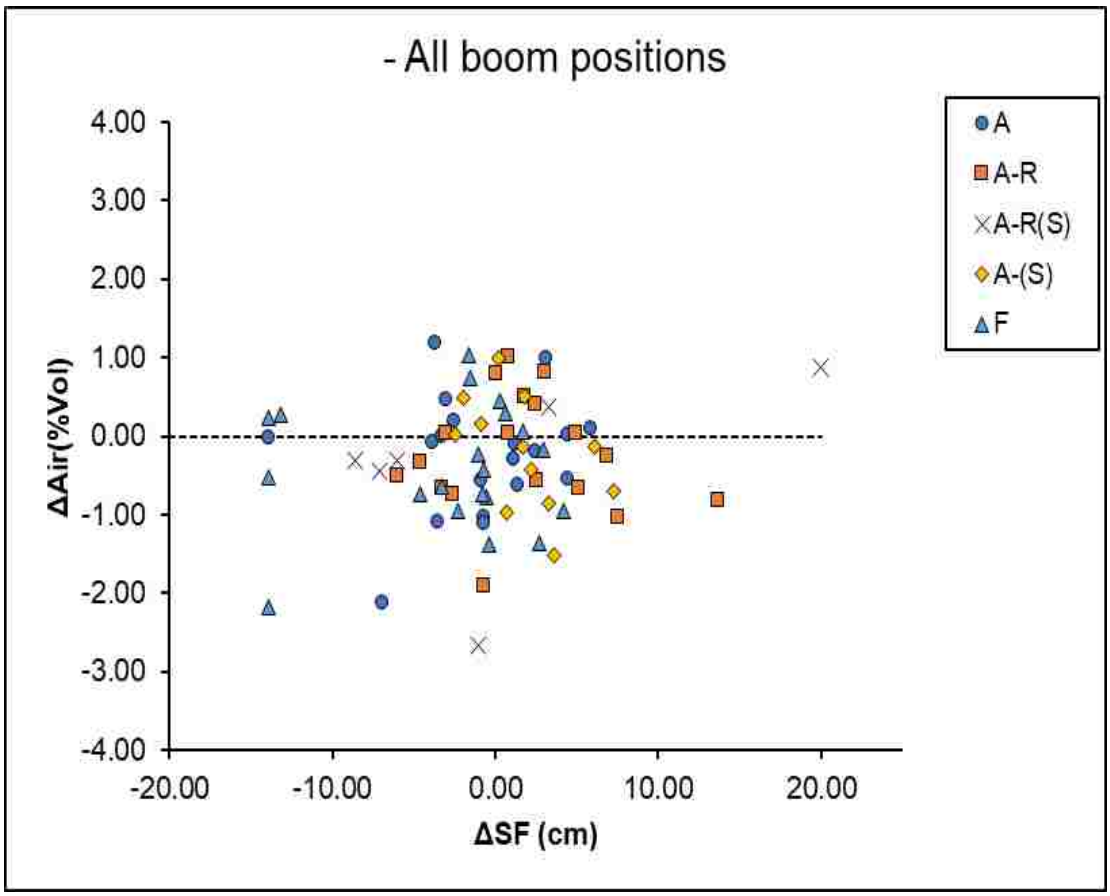

Figure 7-24 Change in air vs change in workability.

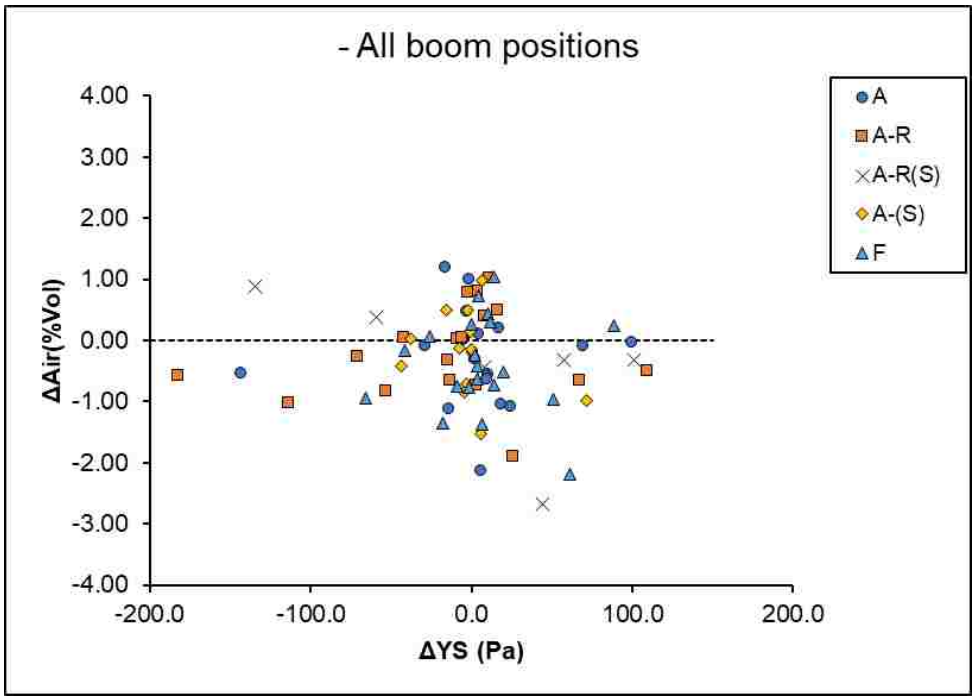

Figure 7-25 Change in air vs change in yield stress.

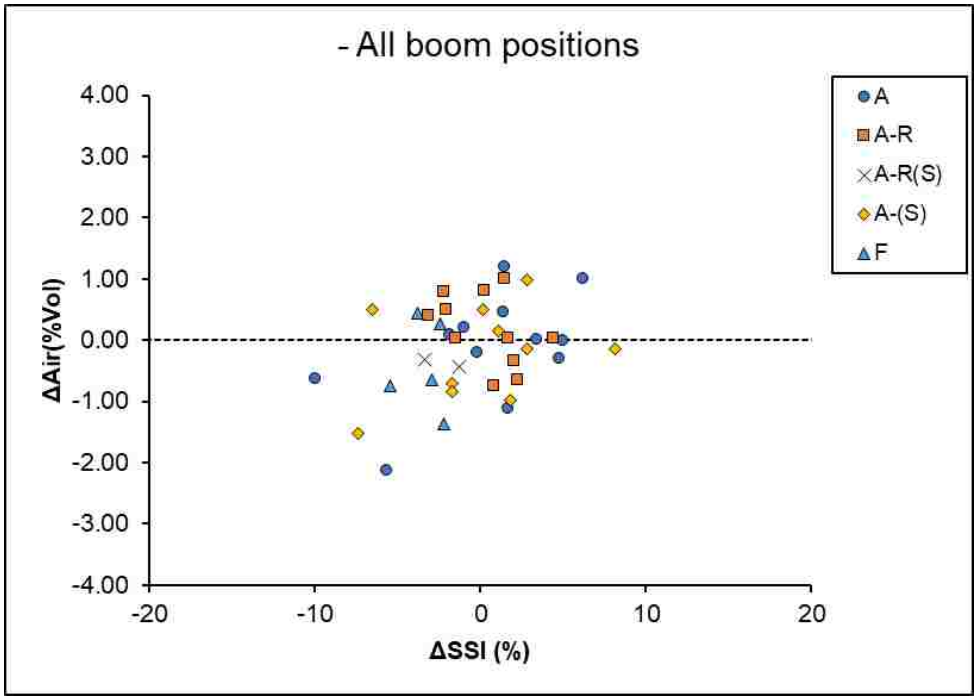

Figure 7-26 Change in air vs change in stability.

7.4. INFLUENCE OF PUMPING PARAMETERS ON ΔSLUMP FLOW

The following changes in consistency were observed with different pumping configurations.

7.4.1. Influence of Reducer and Submerging for Mixtures M1-M10. The same strategy as in 7.2.1 was followed. The use of a reducer decreased the change in Slump flow for mixtures M7-M9, while it increased for M1, M3, M6 and M10 as shown in Figure 7-27. Pumping while hose is submerged includes unpredictable changes to concrete mixtures.

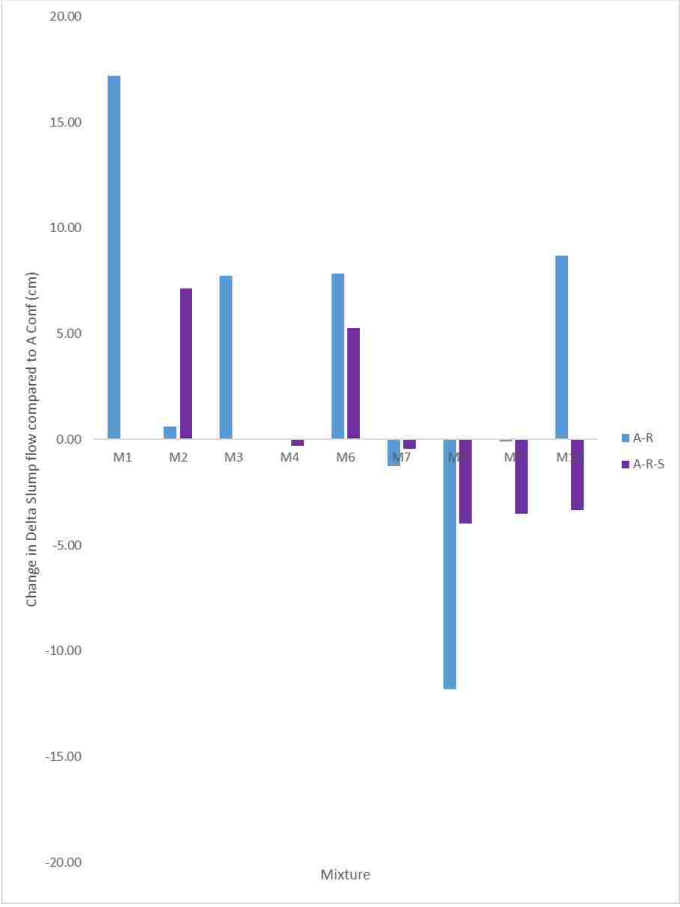

Figure 7-27 ΔSlump flow changes from A-R and A-R-S compared to A configuration.

7.4.2. Influence of Boom Position for Mixtures M1-M10. ΔSlump flow changes from "F" configuration compared to A configuration increased for nearly all mixtures, as shown in Figure 7-28. The reason why the concrete gains more fluidity, or loses less fluidity when pumping in F configuration, compared to A configuration is unknown, although it could be attributed to the duration the concrete is subjected to shearing flow, assuming the downward portion of the A configuration is not always completely filled.

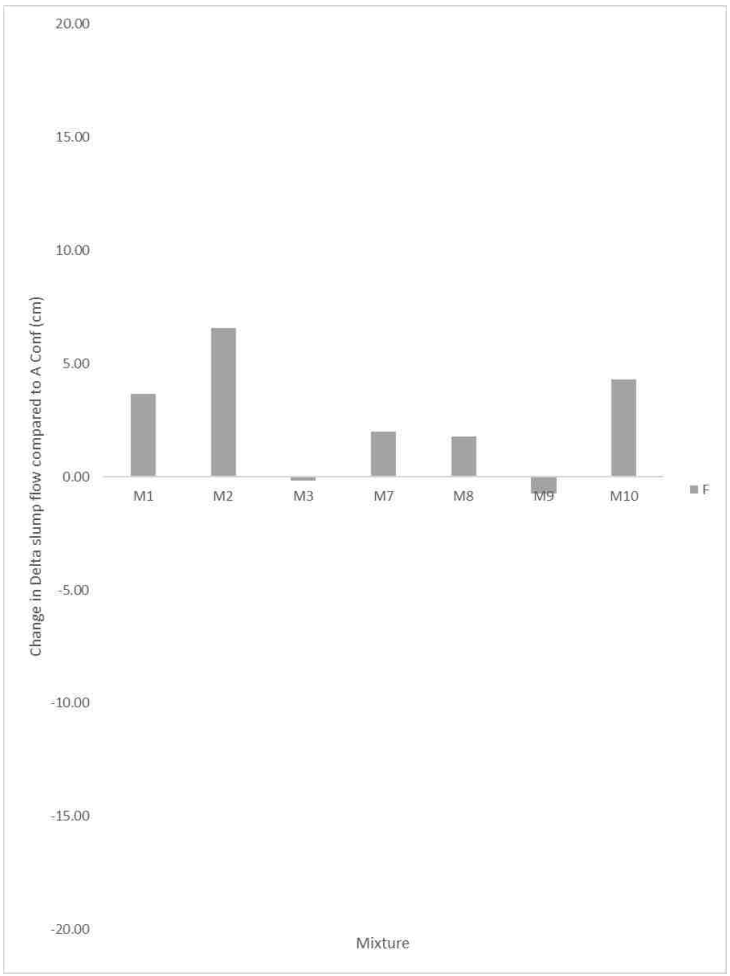

Figure 7-28 ΔAir changes from "F" configuration compared to A configuration.

7.4.3. Influence of Flow Rate in Flat Position for Mixtures M1-M10. It was observed that from available data "slow" "F" configuration always results in a more negative in Δ Slump flow. While in "fast" flow rate, only M1 and M10 got a slight increase in SF as shown in Figure 7-29.

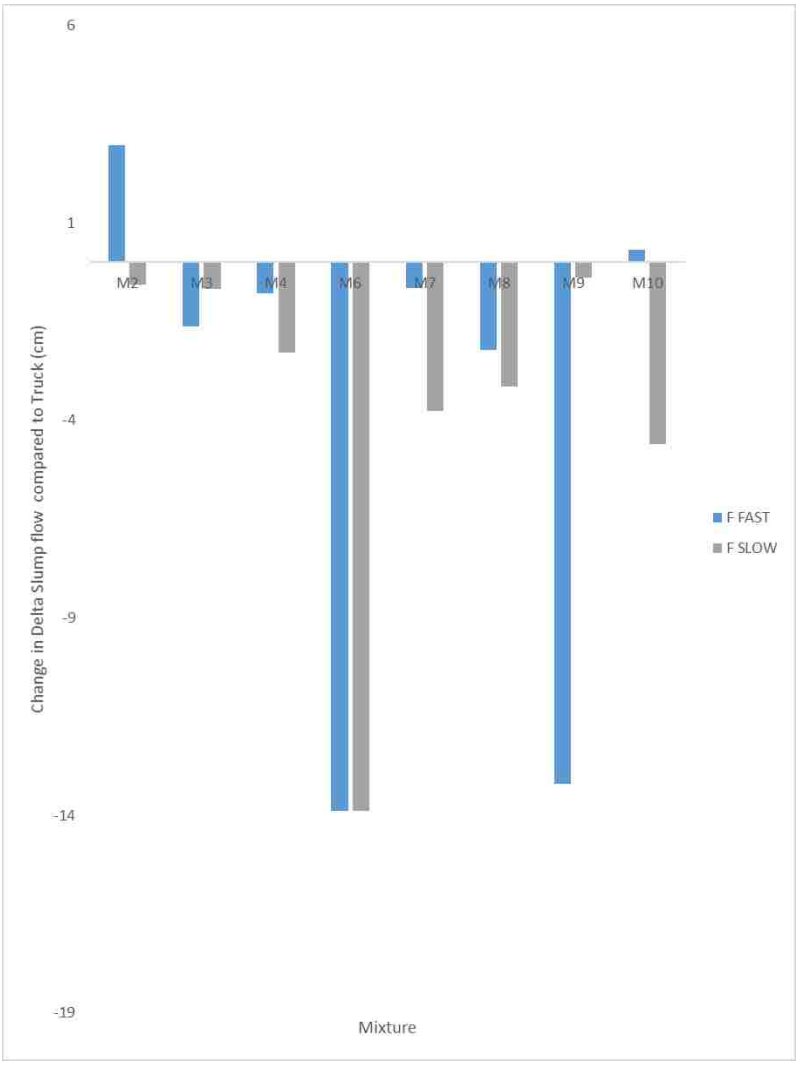

Figure 7-29 ΔSlump flow from "F" configuration in slow and fast flow rate compared to truck measurement.

7.4.4. Influence of Reducer and Submerging for Mixtures M11-M16. The use of a reducer increased the change in slump flow from A configuration from mixtures in "Fast" flow rates in mixtures M11, M12, M13, and M15 and decreased for M14, M16. Pumping while hose is submerged includes unpredictable changes to concrete mixtures as shown in Figure 7-30.

While in slow pumping category, the effect of a reducer increased the change in ΔSlump flow for mixtures M13-M15. The effect of a submerged hose can increase or decrease Δslump flow in an unpredictable manner as shown in Figure 7-31.

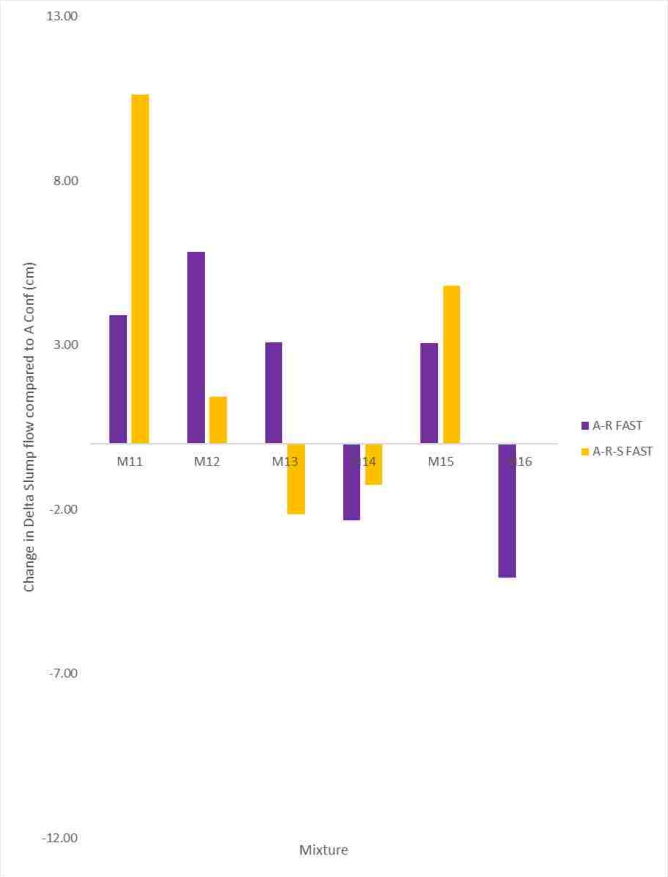

Figure 7-30 ΔSlump flow from A-R and A-R-S configuration in fast flow rate.

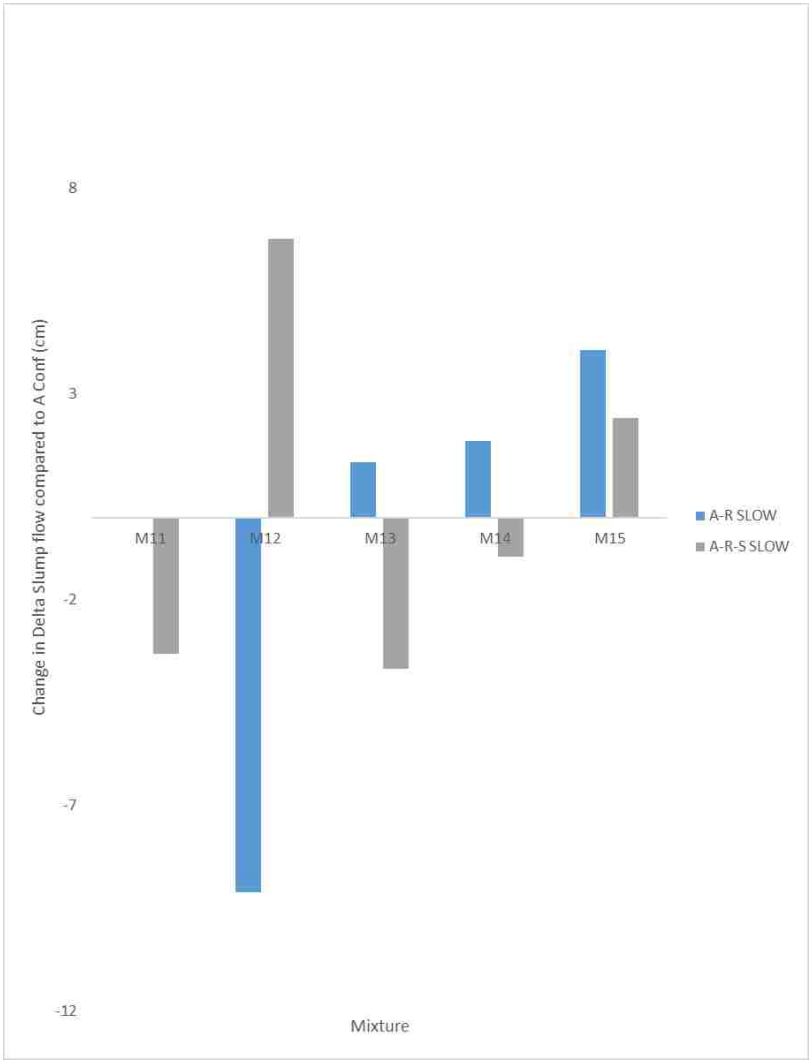

Figure 7-31 ΔSlump flow from A-R and A-R-S configuration in fast flow rate.

7.4.5. Influence of Flow Rate in "A" Boom Position for Mixtures M11-M16.

The influence of flow rate without any reducer is shown in Figure 7-32. The effect of pumping fast increased the changes for mixtures M13 and M14 while decreased for M11, M12 and M13. Slow pumping decreased ΔSlump flow only for M15.

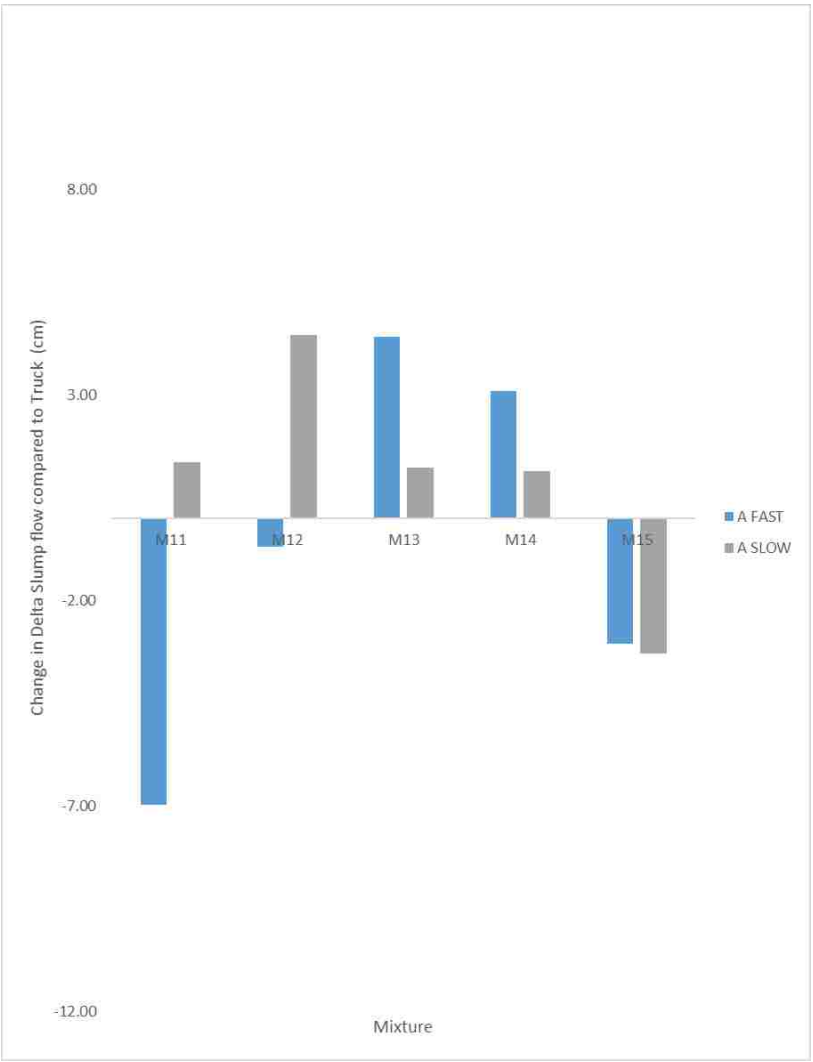

Figure 7-32 ΔSlump flow in A configuration compared to the truck in slow and fast flow rate.

7.5. WORKABILITY LEVELS

It is believed that the effect of pumping on changes in fresh and hardened properties depends on the workability of the concrete.

Based on Kaplan's model, as the yield stress of concrete increases, the possibility of having a plug flow increases and as a result, less concrete is being sheared. Using

empirical measurements, concrete mixtures were divided into two classifications: “slump flow below 550 mm” was considered non-SCC and “above 550 mm” was considered SCC. Pump configurations were separated in “A” and “flat” configuration. Unfortunately, the influence on workability does not depend on the consistency of concrete or boom position as shown in Figure 7-33. No clear tendency is shown to affirm that slump flow is going to increase or decrease depending on tested parameters.

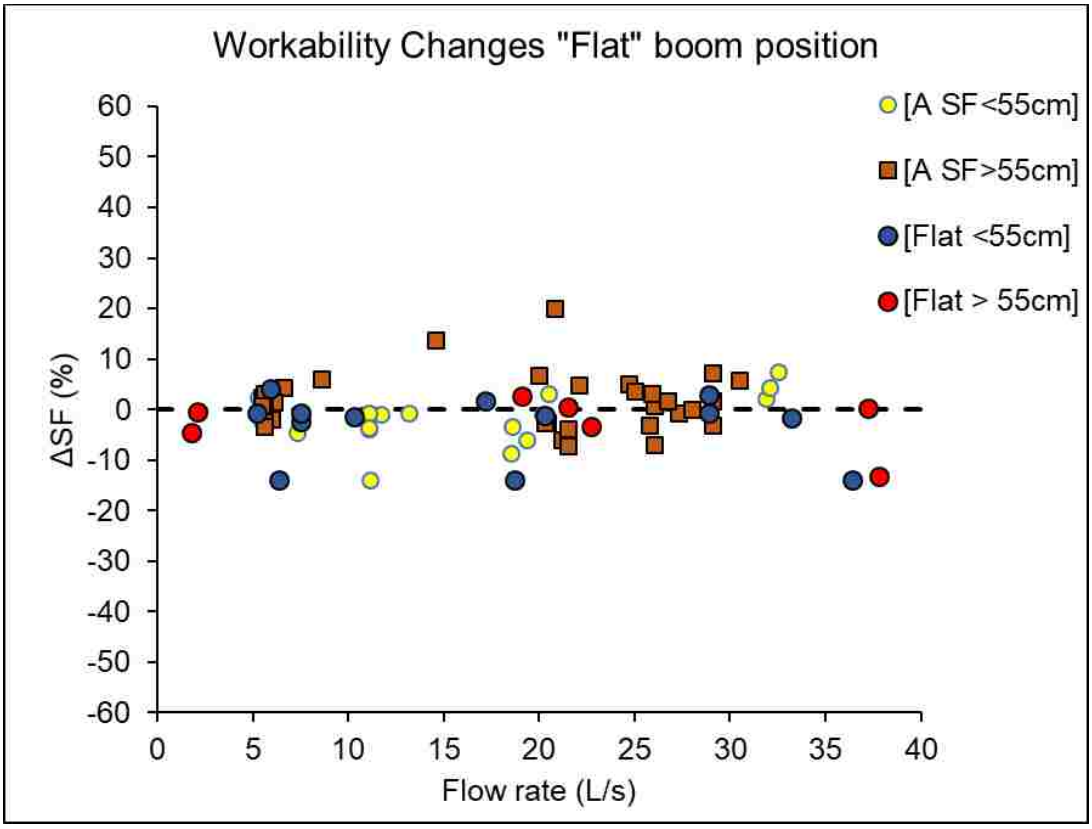

Figure 7-33 Change in slump flow vs flow rate.

Similar to workability loss ΔSlump flow, air loss was measured for all concrete mixtures. ΔAir was between (-3% to +1%). No clear tendency showed that changes in air

depend on consistency, boom position, flow rate or changes in workability, based on Figure 7-34 and Figure 7-35.

Secrieru claims that pumping increases the air content. However, from Figure 7-34, air does not show a tendency to increase. Also, the air content is more likely to decrease regardless of the pump configuration and the flow rate. Figure 7-36 shows the changes in I_{trib} vs the air content of each mixture. Changes in I_{trib} are not related to air content. However, those concrete mixtures that have SCC consistency and which were pumped in "A" configuration had a nearly systematic decrease in $I_{trib.}$

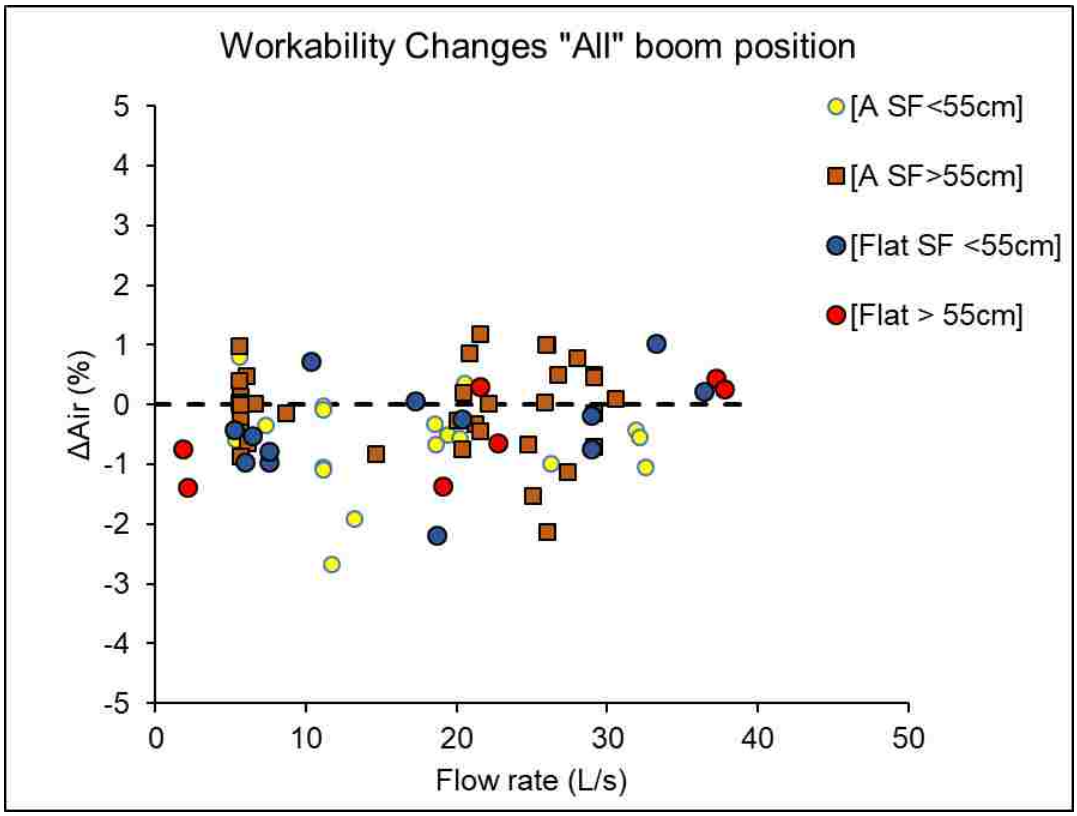

Figure 7-34 Air changes "A" boom position.

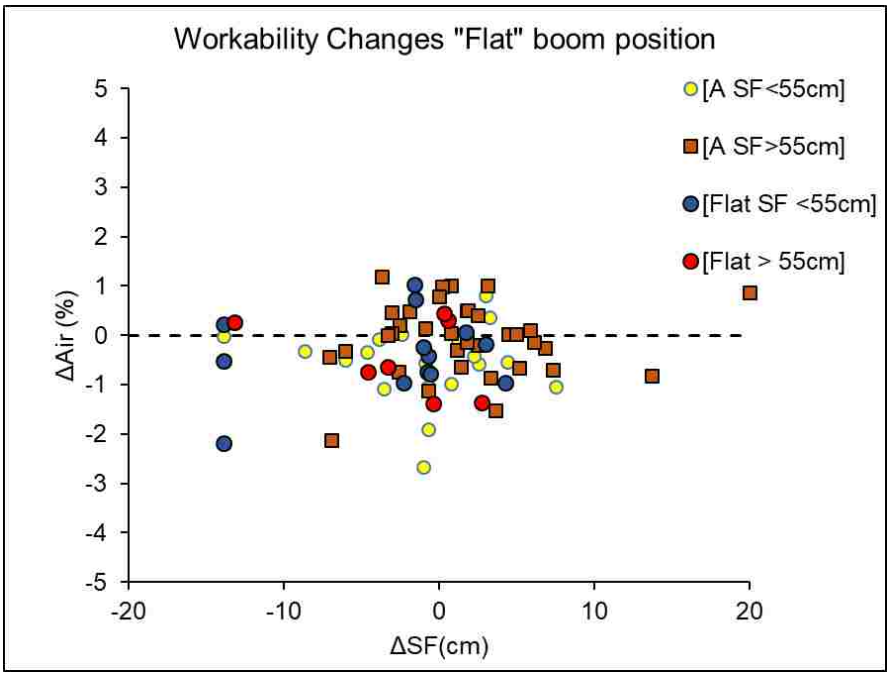

Figure 7-35 Change in air vs change in consistency.

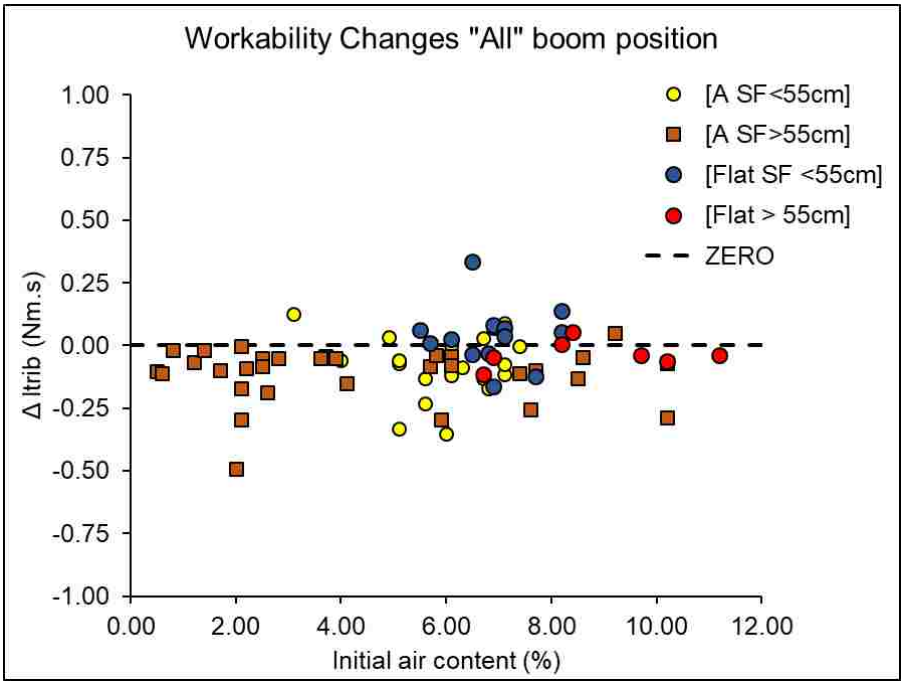

Figure 7-36 Change in Itrib vs air content.

8. CONCLUSIONS

8.1. CONCRETE RHEOMETERS

Previous comparisons have been made between concrete rheoemeters [9,66]. However, most rheometers work at a different shear rate ranges. And if the rheological properties are dependent of the applied shear rate (i.e. shear-thinning, shear-thickening), the comparison becomes much more complicated. Additionally, the selection of the model influences the estimated rheological values (i.e using Bingham model in a shear thinning material will result in an overestimation of the yield stress.)

With the available data, for the reference material used the and for shear rate ranges applied, the following conclusions can be made:

- Using Anton Paar rheometer as a reference, the yield stress measurements of the ConTec 6 seem to be closest in value (slope = 0.82) and had a good curve fit R^2 = 0.98.
- Using Anton Paar rheometer as a reference for plastic viscosity, the ICAR rheometer seems to deliver the closest results (slope = 0.73). The ConTec 5S, ConTec 5W and ConTec 6 show the same results (Slope = 0.64).
- As explained by Ferraris et al[9], even if all rheometers have a different readings overall, they have the same tendency.
- Transformation equations from one rheometer to other could not easily be obtained, as the behavior depends on the shear rate range.

8.1.1. Recommendations.

- Use only one rheometer and the same measuring protocol to investigate the rheological properties, if possible.
- If the material allows, use the rheometer with the smallest gap available.
- If the material shows non-linearity, use the model that better fits the behavior.

8.1.2. Future Work.

- Once plug flow correction is available for non-linear models, transformation equations can be developed with better precision.
- Use a non-shear dependent reference material.
- Find a manner to match the shear rates of all compared rheometers.

8.2. PUMPING PROJECT CONCLUSIONS

A full-scale pumping campaign was conducted to investigate the effect of different pumping parameters and the changes induced to concrete. From the available data, the following conclusions can be made:

8.2.1. Changes in Flow Resistance in the Interface Rheometer.

- The use of a reducer causes lower ΔI_{trib} values only in mixtures that are pumped at a medium flow rate (8-25 l/s). while this is not applicable to low and high flow rates.
- Pumping while the hose is submerged in A configuration and at medium flow rate amplifies the effect of the reducer. This is not observed for pumping at slow or fast flow rate.

- Regardless of the use of a reducer, the "A" configuration, in average, reduces the rheology at the interface zone more than the "F" configuration.
- Flow rate did not show any clear influence in ΔI_{trib} changes.

8.2.2. Changes in Air Content.

- The use of a reducer increased the change in air content only in mixtures that are pumped in "A" configuration and slow flow rate (< 8 l/s).
- The flow rate did not show an influence on ΔAir except for mixtures that were pumped at fast flow rate and in "F" configuration. Those mixtures experienced an increase in ΔAir.
- ΔAir is not a dominant factor for changes in fresh properties.
- The lack of correlation between the changes in I_{trib} and the changes in air content indicate that air is not a dominant factor in influencing the flow resistance in pipes.

8.2.3. Changes in Slump Flow.

- Overall ΔI_{Trib} correlates with Δslump flow, indicating that, for the chosen mix designs, the flow resistance in pipes is affected by the yield stress.
- "F" boom configuration at medium speed results in a higher fluidity of concrete compared to "A" configuration at medium speed.
- "F" boom configuration at slow and fast flow rate tends to decrease fluidity of concrete.
- Changes in fresh properties seem not dependent of the fluidity of the mixture.

8.2.4. Recommendations.

- Overall recommendations depend on the application (i.e. a decrease in ΔI_{trib} is required pump in A configuration at medium speed).
- If concrete compressive strength is at risk, avoid the combination of pumping in "A" configuration slow rate or "F" configuration fast flow rate. (increases air content and that reduces compressive strength)
- Find a way to use a more reliable rheometer on field.

8.2.5. Future Work.

- Develop a practical guide for the use of pumping configuration, flow rates and influence in fresh properties.
- Evaluate the effect of different paste content.
- Evaluate the effect on lower w/c mixtures

8.3. LUBRICATION LAYER CONCLUSIONS

- A methodology was developed to estimate the composition and thickness of the lubrication layer through rheology.
- Special considerations were taken to exclude the effect of increasing shear rate in the paste with increasing particle volume fraction of particles, and the difference between rheometers were taken into account.
- Krieger-Dougherty style parameters were determined for mortars with different volume fractions of particles and different maximum particle sizes.

- A calculation methodology was attempted to replicate the torque-rotational velocity profile from an interface rheometer test through measuring the properties of cement paste and concrete, and calculating the rheological properties of mortars with different volume fractions and particle sizes through the parameters of the Krieger-Dougherty models. The thicknesses of the layers were varied to approach as good as possible the interface rheometer test.
- The 0.35 w/c mixture resulted in a lubrication layer formed of cement paste of 96 μm thick, the 0.4 w/c mixture flowed with a paste layer of 123 μm and the 0.40 w/c mixture with fly ash had a 33 μm thick paste layer. The values are at least one order of magnitude smaller than what is reported in literature. As such, no conclusions can be made and a different characterization methodology must be used.

8.3.1. Recommendations.

- Develop a smooth cylinder for contec 5.
- For all measurements, use only contec 5 and 6.

8.3.2. Future Work.

- Theoretically this approach is correct. But practically, the calculated thickness of each layer may become illogical compared to the theoretical thickness. An alternative to measure the thickness of the lubrication layer is the use of the portable high-pressure filter press (PHPFP) developed at the Institute of Building Materials Science, Leibniz Universität Hannover [67].

REFERENCES

1. Wallevik, O. H., & Wallevik, J. E. (2011). Rheology as a tool in concrete science: The use of rheographs and workability boxes. Cement and Concrete Research, 41(12), 1279-1288.

2. ACI Commitee 238 (2008). "Report on Measurements of Workability and Rheology of Fresh Concrete". ACI 238-08, ACI Manual of Concrete Practice, Detroit, MI, USA.

3. Hackley V. A., Ferraris C. F., "Guide to Rheological Nomenclature: Measurements in Ceramic Particulate Systems, "NIST Special Publication 946, Febrary 2001

4. Browne, R.D. and Bamforth, P.B., 1977, May. Tests to establish concrete pumpability. In Journal Proceedings (Vol. 74, No. 5, pp. 193-203).

5. Secrieru, E., Cotardo, D., Mechtcherine, V., Lohaus, L., Schröfl, C. and Begemann, C., 2018. Changes in concrete properties during pumping and formation of lubricating material under pressure. Cement and Concrete Research, 108, pp.129-139.

6. Jolin, M., Burns, D., Bissonnette, B., Gagnon, F. and Bolduc, L.S., 2009. Understanding the pumpability of concrete.

7. Kaplan, D., De Larrard, F. and Sedran, T., 2005. Avoidance of blockages in concrete pumping process. ACI Materials journal, 102(3), p.183

8. Kaplan, D., 1999. Pompage des bétons. These presentee pour obtenir le titre de de docteur de l'ecole nationale des ponts et chaussees-specialite: structures et materiaux.

9. Ferraris, C.F., Brower, L.E., Banfill, P., Beaupré, D., Chapdelaine, F., de Larrard, F. and Domone, P., 2001. Comparison of Concrete Rheometers: International Test at LCPC (Nantes, France) in October, 2000. US Department of Commerce, National Institute of Standards and Technology.

10. Feys D, De Schutter G, Verhoeven R (2013) Parameters influencing pressure during pumping of self-compacting concrete. Mat Struct 46:533–555

11. Jolin, M., Chapdelaine, F., Gagnon, F. and Beaupré, D., 2006. Pumping concrete: a fundamental and practical approach. In Shotcrete for underground support X (pp. 334-347).

12. Kosmatka, S.H. and Wilson, M.L., 2011. Design and control of concrete mixtures. Portland Cement Assoc.

13. Okamura, H., & Ouchi, M. (2003). Self-compacting concrete. Journal of advanced concrete technology, 1(1), 5-15.

14. De Vicente, J. ed., 2012. Rheology. BoD–Books on Demand.

15. Hackley, V.A. and Ferraris, C.F., 2001. Guide to rheological nomenclature: Measurements in ceramic particulate systems. Gaithersburg: National Institute of Standards and Technology.

16. Newton, I., 1934. Principia mathematica. London, England: Mothe-Cajori.Tattersall, G.H., 1973. The rationale of a two-point workability test. Magazine of Concrete Research, 25(84), pp.169-172.

17. Wallevik, O.H., Feys, D., Wallevik, J.E. and Khayat, K.H., 2015. Avoiding inaccurate interpretations of rheological measurements for cement-based materials. Cement and Concrete Research, 78, pp.100-109.

18. Tattersall, G.H., Banfill, P.F.G., The Rheology of Fresh Concrete, Pitman Advanced Publishing Program, 1983

19. Wallevik, O.H., 2003, August. Rheology—a scientific approach to develop self-compacting concrete. In Proc. of the 3rd Int. Symp. on Self-Compacting Concrete, Reykjavik (pp. 23-31).

20. Feys, D., Verhoeven, R. and De Schutter, G., 2008. Fresh self compacting concrete, a shear thickening material. Cement and Concrete Research, 38(7), pp.920-929.

21. Feys, D., Verhoeven, R. and De Schutter, G., 2009. Why is fresh self-compacting concrete shear thickening?. Cement and concrete Research, 39(6), pp.510-523

22. Yahia, A. and Khayat, K.H., 2001. Analytical models for estimating yield stress of high-performance pseudoplastic grout. Cement and Concrete Research, 31(5), pp.731-738.

23. Yahia A, Khayat KH (2001) Analytical models for estimating yield stress of high-performance pseudoplastic grout. Cem Concr Res 31:731–738

24. Brower, L.E. and Ferraris, C.F., 2003. Comparison of concrete rheometers. Concrete International, 25(8), pp.41-47.

25. Roussel, N., Ovarlez, G., Garrault, S. and Brumaud, C., 2012. The origins of thixotropy of fresh cement pastes. Cement and Concrete Research, 42(1), pp.148-157.

26. Wallevik, J.E., 2009. Rheological properties of cement paste: thixotropic behavior and structural breakdown. Cement and Concrete Research, 39(1), pp.14-29.

27. Mahaut, F., Mokeddem, S., Chateau, X., Roussel, N. and Ovarlez, G., 2008. Effect of coarse particle volume fraction on the yield stress and thixotropy of cementitious materials. Cement and concrete research, 38(11), pp.1276-1285Tattersall, G.H. and Bloomer, S.J., 1979. Further development of the two-point test for workability and extension of its range. Magazine of concrete research, 31(109), pp.202-210.

28. Wallevik, J.E., 2003. Rheology of particle suspensions: fresh concrete, mortar and cement paste with various types of lignosulfonates. Fakultet for ingeniørvitenskap og teknologi.

29. Malvern, L.E., 1969. Introduction to the Mechanics of a Continuous Medium (No. Monograph).

30. Ferraris, C., De Larrard, F., & Martys, N. (2001). Fresh concrete rheology: recent developments. Materials Science of Concrete VI, Amer. Cer. Soc. Ed. S. Mindess, J. Skalny, 215-241.

31. Bentz, D.P., Ferraris, C.F., Galler, M.A., Hansen, A.S. and Guynn, J.M., 2012. Influence of particle size distributions on yield stress and viscosity of cement–fly ash pastes. Cement and Concrete Research, 42(2), pp.404-409.

32. Geiker, M.R., Brandl, M., Thrane, L.N. and Nielsen, L.F., 2002. On the effect of coarse aggregate fraction and shape on the rheological properties of self-compacting concrete. Cement, concrete and aggregates, 24(1), pp.3-6.

33. Kwan, A.K.H. and Fung, W.W.S., 2009. Packing density measurement and modelling of fine aggregate and mortar. Cement and Concrete Composites, 31(6), pp.349-357.

34. Einstein, A., 1906. Eine neue bestimmung der moleküldimensionen. Annalen der Physik, 324(2), pp.289-306.

35. Einstein, A., 1911. Berichtigung zu meiner Arbeit:„Eine neue Bestimmung der Moleküldimensionen" . Annalen der Physik, 339(3), pp.591-592.

36. Batchelor, G.K. and Green, J.T., 1972. The determination of the bulk stress in a suspension of spherical particles to order c 2. Journal of Fluid Mechanics, 56(3), pp.401-427.

37. Erdoğan, S.T., Martys, N.S., Ferraris, C.F. and Fowler, D.W., 2008. Influence of the shape and roughness of inclusions on the rheological properties of a cementitious suspension. Cement and Concrete Composites, 30(5), pp.393-402.

38. Yammine, J., Chaouche, M., Guerinet, M., Moranville, M. and Roussel, N., 2008. From ordinary rhelogy concrete to self compacting concrete: A transition between frictional and hydrodynamic interactions. Cement and Concrete Research, 38(7), pp.890-896Mewis, J. and Wagner, N.J., 2012. Colloidal suspension rheology. Cambridge University Press.

39. Krieger, I.M., 1972. Rheology of monodisperse latices. Advances in Colloid and Interface science, 3(2), pp.111-136.

40. Kaplan, D., de Larrard, F. and Sedran, T., 2005. Design of concrete pumping circuit. ACI materials journal, 102(2), p.110.

41. Ngo, T.T., Kadri, E.H., Bennacer, R. and Cussigh, F., 2010. Use of tribometer to estimate interface friction and concrete boundary layer composition during the fluid concrete pumping. Construction and Building Materials, 24(7), pp.1253-1261

42. Wallevik, J.E., 2008. Minimizing end-effects in the coaxial cylinders viscometer: Viscoplastic flow inside the ConTec BML Viscometer 3. Journal of Non-Newtonian Fluid Mechanics, 155(3), pp.116-123.

43. Phillips, R.J., Armstrong, R.C., Brown, R.A., Graham, A.L. and Abbott, J.R., 1992. A constitutive equation for concentrated suspensions that accounts for shear-induced particle migration. Physics of Fluids A: Fluid Dynamics, 4(1), pp.30-40

44. Feys, D. and Khayat, K.H., 2017. Particle migration during concrete rheometry: How bad is it?. Materials and Structures, 50(2), p.122.

45. Chapdelaine, F., 2007. Fundamental and practical study on pumping of concrete (Doctoral dissertation, Ph-D-thesis (in French), Université Laval, Laval).

46. Roussel, N. (Ed.). (2011). Understanding the rheology of concrete. Elsevier

47. Kwon, S.H., Park, C.K., Jeong, J.H., Jo, S.D. and Lee, S.H., 2013. Prediction of concrete pumping: Part II-analytical prediction and experimental verification. ACI Materials Journal, 110(6), p.657.

48. Choi, M., Roussel, N., Kim, Y. and Kim, J., 2013. Lubrication layer properties during concrete pumping. Cement and Concrete Research, 45, pp.69-78.

49. Feys, D., Khayat, K.H. and Khatib, R., 2016. How do concrete rheology, tribology, flow rate and pipe radius influence pumping pressure?. Cement and Concrete Composites, 66, pp.38-46.

50. Feys, D., De Schutter, G., Khayat, K.H. and Verhoeven, R., 2016. Changes in rheology of self-consolidating concrete induced by pumping. Materials and Structures, 49(11), pp.4657-4677.

51. ASTM, 2012. ASTM C150/C150M-12: Standard specification for Portland cement, ASTM International, West Conshohocken, PA

52. Helmuth, R., 1987. Fly ash in cement and concrete (No. SP040. 01T).

53. ACI Committee 232 1996 "Use of Fly Ash in Concrete" ACI232.2R-96 ACI manual of concrete practice, Detroit, MI,USA

54. ASTM C128-15 Standard Test Method for Relative Density (Specific Gravity) and Absorption of Fine Aggregate. ASTM International, West Conshohocken, PA.

55. ASTM C136/C136M-14 Standard Test Method for Sieve Analysis of Fine and Coarse Aggregates. ASTM International, West Conshohocken, PA

56. ASTM C127-15 Standard Test Method for Relative Density (Specific Gravity) and Absorption of Coarse Aggregate. ASTM International, West Conshohocken, PA

57. ASTM C494 / C494M - 16 Standard Specification for Chemical Admixtures for Concrete. ASTM International, West Conshohocken, PA

58. AASHTO, M., 2006. 194M/M 194-06,". Standard Specification for Chemical Admixtures for Concrete," American Association of State and Highway Transportation Officials, Washington, DC.

59. ASTM, C., 2001. 260. Standard Specification for Air-Entraining Admixtures for Concrete, West Conshohocken, PA

60. AASHTO, M., 2016 154M/M 154-12 "Standard Specification for Air-Entraining Admixtures for Concrete" American Association of State and Highway Transportation Officials, Washington, DC.

61. ASTM C143/C143M-15a. (2015). Standard Test Method for Slump of Hydraulic-Cement Concrete. ASTM International, West Conshohocken, PA.

62. ASTM C1611/C1611M-15a. (2015). Standard Test Method for Slump Flow of Self-Consolidating Concrete. ASTM International, West Conshohocken, PA.

63. ASTM C231-09. (2009). Standard Test Method for Air Content of Freshly Mixed Concrete by the Pressure Method. ASTM International, West Conshohocken, PA

64. The European Guidelines for Self-Compacting Concrete: Specification, Production and Use. (2005).

65. Mahaut F., Mokéddem S., Chateau X., Roussel N., Ovarlez G., "Effect of coarse particle volume fraction on the yield stress and thixotropy of cementitious materials," Cem. Conc. Res. **38** (2008), 1276-1285.

66. Beaupré, D., Chapdelaine, F., Domone, P., Koehler, E., Shen, L., Sonebi, M., Struble, L., Tepke, D., Wallevik, J.E. and Wallevik, O., 2004. Comparison of concrete rheometers: International tests at MBT (Cleveland OH, USA) in May 2003.

67. Abebe, Y.A., 2017. Flowable and Stable Concrete: Design, Characterization and Performance Evaluation. Hannover: Institut für Baustoffe, Leibniz Universität.

68. ACI Committee 238 2008 "Report on Measurements of Workability and Rheology of Fresh Concrete" ACI238-08 ACI manual of concrete practice, Detroit, MI,USA

APPENDIX

LUBRICATION LAYER CALCULATIONS

Table A-1 Example of determination of φm and intrinsic viscosity using Chateau–Ovarlez–Trung model. In portion that passes sieve #8.

Portion Sieved by #8			OUTPUT
		φ_m	0.565079844
INPUT		intr. V	6.273550231
φ	Relative Yield Stress (Pa)	Calculated Yield Stress (Pa)	SQ difference
0	1	1	0
0.2	2.037	1.940	0.00227843
0.3	2.968	3.201	0.006130708
0.4	7.201	6.860	0.00223849
0.45	12.437	12.451	1.22816E-06
0.5	32.462	32.606	1.96662E-05
			0.011

Table A-2 Example of determination of φm and intrinsic viscosity using Chateau–Ovarlez–Trung model. In portion that passes sieve #16.

Portion Sieved by #16			OUTPUT
		φ_m	0.510733793
INPUT		intr. V	6.011260792
φ	Relative Yield Stress (Pa)	Calculated Yield Stress (Pa)	SQ difference
0	1	1	0
0.2	1.536	1.917891299	0.061987836
0.3	2.608	3.256307113	0.06190266
0.4	11.056	8.095345475	0.071712968
0.45	29.093	19.48792484	0.109004741
0.475	38.549	42.98044143	0.01321645
			0.318

Table A-3 Example of determination of φm and intrinsic viscosity using Chateau–Ovarlez–Trung model. In portion that passes sieve #30.

Portion Sieved by #30			**OUTPUT**
		φ_m	0.500668
INPUT		intr. V	9.019492
φ	Relative Yield Stress (Pa)	Calculated Yield Stress (Pa)	SQ difference
0	1	1	0
0.2	2.264	2.828669758	0.062230886
0.3	5.714	6.593127674	0.023676347
0.4	38.435	28.97680638	0.060555214
0.425	76.755	54.04302149	0.087556597
0.45	114.516	130.7260505	0.020037872
			0.254

Table A-4 Example of determination of φm and intrinsic viscosity using Chateau–Ovarlez–Trung model. In portion that passes sieve #50.

Portion Sieved by #50			**OUTPUT**
		φ_m	0.455
INPUT		intr. V	12.37782
φ	Relative Yield Stress (Pa)	Calculated Yield Stress (Pa)	SQ difference
0	1	1	0
0.2	2.970	4.567477149	0.289538972
0.3	16.390	17.35855465	0.003495853
0.325	51.352	27.97193429	0.207293282
0.35	62.734	50.08624149	0.040645637
			0.541

Table A-5 Example of determination of φmax and intrinsic viscosity using Krieger-Dougherty equation. In portion that passes sieve #8.

Portion Sieved by #8			**OUTPUT**
		phimax	0.627965177
INPUT		intr. V	4.532274174
φ	Relative Plastic (Pa.s)	Calculated K-D (Pa.s)	SQ difference
0	1	1	0
0.2	2.927	2.978204978	0.000304709
0.3	5.590	6.351992988	0.018557841
0.4	21.211	17.88460644	0.024598385
0.45	37.316	36.18524683	0.000918383
0.5	89.081	92.51615548	0.001486672
			0.046

Table A-6 Example of determination of φmax and intrinsic viscosity using Krieger-Dougherty equation. In portion that passes sieve #16.

Portion Sieved by #16			**OUTPUT**
		phimax	0.57936
INPUT		intr. V	4.519275
φ	Relative Plastic (Pa.s)	Calculated K-D (Pa.s)	SQ difference
0	1	1	0
0.2	2.071	3.030365955	0.214380801
0.3	4.724	6.751996809	0.184422793
0.4	21.609	21.54228735	9.54594E-06
0.45	59.797	50.68667011	0.023212521
0.475	89.668	88.93869755	6.61469E-05
			0.422

Table A-7 Example of determination of φmax and intrinsic viscosity using Krieger-Dougherty equation. In portion that passes sieve #30.

Portion Sieved by #30			**OUTPUT**
		phimax	0.591014
INPUT		intr. V	5.508883
φ	Relative Plastic (Pa.s)	Calculated K-D (Pa.s)	SQ difference
0	1	1	0
0.2	3.252	3.838072205	0.032523077
0.3	9.852	10.04073482	0.000367766
0.4	50.778	39.54478082	0.048941489
0.425	69.724	62.43609501	0.010924562
0.45	93.948	106.222576	0.017070074
			0.110

Table A-8 Example of determination of φmax and intrinsic viscosity using Krieger-Dougherty equation. In portion that passes sieve #50.

Portion Sieved by #50			**OUTPUT**
		phimax	0.49382
INPUT		intr. V	7.051051
φ	Relative Plastic (Pa.s)	Calculated K-D (Pa.s)	SQ difference
0	1	1	0
0.2	5.422	6.097272114	0.015526028
0.3	27.541	25.95756395	0.003307019
0.325	53.244	41.98487033	0.044718555
0.35	65.848	73.35886335	0.01300882
			0.077

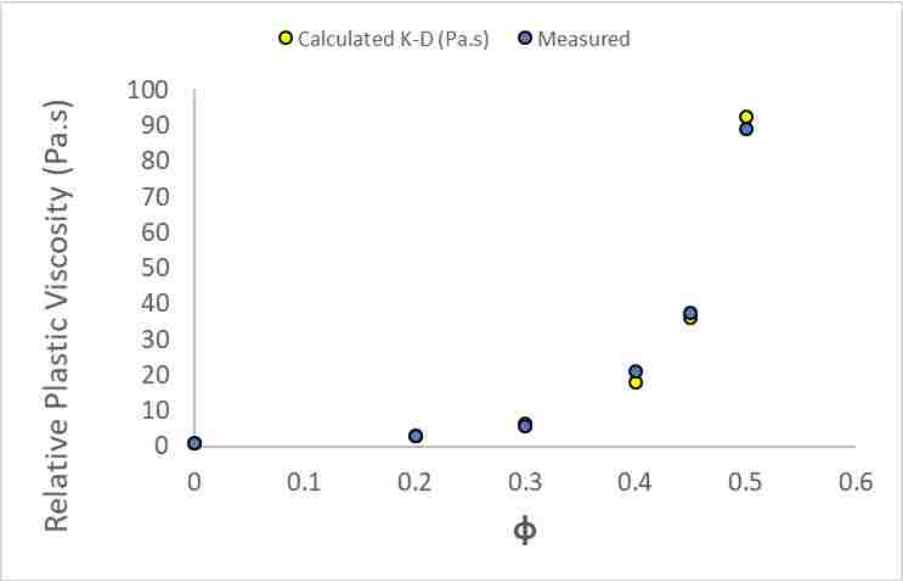

Figure A-1 Relative plastic viscosity evolution with volume fraction. In portion that passes sieve #8.

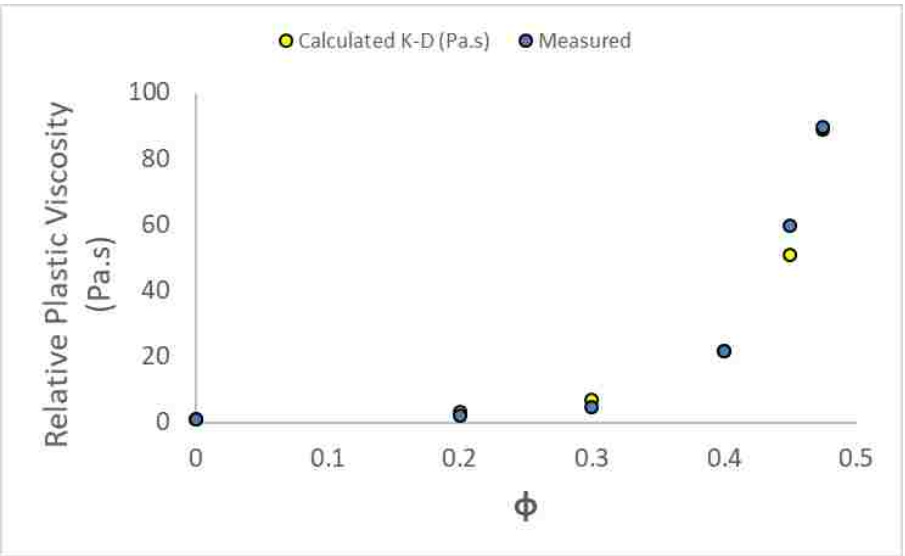

Figure A-2 Relative plastic viscosity evolution with volume fraction. In portion that passes sieve #16.

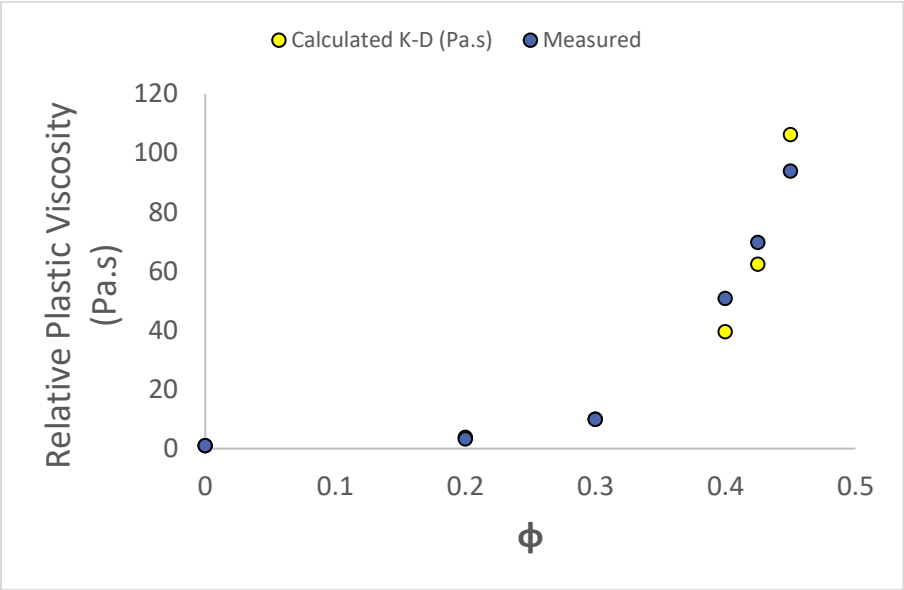

Figure A-3 Relative plastic viscosity evolution with volume fraction. In portion that passes sieve #30.

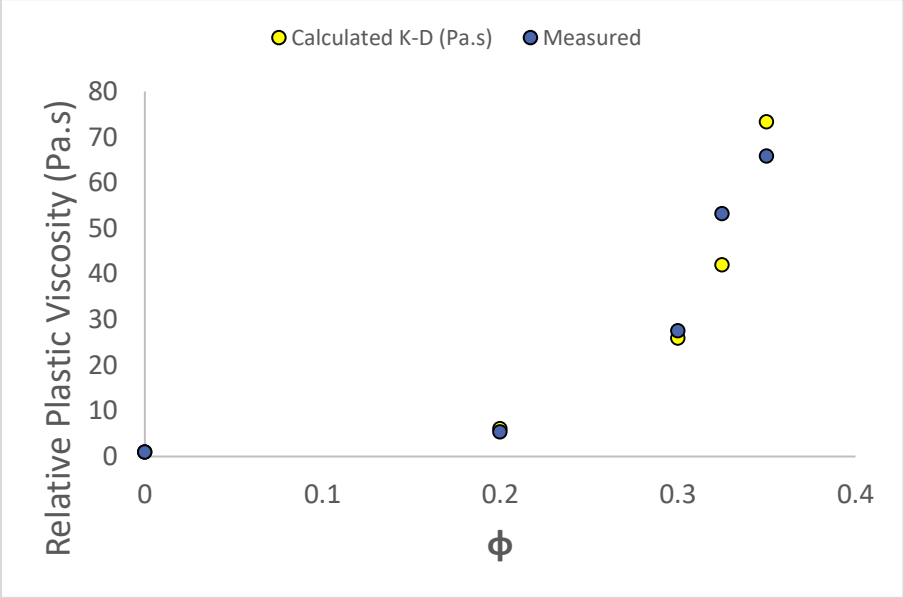

Figure A-4 Relative plastic viscosity evolution with volume fraction. In portion that passes sieve #50.

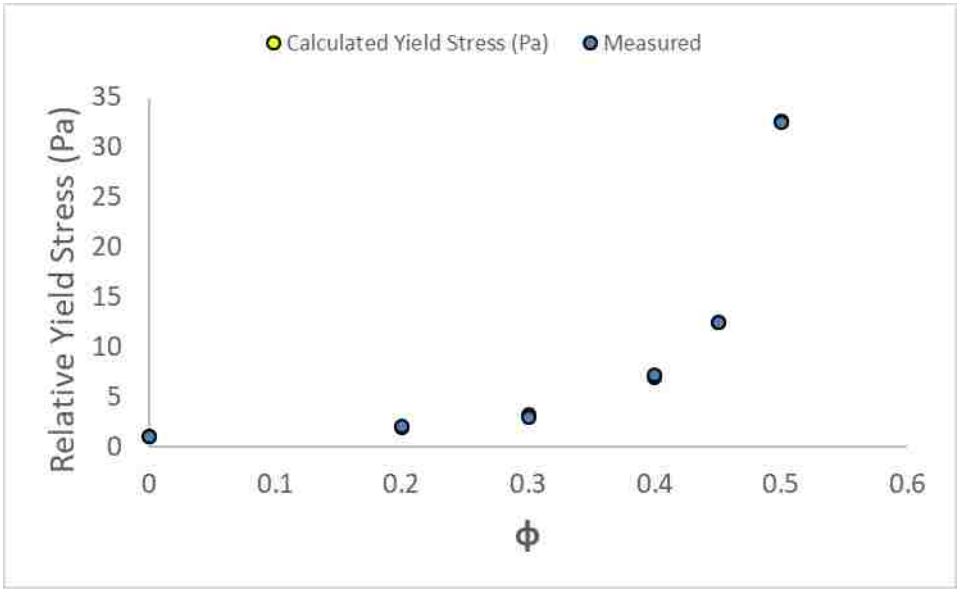

Figure A-5 Relative yield stress evolution with volume fraction. In portion that passes sieve #8.

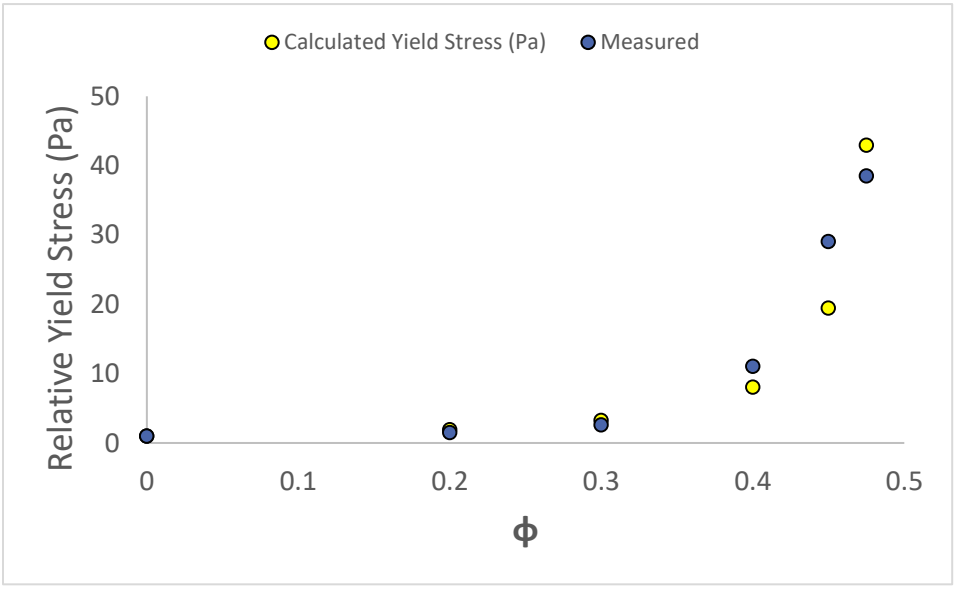

Figure A-6 Relative yield stress evolution with volume fraction. In portion that passes sieve #16.

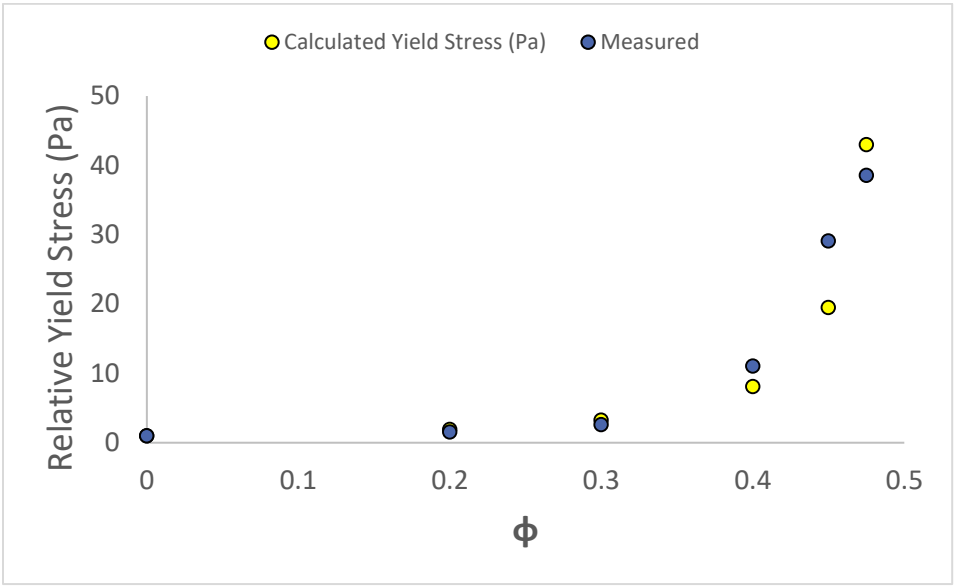

Figure A-7 Relative yield stress evolution with volume fraction. In portion that passes sieve #30.

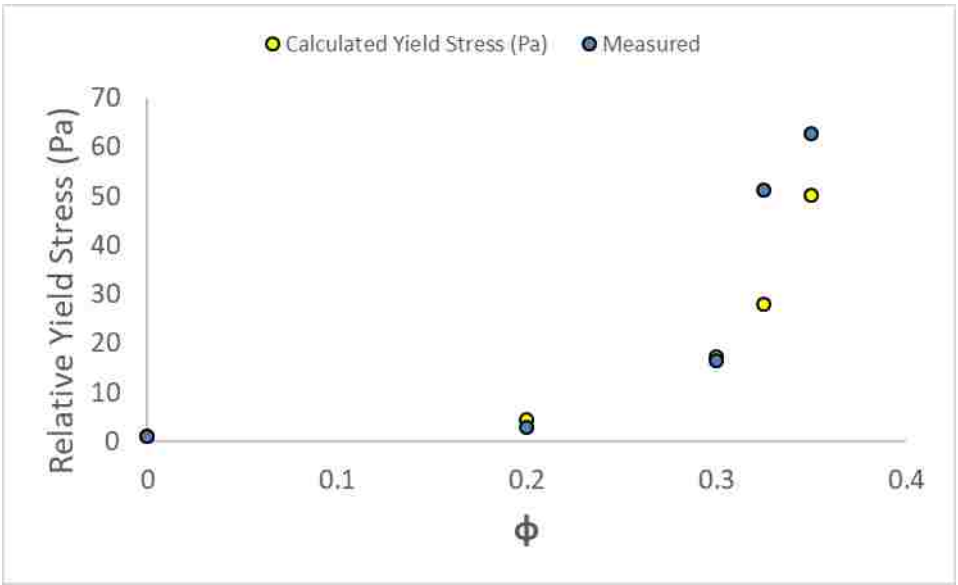

Figure A-8 Relative yield stress evolution with volume fraction. In portion that passes sieve #50.

Table A-9 Calculation procedure for determination of thickness of each layer. Mix with w/c=0.35 (Scenario1).

Step 1. Measured properties									
			Ri	Ri+2	Ri+3	Ri+4	Ri+5	Ri+6	Ri+7
Torque (Nm)	Velocity	YS (Pa)	0.720	1.253	1.620	1.874	4.181	12.389	39.659
		PV (Pa.s)	0.130	0.256	0.377	0.632	1.877	6.629	33.477
0.897	0.500	Rp	0.996	0.755	0.664	0.617	0.413	0.240	0.134
0.784	0.424		0.931	0.706	0.621	0.577	0.386	0.224	0.125
0.614	0.350		0.824	0.624	0.549	0.511	0.342	0.199	0.111
0.487	0.275		0.733	0.556	0.489	0.455	0.304	0.177	0.099
0.370	0.200		0.640	0.485	0.426	0.397	0.265	0.154	0.086
0.216	0.125		0.489	0.371	0.326	0.303	0.203	0.118	0.066
0.081	0.050		0.299	0.227	0.199	0.185	0.124	0.072	0.040
		Step2. Determination of plug flow at Inner Radius							
		plug flow	0.063	0.063	0.063	0.063	0.063	0.063	0.063
		at Ri?	0.063	0.063	0.063	0.063	0.063	0.063	0.063
			0.063	0.063	0.063	0.063	0.063	0.063	0.063
			0.063	0.063	0.063	0.063	0.063	0.063	0.063
			0.063	0.063	0.063	0.063	0.063	0.063	0.063
			0.063	0.063	0.063	0.063	0.063	0.063	0.063
			0.063	0.063	0.063	0.063	0.063	0.063	0.000
		Step 3. Determination of plug flow at Outer Radius							
N/A	N/A	plug flow	0.063	0.063	0.063	0.063	0.063	0.063	0.134
		at Ro	0.063	0.063	0.063	0.063	0.063	0.063	0.125
			0.063	0.063	0.063	0.063	0.063	0.063	0.111
			0.063	0.063	0.063	0.063	0.063	0.063	0.099
			0.063	0.063	0.063	0.063	0.063	0.063	0.086
			0.063	0.063	0.063	0.063	0.063	0.063	0.066
			0.063	0.063	0.063	0.063	0.063	0.063	0.000
		Step 4. Contribution to speed of each layer							
		Ri	Ri+2	Ri+3	Ri+4	Ri+5	Ri+6	Ri+7	Sum of Velocities (rps)
0.897	0.500	0.342	0.000	0.000	0.000	0.000	0.000	0.195	0.536
0.784	0.424	0.299	0.000	0.000	0.000	0.000	0.000	0.153	0.452
0.614	0.350	0.233	0.000	0.000	0.000	0.000	0.000	0.094	0.327
0.487	0.275	0.185	0.000	0.000	0.000	0.000	0.000	0.055	0.239
0.370	0.200	0.140	0.000	0.000	0.000	0.000	0.000	0.024	0.164
0.216	0.125	0.081	0.000	0.000	0.000	0.000	0.000	0.001	0.082
0.081	0.050	0.030	0.000	0.000	0.000	0.000	0.000	0.000	0.030
		Step5. Optimal thickness (m)							
N/A	N/A	0	0.0625	0.062596	0.062596	0.062596	0.062596	0.062596	0.143
		0.0625	0.062596	0.062596	0.062596	0.062596	0.062596	0.062596	0.143
		N/A	9.60394E-05	0	0	0	0	0	N/A

Table A-10 Calculation procedure for determination of thickness of each layer. Mix with w/c=0.40 (Scenario1).

Step 1. Measured properties									
			Ri	Ri+2	Ri+3	Ri+4	Ri+5	Ri+6	Ri+7
Torque (Nm)	Velocity	YS (Pa)	0.612	1.065	1.378	1.593	3.554	10.533	54.409
		PV (Pa.s)	0.094	0.184	0.271	0.455	1.351	4.772	24.262
0.584	0.500	Rp	0.871	0.660	0.581	0.540	0.361	0.210	0.092
0.528	0.425		0.828	0.628	0.552	0.513	0.344	0.200	0.088
0.463	0.350		0.776	0.588	0.517	0.481	0.322	0.187	0.082
0.397	0.275		0.718	0.545	0.479	0.445	0.298	0.173	0.076
0.331	0.200		0.656	0.498	0.437	0.407	0.272	0.158	0.070
0.254	0.125		0.574	0.435	0.383	0.356	0.238	0.138	0.061
0.157	0.050		0.452	0.343	0.301	0.280	0.188	0.109	0.048
		Step2. Determination of plug flow at Inner Radius							
		plug flow	0.063	0.063	0.063	0.063	0.063	0.063	0.063
		at Ri?	0.063	0.063	0.063	0.063	0.063	0.063	0.063
			0.063	0.063	0.063	0.063	0.063	0.063	0.063
			0.063	0.063	0.063	0.063	0.063	0.063	0.063
			0.063	0.063	0.063	0.063	0.063	0.063	0.063
			0.063	0.063	0.063	0.063	0.063	0.063	0.000
			0.063	0.063	0.063	0.063	0.063	0.063	0.000
		Step 3. Determination of plug flow at Outer Radius							
N/A	N/A	plug flow	0.063	0.063	0.063	0.063	0.063	0.063	0.092
		at Ro	0.063	0.063	0.063	0.063	0.063	0.063	0.088
			0.063	0.063	0.063	0.063	0.063	0.063	0.082
			0.063	0.063	0.063	0.063	0.063	0.063	0.076
			0.063	0.063	0.063	0.063	0.063	0.063	0.070
			0.063	0.063	0.063	0.063	0.063	0.063	0.000
			0.063	0.063	0.063	0.063	0.063	0.063	0.000
		Step 4. Contribution to speed of each layer							
		Ri	Ri+2	Ri+3	Ri+4	Ri+5	Ri+6	Ri+7	Sum of Velocities (rps)
0.584	0.500	0.394	0.000	0.000	0.000	0.000	0.000	0.071	0.465
0.528	0.425	0.356	0.000	0.000	0.000	0.000	0.000	0.052	0.408
0.463	0.350	0.312	0.000	0.000	0.000	0.000	0.000	0.032	0.344
0.397	0.275	0.267	0.000	0.000	0.000	0.000	0.000	0.016	0.283
0.331	0.200	0.223	0.000	0.000	0.000	0.000	0.000	0.004	0.227
0.254	0.125	0.170	0.000	0.000	0.000	0.000	0.000	0.000	0.170
0.157	0.050	0.105	0.000	0.000	0.000	0.000	0.000	0.000	0.105
		Step5. Optimal thickness (m)							
N/A	N/A	0	0.0625	0.062596	0.062596	0.062596	0.062596	0.062596	0.143
		0.0625	0.062596	0.062596	0.062596	0.062596	0.062596	0.062596	0.143
		N/A	0.0625	0.062622663	0.062622663	0.062622663	0.062622663	0.062622663	0.062622663

Table A-11Calculation procedure for determination of thickness of each layer. Mix with w/c=0.40 (Scenario2).

Step 1. Measured properties									
			Ri	Ri+2	Ri+3	Ri+4	Ri+5	Ri+6	Ri+7
Torque (Nm)	Velocity	YS (Pa)	0.612	1.065	1.378	1.593	3.554	10.533	54.409
		PV (Pa.s)	0.094	0.184	0.271	0.455	1.351	4.772	24.262
0.584	0.500	Rp	0.871	0.660	0.581	0.540	0.361	0.210	0.092
0.528	0.425		0.828	0.628	0.552	0.513	0.344	0.200	0.088
0.463	0.350		0.776	0.588	0.517	0.481	0.322	0.187	0.082
0.397	0.275		0.718	0.545	0.479	0.445	0.298	0.173	0.076
0.331	0.200		0.656	0.498	0.437	0.407	0.272	0.158	0.070
0.254	0.125		0.574	0.435	0.383	0.356	0.238	0.138	0.061
0.157	0.050		0.452	0.343	0.301	0.280	0.188	0.109	0.048
		Step2. Determination of plug flow at Inner Radius							
		plug flow	0.063	0.063	0.063	0.063	0.063	0.063	0.072
		at Ri?	0.063	0.063	0.063	0.063	0.063	0.063	0.072
			0.063	0.063	0.063	0.063	0.063	0.063	0.072
			0.063	0.063	0.063	0.063	0.063	0.063	0.072
			0.063	0.063	0.063	0.063	0.063	0.063	0.000
			0.063	0.063	0.063	0.063	0.063	0.063	0.000
			0.063	0.063	0.063	0.063	0.063	0.063	0.000
		Step 3. Determination of plug flow at Outer Radius							
N/A	N/A	plug flow	0.063	0.063	0.063	0.063	0.063	0.072	0.092
		at Ro	0.063	0.063	0.063	0.063	0.063	0.072	0.088
			0.063	0.063	0.063	0.063	0.063	0.072	0.082
			0.063	0.063	0.063	0.063	0.063	0.072	0.076
			0.063	0.063	0.063	0.063	0.063	0.072	0.000
			0.063	0.063	0.063	0.063	0.063	0.072	0.000
			0.063	0.063	0.063	0.063	0.063	0.072	0.000
		Step 4. Contribution to speed of each layer							
		Ri	Ri+2	Ri+3	Ri+4	Ri+5	Ri+6	Ri+7	Sum of Velocities (rps)
0.584	0.500	0.000	0.000	0.010	0.001	0.000	0.429	0.027	0.467
0.528	0.425	0.000	0.000	0.009	0.001	0.000	0.383	0.017	0.410
0.463	0.350	0.000	0.000	0.008	0.001	0.000	0.330	0.007	0.346
0.397	0.275	0.000	0.000	0.007	0.000	0.000	0.276	0.001	0.285
0.331	0.200	0.000	0.000	0.006	0.000	0.000	0.223	0.000	0.229
0.254	0.125	0.000	0.000	0.004	0.000	0.000	0.159	0.000	0.164
0.157	0.050	0.000	0.000	0.003	0.000	0.000	0.080	0.000	0.083
		Step5. Optimal thickness (m)							
N/A	N/A	0	0.0625	0.062596	0.062596	0.062596	0.062596	0.062596	0.143
		0.0625	0.062596	0.062596	0.062596	0.062596	0.062596	0.062596	0.143
		N/A	0.062500	0.062500	0.062500	0.062509	0.062510	0.062510	0.071743

Table A-12 Calculation procedure for determination of thickness of each layer. Mix with w/c=0.40 +fly ash (Scenario1).

Step 1. Measured properties									
			Ri	Ri+2	Ri+3	Ri+4	Ri+5	Ri+6	Ri+7
Torque (Nm)	Velocity	YS (Pa)	0.479	0.833	1.077	1.246	2.780	8.238	50.581
		PV (Pa.s)	0.071	0.140	0.206	0.345	1.024	3.617	26.624
0.584	0.500	Rp	1.301	0.986	0.867	0.806	0.540	0.314	0.127
0.528	0.425		1.216	0.922	0.811	0.754	0.505	0.293	0.118
0.463	0.350		1.137	0.862	0.758	0.705	0.472	0.274	0.111
0.397	0.275		1.076	0.816	0.717	0.667	0.446	0.259	0.105
0.331	0.200		0.945	0.716	0.630	0.586	0.392	0.228	0.092
0.254	0.125		0.858	0.650	0.572	0.532	0.356	0.207	0.083
0.157	0.050		0.708	0.537	0.472	0.439	0.294	0.171	0.069
		Step2. Determination of plug flow at Inner Radius							
		plug flow	0.063	0.063	0.063	0.063	0.063	0.063	0.063
		at Ri?	0.063	0.063	0.063	0.063	0.063	0.063	0.063
			0.063	0.063	0.063	0.063	0.063	0.063	0.063
			0.063	0.063	0.063	0.063	0.063	0.063	0.063
			0.063	0.063	0.063	0.063	0.063	0.063	0.063
			0.063	0.063	0.063	0.063	0.063	0.063	0.063
			0.063	0.063	0.063	0.063	0.063	0.063	0.063
		Step 3. Determination of plug flow at Outer Radius							
N/A	N/A	plug flow	0.063	0.063	0.063	0.063	0.063	0.063	0.127
		at Ro	0.063	0.063	0.063	0.063	0.063	0.063	0.118
			0.063	0.063	0.063	0.063	0.063	0.063	0.111
			0.063	0.063	0.063	0.063	0.063	0.063	0.105
			0.063	0.063	0.063	0.063	0.063	0.063	0.092
			0.063	0.063	0.063	0.063	0.063	0.063	0.083
			0.063	0.063	0.063	0.063	0.063	0.063	0.069
		Step 4. Contribution to speed of each layer							
		Ri	Ri+2	Ri+3	Ri+4	Ri+5	Ri+6	Ri+7	Sum of Velocities (rps)
1.018	0.500	0.248	0.000	0.000	0.000	0.000	0.000	0.255	0.502
0.890	0.425	0.216	0.000	0.000	0.000	0.000	0.000	0.197	0.414
0.777	0.350	0.189	0.000	0.000	0.000	0.000	0.000	0.149	0.338
0.696	0.275	0.169	0.000	0.000	0.000	0.000	0.000	0.116	0.286
0.537	0.200	0.130	0.000	0.000	0.000	0.000	0.000	0.059	0.189
0.442	0.125	0.107	0.000	0.000	0.000	0.000	0.000	0.031	0.138
0.302	0.050	0.073	0.000	0.000	0.000	0.000	0.000	0.003	0.076
		Step5. Optimal thickness (m)							
N/A	N/A	0	0.0625	0.062596	0.062596	0.062596	0.062596	0.062596	0.143
		0.0625	0.062596	0.062596	0.062596	0.062596	0.062596	0.062596	0.143
		N/A	0.062500	0.062533	0.062533	0.062533	0.062533	0.062533	0.062534

Table A-13 Calculation procedure for determination of thickness of each layer. Mix with w/c=0.40 (Scenario2).

Step 1. Measured properties									
			Ri	Ri+2	Ri+3	Ri+4	Ri+5	Ri+6	Ri+7
Torque (Nm)	Velocity	YS (Pa)	0.479	0.833	1.077	1.246	2.780	8.238	50.581
		PV (Pa.s)	0.071	0.140	0.206	0.345	1.024	3.617	26.624
0.584	0.500	Rp	1.301	0.986	0.867	0.806	0.540	0.314	0.127
0.528	0.425		1.216	0.922	0.811	0.754	0.505	0.293	0.118
0.463	0.350		1.137	0.862	0.758	0.705	0.472	0.274	0.111
0.397	0.275		1.076	0.816	0.717	0.667	0.446	0.259	0.105
0.331	0.200		0.945	0.716	0.630	0.586	0.392	0.228	0.092
0.254	0.125		0.858	0.650	0.572	0.532	0.356	0.207	0.083
0.157	0.050		0.708	0.537	0.472	0.439	0.294	0.171	0.069
		Step2. Determination of plug flow at Inner Radius							
		plug flow	0.063	0.063	0.063	0.063	0.063	0.063	0.063
		at Ri?	0.063	0.063	0.063	0.063	0.063	0.063	0.063
			0.063	0.063	0.063	0.063	0.063	0.063	0.063
			0.063	0.063	0.063	0.063	0.063	0.063	0.063
			0.063	0.063	0.063	0.063	0.063	0.063	0.063
			0.063	0.063	0.063	0.063	0.063	0.063	0.063
			0.063	0.063	0.063	0.063	0.063	0.063	0.063
		Step 3. Determination of plug flow at Outer Radius							
N/A	N/A	plug flow	0.063	0.063	0.063	0.063	0.063	0.063	0.127
		at Ro	0.063	0.063	0.063	0.063	0.063	0.063	0.118
			0.063	0.063	0.063	0.063	0.063	0.063	0.111
			0.063	0.063	0.063	0.063	0.063	0.063	0.105
			0.063	0.063	0.063	0.063	0.063	0.063	0.092
			0.063	0.063	0.063	0.063	0.063	0.063	0.083
			0.063	0.063	0.063	0.063	0.063	0.063	0.069
		Step 4. Contribution to speed of each layer							
		Ri	Ri+2	Ri+3	Ri+4	Ri+5	Ri+6	Ri+7	Sum of Velocities (rps)
1.018	0.500	0.000	0.134	0.088	0.022	0.005	0.000	0.254	0.502
0.890	0.425	0.000	0.117	0.077	0.019	0.004	0.000	0.196	0.414
0.777	0.350	0.000	0.102	0.067	0.017	0.004	0.000	0.149	0.338
0.696	0.275	0.000	0.092	0.060	0.015	0.003	0.000	0.116	0.286
0.537	0.200	0.000	0.070	0.046	0.011	0.003	0.000	0.059	0.189
0.442	0.125	0.000	0.058	0.038	0.009	0.002	0.000	0.031	0.138
0.302	0.050	0.000	0.039	0.026	0.006	0.001	0.000	0.003	0.076
		Step5. Optimal thickness (m)							
N/A	N/A	0	0.0625	0.062596	0.062596	0.062596	0.062596	0.062596	0.143
		0.0625	0.062596	0.062596	0.062596	0.062596	0.062596	0.062596	0.143
		N/A	0.062500	0.062500	0.062536	0.062570	0.062584	0.062594	0.062594

VITA

Alexis Salinas was born in Mission, Texas to parents Florentino Salinas and Maria Reyes. He started his undergraduate studies in fall 2011. During his time as an undergraduate student he worked as an electrician journeyman to pay his studies. He received is Bachelors in Science in Facultad de Ingenieria Civil. UANL in Monterrey. Nuevo Leon In fall 2016. He stared is Civil Engineering Master's program In Fall 2017 at Missouri University of Science and Technology. He held the position of Graduate teaching Assistant, and Graduate research assistant. In spring 2019 he started working as a Quality Assurance Engineer for Air Force Civil Engineering Center (AFCEC). He completed his Masters of Science in Civil Engineering in December 2019.